

CONJUGATED PHOTOACTIVE POLYELECTROLYTES AND HYBRID MATERIALS
BASED ON CONJUGATED OLIGOMERS: SYNTHESIS, PHOTOPHYSICS AND
APPLICATION IN SOLAR CELLS

By

DONGPING XIE

A DISSERTATION PRESENTED TO THE GRADUATE SCHOOL
OF THE UNIVERSITY OF FLORIDA IN PARTIAL FULFILLMENT
OF THE REQUIREMENTS FOR THE DEGREE OF
DOCTOR OF PHILOSOPHY

UNIVERSITY OF FLORIDA

2012

© 2012 Dongping Xie

To My parents

ACKNOWLEDGMENTS

I want to express my deepest appreciation to many people who have shared their support, advice, love and friendship during my time here in Florida. First I give my sincerest gratitude to my advisor Kirk Schanze. With his teaching which is full of wisdom and knowledge I have learnt a lot more than just chemistry. With his unending patience and support, I have had chance to explore myself as a person, instead of worrying about turning into an obedient machine whose data matters larger than life. Having been working with him is indeed an invaluable asset to me.

I am very much obliged to those who have contributed to this dissertation. My collaborators Dr. John Reynolds, Dr. Jiangeng Xue, and Dr. Paul Holloway have all been extremely supportive. Their wisdoms and expertise on research added many inspirations to the work. My committee professors Dr. Ronald Castellano, Dr. Valeria Kleiman and Dr. Sukwon Hong have spared their valuable time providing suggestions and revisions on the writing, to which I am sincerely grateful. I also owe my appreciate to the student researchers who have worked side by side with me for almost the entire graduate study: Romain Stalder is a handsome intelligent man who also becomes a PhD this semester, and Renjia Zhou is almost a “mobile library” of his field whose energy seems endless. Those late night (or early morning) experiments, meetings before deadlines on the turf, and of course, the happy conversations on the highways with them are my precious “clips” that will always be cherished.

I would like to thank my former and current colleagues who have shared their advice and friendships. Dr. Zhen Fang, Dr. Fude Feng and Dr. Chen Liao offered many useful tips and trainings that paved my way to this career point. Dr. Anand Parthasarathy tirelessly assisted me editing my writings, and kindly discussed problems

that I encountered during research. Randi Price is a cool “laser girl”, she contributed to this work by conducting many transient absorption experiments. Zhuo Chen, Xuzhi Zhu, Zhenxing Pan, Jie Yang and Danlu Wu, who are also thousands miles away from homes, have provided many joyful times.

I am grateful to my best friends who are always there for me. Yiheng Huang is the smartest person I have ever met. His funny yet witty ideas really have catalyzed my process of self-recognition, and his unremittingly pursue on his goals has been encouraging all the time. Jinhua Tu is a self-taught astronomist and engineer. He shared with me a great deal of happy time of childhood and teenage, and this friendship has never ceased growing up with us. I also want to give Yiheng and Jinhua my innermost gratitude for taking care of my parents while I am oceans apart.

Special thanks go to the great composers Frédéric Chopin, Ludwig van Beethoven et al. whose fantastic music have conquered the hard times along the way.

Last but not the least, I am feeling lucky to be endowed with a happy and warm family. I thank my parents and grandparents for their constant supports and love during the past 27 years. I give my heart-whole acknowledgement to my mother Hui Peng. Beyond any word, this work is dedicated solely to her.

TABLE OF CONTENTS

	<u>Page</u>
ACKNOWLEDGMENTS	4
LIST OF TABLES	8
LIST OF FIGURES	9
ABSTRACT	12
CHAPTER	
1 INTRODUCTION	15
Conjugated Polyelectrolytes	15
Synthesis Approaches	16
Pd catalyzed cross-coupling reactions	16
Other approaches used in CPE synthesis	18
Synthetic methodologies	20
Photophysical Properties: Aggregation and Amplified Quenching of CPEs	21
Aggregation and self-assembly	22
Amplified photoluminescence quenching	25
Application of CPEs as Functional Materials	28
Bio/chemo sensory materials	28
Dye-sensitized solar cells	31
Summary for CPEs	36
Conjugated Polymer/Oligomer-Semiconductor Nanocrystal Hybrid Materials	36
Synthetic Strategies	37
“Graft to” method	38
“Graft from” method	41
Characterization-Interfaces of the Hybrids	43
Compositional analysis	43
Photophysical and electrochemical analysis	46
The Hybrids’ Applications in Solar Cells	48
Summary for Polymer/Oligomer-Semiconductor Nanoparticle Hybrids	50
2 AGGREGATION INDUCED AMPLIFIED QUENCHING IN CONJUGATED POLYELECTROLYTES WITH INTERRUPTED CONJUGATION	52
Conjugated Polyelectrolytes	52
Results and Discussion	54
Synthesis and Structural Characterization	54
Photophysics	57
Summary and Conclusions	67
Experimental	68
Materials and Methods	68

	Synthetic Procedures	68
3	SYNTHESIS AND CHARACTERIZATION OF BODIPY BASED POLYELECTROLYTES AND THEIR INTERACTIONS WITH QUENCHERS	73
	Incorporating BODIPY into Polymer Backbones	73
	Results and Discussion.....	76
	Synthesis and Structural Characterization.....	76
	Photophysical Properties.....	80
	Interaction with Quenchers-Amplified Quenching and Ion Sensing	84
	Application of PB-a in Dye-sensitized Solar Cells	90
	Summary and Conclusions	94
	Experimental.....	95
	Materials and Methods	95
	Synthetic Procedures	97
4	PHOSPHONIC ACID FUNCTIONALIZED Π -CONJUGATED PHOTOACTIVE OLIGOMERS: PHOTOPHYSICAL PROPERTIES, INTERACTIONS WITH CDSE NANOCRYSTALS, AND APPLICATION IN DYE-SENSITIZED SOLAR CELLS	104
	Hybrid Materials Based on Conjugated Oligomers	104
	Results and Discussions.....	107
	Synthesis and Structural Characterizations.....	107
	Photophysics of the Oligomers and CdSe NCs	110
	E-chem Characterizations	112
	Photoluminescence Quenching of the Oligomers and NCs.....	114
	Oligomer-CdSe Hybrids and IPCE Results	118
	Application of the Oligomers in Dye-sensitized Solar Cells	125
	Summary and Conclusions	127
	Experimental.....	128
	Materials and Methods	128
	Synthetic Procedures	130
5	CONCLUSIONS AND FUTURE WORK	136
	Aggregation Induced Amplified Quenching.....	136
	BODIPY in the Backbone.....	137
	Conjugated Oligomers with Mono Phosphonic Acid Functionality	138
	LIST OF REFERENCES	140
	BIOGRAPHICAL SKETCH.....	152

LIST OF TABLES

<u>Table</u>	<u>page</u>
1-1 Palladium catalyzed cross-coupling reactions	17
1-2 Examples of CPEs that were synthesized by Pd-catalyzed cross-coupling reactions	18
2-1 Photophysical data of C-PPE and O-PPE	59
3-1 Photophysical data of PB-e , PB-a and PB-Na	83
4-1 Contributions made by several groups to the project.....	106
4-2 Photophysical data for the oligomers and CdSe NCs in CHCl ₃ solution.....	112
4-3 Optical data of the oligomer/CdSe hybrids in CHCl ₃ solution.	123

LIST OF FIGURES

<u>Figure</u>	<u>page</u>
1-1 Examples of typical CPEs	16
1-2 A general catalytic cycle for Pd-catalyzed cross-coupling.	17
1-3 Electropolymerization of thiophenes.....	19
1-4 Synthetic approach for PPV type of CPE	20
1-5 Photophysics of CPEs with variable bandgaps.....	22
1-6 Schematic representation of the aggregative interactions between polymer 1 and different diamine analytes.....	24
1-7 Equations of Photoluminescence Quenching.	26
1-8 “Molecular-wire effect” in conjugated polymers with receptors.	27
1-9 Stern–Volmer plots of polyfluorene quenched by 5-nm gold nanoparticles.	30
1-10 A “turn on” fluorescence sensor for avidin.	31
1-11 Principle of operation of DSSCs.	33
1-12 J–V characteristics under AM1.5 conditions for solar cells sensitized with PPE, PT, and PPE/PT mixture.	34
1-13 Structures of the repeat units for variable-gap PPE-based CPEs used in TiO ₂ -sensitized photovoltaic devices.	35
1-14 Schematic presentation of molecular recognition between MHT functionalized CdSe NCs and DAP modified P3HT.....	39
1-15 Schematic presentations of different routes the oligomers/polymers are attached to the NC surfaces.	40
1-16 “Graft from” synthetic scheme for PPV/CdSe hybrids.....	42
1-17 <i>In situ</i> synthesis of CdS nanorods template by P3HT.....	43
1-18 ¹ H NMR broadening as free oligothiophenes bind to CdSe NCs.....	45
1-19 TEM characterizations of the hybrid films.....	46
1-20 Energy level alignment in a conjugated polymer/CdSe NC hybrid film facilitating charge separations.	47

1-21	Schematic presentation of the proposed energy level alignment in CdSe-oligothiophene complexes	48
2-1	Structures of C-PPE and O-PPE	54
2-2	Synthetic scheme of C-PPE and O-PPE	55
2-3	¹ H NMR and peak assignment for C-PPE and O-PPE	56
2-4	Absorption and fluorescence spectra of C-PPE and O-PPE in MeOH..	58
2-5	Fluorescence spectra of C-PPE and O-PPE in a mixture of methanol and water.....	59
2-6	Fluorescence spectra of O-PPE with added MV ²⁺	60
2-7	Fluorescence quenching of O-PPE by adding DOC..	61
2-8	Fluorescence quenching of O-PPE by DODC.	62
2-9	Stern-Volmer plots of C-PPE and O-PPE with MV ²⁺ in MeOH Water.....	63
2-10	Distribution of particle sizes of C-PPE and O-PPE in MeOH and H ₂ O	65
2-11	Interaction between Ru(bpy) ₂ (dppz) ²⁺ and O-PPE	66
2-12	Photophysics of O-PPE at different concentrations.	67
2-13	Fluorescence spectra of O-PPE at different temperatures in MeOH.	67
3-1	Chemical structure of BODIPY	74
3-2	Two examples of conjugated polymers incorporating BODIPY.	75
3-3	Synthesis of monomer 6	76
3-4	Synthesis of monomer 10	77
3-5	Polymerization and deprotection..	78
3-6	¹ H NMR spectra and peak assignment for monomer 6 , monomer 10 , PB-e and PB-a	79
3-7	Normalized absorption and fluorescence spectra of PB-e , PB-a and PB-Na	81
3-8	Absorption and Fluorescence spectra of PB-Na in a mixture of methanol and water.....	82
3-9	Absorption and fluorescence response of PB-Na in MeOH upon adding MV ²⁺ ..	85

3-10	CV and DPV of PB-a	87
3-11	Fluorescence quenching of PB-Na by Cu^{2+}	88
3-12	Chemical structure of DOTC.....	89
3-13	Fluorescence quenching of PB-Na by DOTC.....	90
3-14	PB-a on TiO_2 films.....	91
3-15	PB-a - TiO_2 film transient absorption and decay profile at 700 nm.	93
3-16	Transient absorption setup for films.....	97
4-1	Chemical structures of conjugated oligomers studied in this work.....	107
4-2	Synthesis of OPE-E and OPE-A	109
4-3	Photophysical characterization of the oligomers.....	111
4-4	Energy level alignment of the oligomers and CdSe.....	113
4-5	Fluorescence quenching of the oligomers by CdSe.	115
4-6	Evolution of the fluorescence of CdSe NCs upon addition of OPE-E and OPE-A	117
4-7	Absorbance comparison of the hybrids with parental CdSe NCs..	119
4-8	TGA thermograms of the pristine CdSe NCs and the hybrids.	121
4-9	Comparison of absorption of T6-A /CdSe hybrid and the free components.	122
4-10	IPCE of OPE /CdSe, T6 /CdSe and T4BTD /CdSe hybrids films.	125
4-11	J-V curve and IPCE of T6 and T4BTD in TiO_2 base DSSCs.....	127

Abstract of Dissertation Presented to the Graduate School
of the University of Florida in Partial Fulfillment of the
Requirements for the Degree of Doctor of Philosophy

CONJUGATED PHOTOACTIVE POLYELECTROLYTES AND HYBRID MATERIALS
BASED ON CONJUGATED OLIGOMERS: SYNTHESIS, PHOTOPHYSICS AND
APPLICATION IN SOLAR CELLS

By

Dongping Xie

May 2012

Chair: Kirk S. Schanze
Major: Chemistry

This dissertation focuses on fundamental investigations of the structure-property relationships of conjugated polyelectrolytes (CPE) and conjugated oligomers, as well as their application to the dye-sensitized solar cells (DSSCs).

First, a pair of conjugated polyelectrolytes with sulfonate side groups that contain three-ring (phenylene ethynylene) units linked by a single $-\text{CH}_2-$ or $-\text{O}-$ tether (**C-PPE** and **O-PPE**, respectively) were studied. The linkers served to interrupt the π conjugation along the polymer backbone. Fluorescence spectroscopy revealed that **O-PPE** forms a fluorescent aggregate in methanol and water; however, the fluorescence of **C-PPE** is much weaker in water, and **C-PPE** exhibits only weak aggregate fluorescence. Fluorescence quenching of the polymers was examined using methylviologen (MV^{2+}) as a cationic quencher. **C-PPE** showed only a weak amplified quenching effect, with a Stern–Volmer quenching constant of $K_{\text{SV}} \sim 6 \times 10^5 \text{ M}^{-1}$ in methanol. Interestingly, for **O-PPE** in methanol, the aggregate emission is strongly quenched with $K_{\text{SV}} \sim 5 \times 10^6 \text{ M}^{-1}$, which is comparable to the highest quenching efficiency observed for fully π -conjugated polyelectrolytes. By contrast, the monomer emission is quenched much less efficiently,

with $K_{SV} \sim 2 \times 10^5 \text{ M}^{-1}$. The results are explained by a model in which **O-PPE** is able to fold into a helical conformation in solution, which facilitates the formation of extended π -stacked aggregates for long-distance exciton transport.

Second, a novel type of CPE bearing BODIPY-phenylene-ethynylene copolymer backbone and branched sodium-carboxylate side chains (**PB-Na**) was synthesized by a precursor route via Sonogashira coupling reaction. **PB-Na** was less likely to aggregate in both MeOH and H₂O, resulting in moderate fluorescence quantum yields. The fluorescence quenching experiment showed that **PB-Na** could be quenched by Cu²⁺ selectively among a series of metal ions in an amplified quenching manner ($K_{SV} \sim 10^6 \text{ M}^{-1}$). Also, fluorescence quenching of **PB-Na** was observed with cyanine dye DOTC ($K_{SV} \sim 10^6 \text{ M}^{-1}$) by an energy transfer mechanism. However, treatment with the commonly used electron acceptor MV²⁺ caused little change to the photophysical properties of the CPE. Electrochemical analysis showed that MV²⁺ is not a sufficiently strong oxidant to allow the electron transfer process to occur, presumably due to low LUMO energy level of the novel CPE **PB-Na**. On the other hand, the carboxylic acid form **PB-a** was utilized as sensitizer in DSSC cells with TiO₂. Evidence for electron injection between **PB-a** and TiO₂ was provided by fluorescence lifetime measurements and transient absorption experiments on **PB-a**-TiO₂ films. The low transient absorption signal and inadequate IPCE data suggested that there was insufficient electron injection yield. Possible solutions towards optimization of **PB-a**-TiO₂ DSSCs were pointed out.

Third, in a collaborative project, we conducted a systematic study of functionalized conjugated oligomers with variable band gaps and their interactions with CdSe nanocrystals (NCs). The chromophores-oligo(phenylene ethynylene) (**OPE**),

oligothiophene (**T6**) and donor-acceptor-donor oligothiophenes with a benzothiadiazole acceptor (**T4BTD**) (the latter two synthesized by Romain Stalder from Reynolds group)- were designed with decreasing HOMO-LUMO energy gaps, so that increasing amounts of light could be absorbed toward longer wavelengths up to 600 nm. In this dissertation, the work performed by Schanze group is reviewed in detail. Synthetically, a newly designed route, which is less tedious without compromising the overall yield, was employed to replace the conventional **OPE** synthesis. Photoluminescence quenching studies on both the oligomers and CdSe NCs indicated that charge separation occurred at the interface of the oligomer/NCs, and this photophysical process was assisted by the phosphonic acid groups on the oligomers. Hybrid materials based on the oligomer/ NCs complex were synthesized. The incident photon to current efficiency (IPCE) provided solid evidence for an electron transfer process in the hybrids. Finally, studies on the performance of the oligomers in two different solar cell formats indicated that the oligomers have promising application potential in dye-sensitized solar cells.

CHAPTER 1 INTRODUCTION

Conjugated Polyelectrolytes

Conjugated polyelectrolytes (CPEs) are a class of polymers that contain π -conjugated backbones and ionic side chains.¹ Incorporation of ionic side chains such as carboxylate and sulfonate on the backbones usually enables the polymers, which are otherwise hydrophobic, to dissolve in water and other polar solvents (eg. MeOH). The advantage of this modification is obvious. First, fundamental studies on areas such as charge transport, amplified quenching, and self-assembly benefit from the aqueous solubility of the CPEs. Second, the drastic change in the photophysical properties upon binding to oppositely charged ions gives CPEs great potential for applications in sensing, labeling and other biological studies. Third, solubility in aqueous media allows CPEs to be processed in an environmental-friendly manner.

Since Wudl and co-workers' pioneering work on water soluble polythiophene and poly(phenylene vinylene)s,^{2,3} the field of CPEs has experienced phenomenal growth, leading to development of new polymers with broad applications in optoelectronic devices and bio/chemo sensory materials.⁴⁻¹² Figure 1-1 exhibits some typical CPEs that have been subjects of intensive research. Engineering of CPEs has been active both on the polymer backbones by including different electrochemical properties, and the diverse ionic side groups that add functionalities to the polymers. In this chapter, we will first introduce the syntheses of CPEs, then the self-assembly and photophysical property relations of CPEs will be discussed, and last a few examples of their applications in several areas such as bio/chemo sensors and dye sensitized solar cells (DSSCs) will be described.

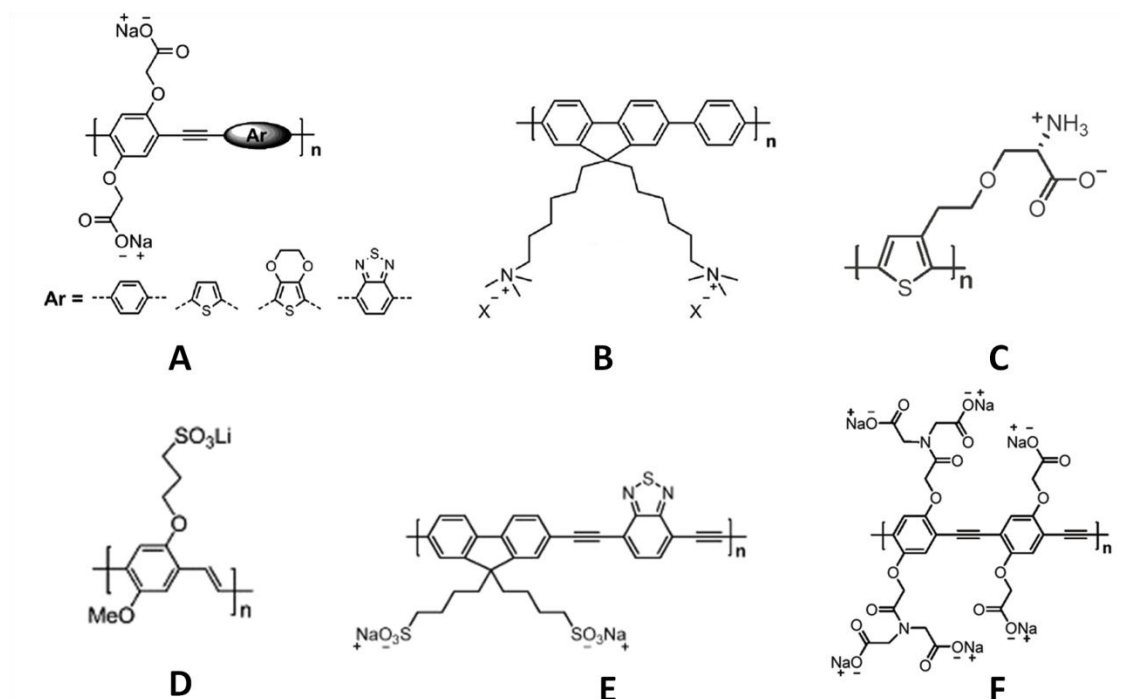


Figure 1-1. Examples of typical CPEs^{10,11,13-16}

Synthesis Approaches

In this section, we briefly review the synthetic methodologies for CPEs, including both “Pd method” and alternative paths.

Pd catalyzed cross-coupling reactions

The facile syntheses of CPEs are largely attributed to the development of transition-metal-catalyzed cross-coupling reactions. Specifically, Palladium-catalyzed carbon-carbon bond formation is one of the most utilized transformations in organic chemistry. The broad substrate scope, tolerance of variable functional groups, and mild reaction conditions associated with the “Palladium method” impart them noticeable importance in organic synthesis. As a matter of fact, the 2010 Nobel Prize in Chemistry was awarded to Heck, Negishi and Suzuki “for palladium-catalyzed cross couplings in organic synthesis”. Table 1-1 presents a summary of some common name reactions that are related to Pd-catalyzed cross-couplings, and the general mechanism for this

type of reaction is illustrated in Figure 1-2. The reactions usually begin with oxidative addition of organic halides (R^2-X) onto the Pd, followed by substitution of the partner substrate R^1 on the same catalytic center via transmetallation. The final step is the formation of the coupling product along with the regeneration of the catalyst by reductive elimination.

Table 1-1. Palladium catalyzed cross-coupling reactions

Reaction	Reagent A		Reagent B		Catalyst
	substrate	hybridization	substrate	hybridization	
Heck	alkene	sp^2	$R-X$	sp^2	Pd
Negishi	$R-Zn-X$	sp, sp^2, sp^3	$R-X$	sp^2, sp^3	Pd or Ni
Suzuki	$R-B(OR)_2$	sp^2	$R-X$	sp^2, sp^3	Pd
Stille	$R-SnR_3$	sp, sp^2, sp^3	$R-X$	sp^2, sp^3	Pd
Sonogashira	$RC\equiv CH$	sp	$R-X$	sp^2, sp^3	Pd and Cu(I)

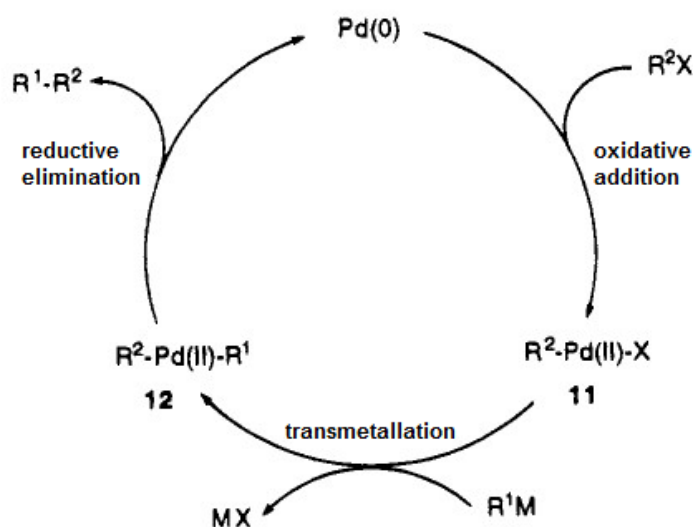
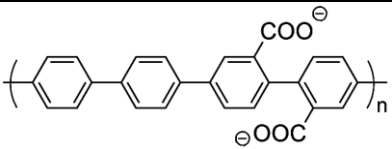
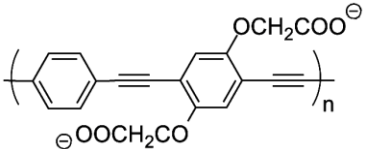
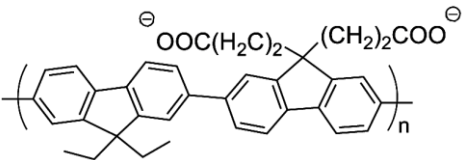
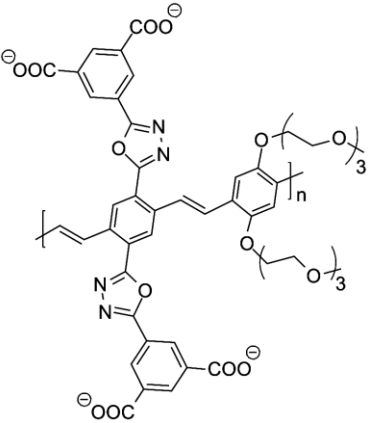


Figure 1-2. A general catalytic cycle for Pd-catalyzed cross-coupling. Figure was reprinted from Suzuki et al.¹⁷

Listed in Table 1-2 is a series of CPEs that have been produced via “Pd-catalyzed cross-coupling reactions”, emphasizing the importance of the Pd chemistry in CPE syntheses.

Table 1-2. Examples of CPEs that were synthesized by Pd-catalyzed cross-coupling reactions

CPE structures	Name/abbreviation	Reaction	Reference
	Poly(<i>para</i> -phenylene) /PPP	Suzuki	18
	Poly(phenylene-ethynylene) /PPE	Sonogashira	14
	Polyfluorene /PF	Suzuki	19
	Poly(phenylenevinylene) /PPV	Heck	20

Other approaches used in CPE synthesis

Admittedly that the Pd-catalyzed cross-coupling reactions are the most utilized means of preparing CPEs, it is necessary to point out that alternative approaches have

been investigated as well. In the synthesis of water soluble polythiophene, Wudl and co-workers employed the so called “electropolymerization” method to construct the backbone of the CPE.² The mechanism of the thiophenes polymerization is illustrated in Figure 1-3. When an electrical potential is applied across a solution containing thiophene and an electrolyte, a thiophene monomer is oxidized to produce a radical cation, which is either coupled with another radical cation to form a dication dimer, or coupled with a monomer to form a radical cation dimer, which is further oxidized to yield the dication dimer. Bithiophene is obtained upon losing two equivalents of protons. This process is repeated before polythiophenes are deposited in the form of polymer films on the anodes.

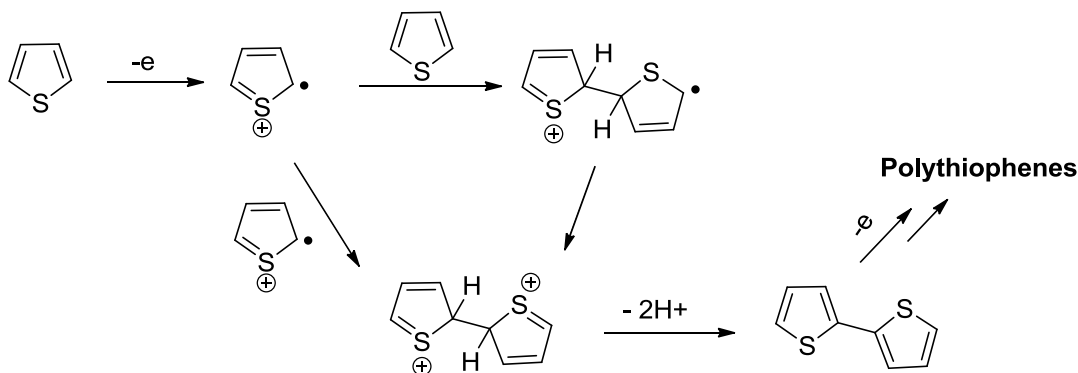


Figure 1-3. Electropolymerization of thiophenes

Another important class of CPEs is poly (phenylenevinylene) (PPV). Table 1-2 shows that the PPV type of CPE can be prepared by the Heck reaction, where divinylbenzenes and diiodobenzenes were coupled via Pd catalysis.²⁰ Nevertheless, the first reported CPE that bear PPV backbone was synthesized via a “Gilch route”,³ as shown in Figure 1-4. In this work, a precursor polymer with sulfonyl chloride side groups was first obtained by anionic or radical addition polymerization before it was hydrolyzed in DMF and water for conversion into a fully conjugated system.

realized via either of two pathways. One approach is direct polymerization of monomers containing ionic side groups that are soluble in water or polar organic solvents.

Alternatively, in “precursor approach”¹, the polymer precursors are first prepared in organic solvents before the protecting groups are removed (usually via hydrolysis) to give rise to the functional ionic side groups. Comparing the two methods, the former is synthetically straightforward, but has drawbacks that it is difficult to obtain precise information on the molecular weight of the CPEs.²¹ The “precursor approach” requires more steps for protection of the ionic groups and removal of the protecting groups, but this method has the advantage of facile purification of the precursor polymers, which can be characterized by gel permeation chromatography (GPC) before they are hydrolyzed to form CPEs. In addition, the completeness of hydrolysis can be monitored by NMR, IR and UV-vis spectra.

Photophysical Properties: Aggregation and Amplified Quenching of CPEs

The applications of CPEs in either sensory materials or optoelectronic devices are closely related to their unique photophysical properties. Fundamentally, the photophysical properties of CPEs are determined by the chemical structures of the conjugated backbones. CPEs bearing the same chromophores in the backbones should show similar absorption and photoluminescence spectra. Figure 1-5 gives a typical example for PPE type of CPEs containing chromophores with variable band gaps. Both absorption and fluorescence spectra of the CPEs were drastically red shifted as lower band gap chromophore was incorporated.²² Another factor that can have a major effect on CPE photophysical behavior is the tendency to form secondary structures in aqueous or polar organic solvents, due to the amphiphilic nature of CPEs (hydrophobic backbone and hydrophilic side groups). The formation of the aggregates in many cases

significantly changes the photophysical properties of the CPEs. Examples will be shown in the following discussions.

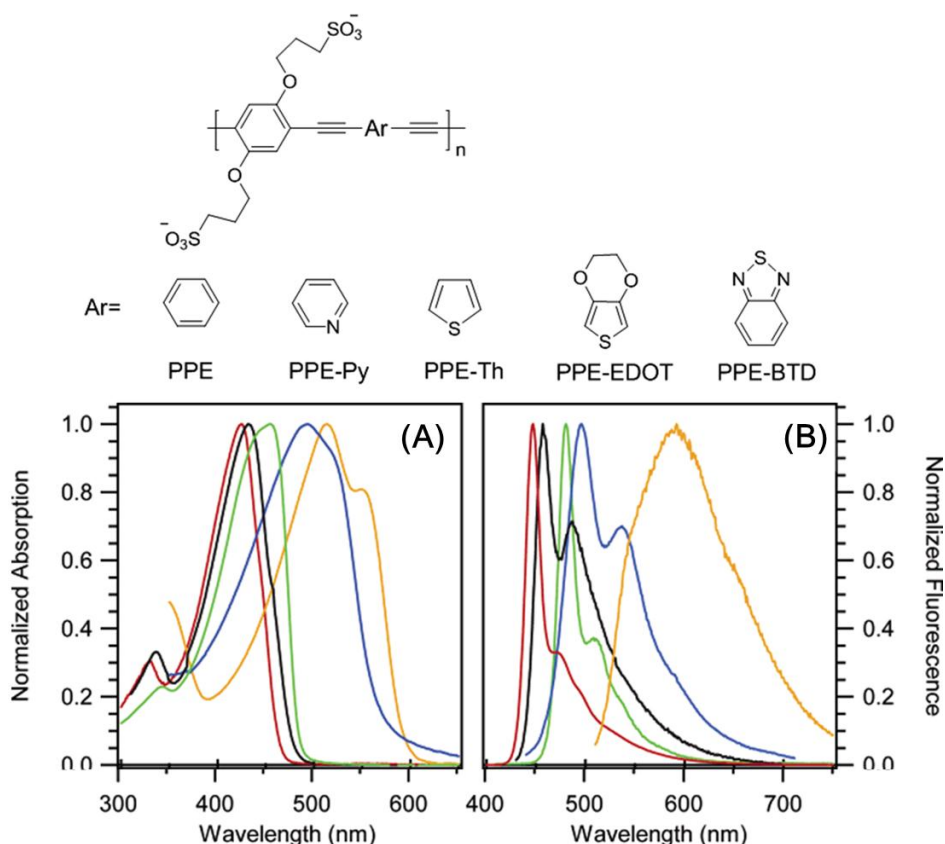


Figure 1-5. Photophysics of CPEs with variable bandgaps. A) Normalized absorption and B) fluorescence of PPE (red), PPE-Py (black), PPE-Th (green), PPE-EDOT (blue), and PPE-BTD (yellow) in methanol solution. Figure was reprinted with permission from Schanze et al.²²

Aggregation and self-assembly

It is not possible to discuss the photophysical properties of CPEs without mentioning the aggregation and self-assembling of the CPEs under specific solution conditions. As described above, due to their amphiphilic nature CPEs have a tendency to aggregate in aqueous solution or polar organic solvents, and the aggregation process usually induces significant changes in both the absorption and fluorescence spectra.^{21,23-25} Taking the poly (arylene-ethynylene) type of CPEs as an example, the CPEs with anionic side groups such as sulfonate (SO_3^-) or carboxylate (CO_2^-) exist as

molecularly dissolved chains in methanol, but when the solvent is changed to water, the CPEs aggregate.^{21,24} The formation of aggregates is reflected by photophysical changes which usually include a red-shift in the absorption and fluorescence spectra, a decrease in the fluorescence quantum yield, and an increase in the fluorescence lifetime.

While the formation of CPE aggregates is largely dependent on the nature of the solvent, other factors can induce aggregation in CPE systems. For example, when a divalent cation, such as Ca^{2+} is added to the methanol solution of anionic PPE type of CPEs bearing carboxylate side groups **PPE-CO₂⁻**, aggregates form,²³ and as a result, the spectral changes mimicking the effect of adding water to the CPE solutions are observed. It is believed that Ca^{2+} induces aggregation of the CPE by cross-linking **PPE-CO₂⁻** chains while complexing with the carboxylate side groups of the polymer.

More direct evidence of the inducing aggregation was observed in a study of analyte-directed polymer aggregation.²⁶ In this clever design, a series of α, ω -diamines varying successively by only one methylene unit separating the amines were allowed to interact with polythiophenes with carboxylate side groups. Not only did the diamines induce the aggregation of the polythiophenes, but the extent of communication between polymer chains was controlled by the degree of flexibility of the tether between the two amines.²⁶ Illustrated in Figure 1-6 is a schematic representation of how the different diamines affected the aggregative interactions with polymer 1, giving rise to different absorption spectra. Similarly, when CPEs with cationic side groups were treated with an anionic dicarboxylate analyte,²⁷ the formation of aggregation was dependent on the length of the tethers between carboxylates. When short-tethered oxalic acid was added,

“tight aggregates” (Figure 1-6, path A) formed, and by contrast “loose aggregates” (Figure 1-6, path C) resulted from the addition of long-tethered glutaric acid.

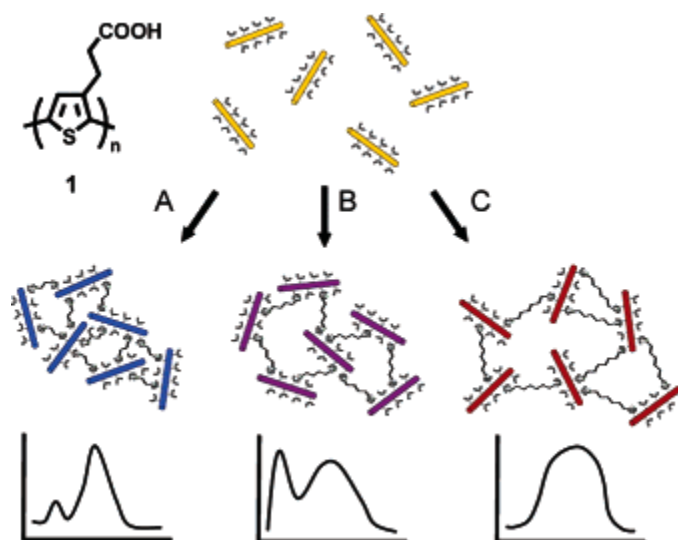


Figure 1-6. Schematic representation of the aggregative interactions between polymer 1 (colored rods) and different diamine analytes (A-C). Different colored aggregates are formed depending on the added diamines. Figure was taken from John Lavigne et al.²⁶

Many other factors that are related to aggregate formation of CPEs have been investigated. For example, CPEs substituted with weakly ionized polyelectrolyte groups, such as phosphonate (PO_3^{2-}), aggregate in water at neutral pH, but the aggregates disperse when the pH increases above 8.²⁵ In addition, factors such as concentration, temperature, solution ionic strength, and added surfactant, have also been carefully studied.²⁸

Furthermore, studies of CPE aggregation have not been limited to the formation of the aggregates and the resulting photophysical property changes. Additional efforts have been made to understand the conformations of the secondary structures of the CPEs and to explore their applications. One typical example is the *meta*-linked PPE (*m*-PPE) system. Initiated by Moore and co-workers,²⁹ several studies were reported on

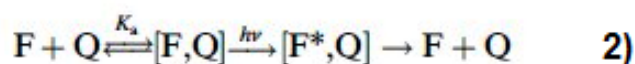
investigations of *m*-PPE polyelectrolytes.³⁰⁻³² Direct evidence for the helical conformation was afforded by the negative chirality in the bisignate CD spectrum exhibited by the polymer in solution.³¹ The helical structure was found to serve as a host supermolecule to bind with planar guests in an intercalation manner. Based on this property, the helical CPE was used as template for the formation of supramolecular helical aggregates of cyanine dyes.

It is also necessary to point out that, although there have been extensive investigations on aggregates of CPEs, there is no “general rule” to follow for predicting the status of aggregation for a given CPE structure. Thus, studies of aggregation of CPEs are still case dependent. For example, in many cases MeOH is a good solvent for CPEs where they exist as monomeric states and H₂O on the other side is a “poor” solvent. However, exceptions were also seen in literature where a mixture of MeOH and H₂O solvates the CPE optimally.^{19,33}

Amplified photoluminescence quenching

Fluorescence quenching of CPE is one of the most popular research topics in this field from both the fundamental and application viewpoints.¹ Fluorescence quenching occurs by two limiting mechanisms,³⁴ namely dynamic quenching and static quenching. The quenching processes are depicted in Figure 1-7. Dynamic quenching, also known as collisional quenching, occurs when the excited fluorophore experiences contact with a quencher that can facilitate non-radiative transitions to the ground state (Figure 1-7, equation 1). Static quenching, by contrast, involves formation of a stable non-emissive complex between the fluorophore and quencher (Figure 1-7, equation 2). Treatment of fluorescence-intensity quenching data by the standard Stern–Volmer method yields equation 3), where I_0 and I are the fluorescence intensities in the absence and presence

of Q, respectively, and K_{SV} is the Stern–Volmer quenching constant. According to equation 3), the Stern–Volmer plot of I_0/I versus quencher concentration is expected to be linear. However, in many situations with quencher–CPE systems, the Stern–Volmer plots are curved upward (i.e., superlinear). Many factors could be responsible for this observation, such as variation in the association constant with quencher concentration, mixed static and dynamic quenching, and CPE aggregation.



$$I_0/I = 1 + K_{sv}[Q] \quad 3)$$

Figure 1-7. Equations of Photoluminescence Quenching. F^* is an excited-state chromophore, Q is a quencher, k_q is the bimolecular quenching rate constant, and K_a is the association constant for formation of the ground-state complex $[F, Q]$. Equations were taken from Lakowicz.³⁴

The concept of “amplified quenching” was first described by Swager and co-workers in 1995.³⁵ In that work the authors reported the fluorescence quenching of PPE polymers bearing cyclophane receptors on the repeat units. Methylviologen (MV^{2+}) was chosen as the quencher for its ability to associate with the cyclophanes. Interestingly, the quenching effect was much more pronounced for the polymers compared to that of monomeric model compound. Furthermore, the Stern- Volmer quenching constant K_{SV} increased with polymer chain length. To rationalize the observation, the authors proposed a theory involving the delocalization and migration of excitons along the polymer chain, called the “molecular-wire effect”. Figure 1-8 indicates the mechanism of the molecular-wire effect. When an exciton is generated, the polymer chain acts as a conduit that allows the exciton to migrate rapidly along the chain. Within its lifetime, the

exciton is quenched once it reaches the repeat unit with a quencher-attached acceptor. Given the efficient exciton migration along the polymer chain, one quencher molecule binding to the acceptor can cause quenching of the excitons that are generated many other places, leading to the amplified quenching response of the polymer to the quencher.

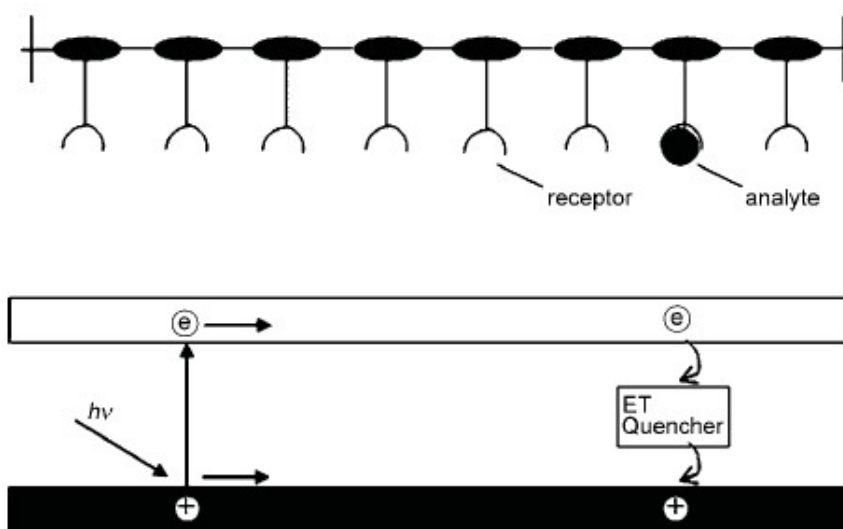


Figure 1-8. “Molecular-wire effect” in conjugated polymers with receptors. Figure was taken from Swager et al.³⁵

The study of amplified quenching effect in CPE systems was initiated by Whitten and co-workers with their investigation of fluorescence quenching of PPV-type CPE by MV^{2+} .¹⁰ It was found in this study that in aqueous solution, the PPV is quenched by MV^{2+} with an extremely large K_{SV} value ($\sim 10^7 \text{ M}^{-1}$). While presumably the “molecular wire effect” contributed to the amplified quenching, the authors also proposed that the aggregation of CPE further enhanced amplified quenching by facilitating exciton hopping between polymers chains.¹⁰ More direct studies of aggregation-amplified quenching relations were conducted by Schanze and co-workers. As previously reviewed, Ca^{2+} ions induce aggregation of PPE polyelectrolytes. More importantly, the

fluorescence quenching response to MV^{2+} was found to have a positive correlation with the concentration of Ca^{2+} .²³ In other words, the amplified quenching effect is more pronounced in the systems with more aggregation, underlying the contribution of aggregation to the exciton hopping between polymer chains.

To conclude, amplified photoluminescence quenching of CPEs arises from the rapid exciton migration either along a single polymer chain or between different chains. This unique property of CPE paves its way to many ultra-sensitive sensory applications.

Application of CPEs as Functional Materials

The applications of CPEs have widely expanded into many fields such as bio/chemo sensory materials,^{1,36,37} polymer light-emitting diodes,³⁸⁻⁴² photovoltaic devices,⁴³ cell imaging^{44,45} and biocidal materials.^{46,47} Space limitations make it impossible to review all the works related to the CPE applications. Instead, this dissertation will use a few examples to elucidate the property-application relation of the CPEs.

Bio/chemo sensory materials

CPEs are ideal materials for bio/chemo sensors for several reasons. 1) They are generally fluorescent. This basic photophysical nature of CPEs makes it possible to detect target molecules/ions from the change of photoluminescence. 2) They usually have considerable solubility in aqueous solutions. This feature largely broadens the applications of CPEs as sensory materials since water is the most commonly applied medium for many molecules/ions of biological importance. 3) They bear ionic functional groups on their side chains. Besides enhancing solubilities, the ionic groups provide substantial affinity between CPEs and the targets through electrostatic⁶ or/and coordinating⁴⁸ interactions. 4) The amplified quenching properties. As described above, exciton delocalization and transport within/between the polymer chains lead to an

amplified quenching effect, which allows the fluorescence of CPEs to be quenched at very low quencher concentrations. When applied to sensory materials, this property affords the CPEs substantially high sensitivity and low detection limits for analyte detection.

Depending on how the sensor systems are designed, there are two separate modes, “turn off” and “turn on” for the fluorescent-based CPEs to respond to the target molecules. In the “turn off” mode, the fluorescence of CPEs is quenched by the added analyte. Generally, the analytes quench via energy/charge transfer,⁴⁹ or/and by inducing a change in the physical state of the CPE (aggregation and conformation).⁴⁸ By contrast, in the “turn on” mode, the addition of analytes recovers the fluorescence of CPE. Specifically, the CPEs first interact with quenchers to form non-fluorescent CPE-Quencher (C-Q) complexes. When analytes are introduced to the system, the quencher molecules redistribute between the CPEs and analytes, and thus the fluorescence of CPEs is “turned on” by the analytes.

Illustrated in Figures 1-9 and 1-10 are two CPE-sensor examples based on “turn-off” and “turn-on” modes, respectively. In 2003, Heeger and co-workers reported that cationic polyfluorene (PF) was quenched with extraordinarily high efficiency by gold nanoparticles ($K_{SV} \sim 8.3 \times 10^{10} \text{ M}^{-1}$) in water (Figure 1-9).⁴⁹ In this work, a series of gold nanoparticles were treated with tertiary amine-functionalized PF. The quenching response was significantly reduced in solutions of high ionic strength, indicating that the PF interacted with gold nanoparticles via electrostatic attractions. Nanoparticles with diameters of 5, 10, and 20 nm, which all absorbed strongly in the region of polymer emission, produced similar quenching response. However, the smaller gold

nanoparticles (2 nm in diameter) showed approximately 10^4 lower quenching efficiency, due to poor overlap of the absorption spectra of 2 nm nanoparticles with the PF fluorescence. Based on this observation, the authors concluded that resonance energy transfer was the dominant quenching mechanism. On the other hand, the monomeric model compound oligofluorene was 10 times less sensitive to the addition of nanoparticles, clearly indicating that exciton migration along the polymer backbones contributed to the amplified quenching. This work demonstrated that strong electrostatic nanoparticle-polymer complexation, long-distance energy-transfer quenching and conjugated polymer-based excitation mobilization are all critical factors in the amplified quenching effects, which are fundamental to the design of sensor materials.

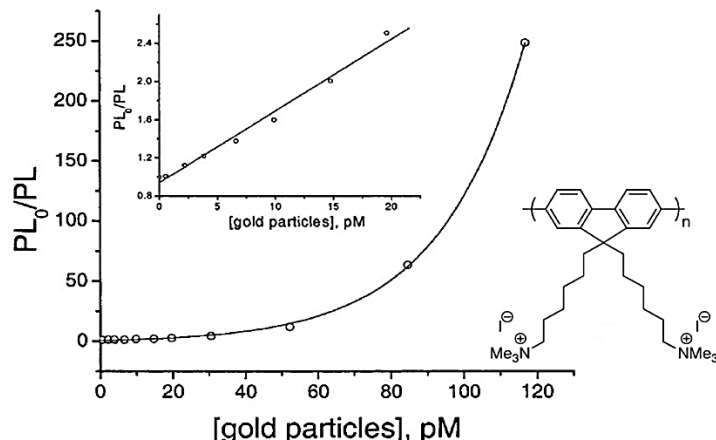


Figure 1-9. Stern–Volmer plots of polyfluorene quenched by 5-nm gold nanoparticles. Figure was taken from Heeger et al.⁴⁹

A “turn-on” sensory system is portrayed in Figure 1-10. This so called “quencher-tether-ligand” strategy for detection of avidin was introduced by Whitten and co-workers in 1999.¹⁰ The authors designed a biotin functionalized viologen quencher that quenched the fluorescence of the PPV type of CPE in aqueous solution. The biotin functionality on the quencher was able to bind with avidin, so when avidin was added to the system, the avidin-bound quencher was prevented to be associated with CPEs due

to enhanced spatial hinderance, resulting in the recovery of the CPE fluorescence. A control experiment was conducted to investigate the role of the “quencher-tether-ligand” in CPE fluorescence recovery. Avidin alone did not modulate the intensity of the CPE fluorescence, and the CPE quenched by methyl viologen quencher (which has no affinity to avidin) showed no fluorescence recovery upon avidin addition. All the evidence pointed to the conclusion that the “turn-on” response of the CPE was due to the specific biotin-avidin interaction. This pioneering work triggered a tremendous amount of research interest in CPE-based biosensing materials.

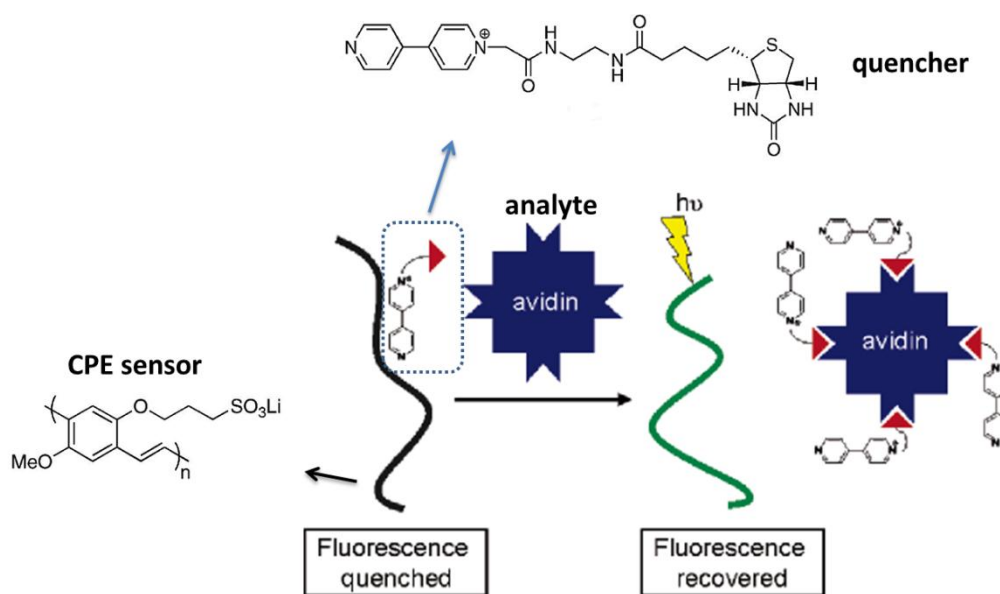


Figure 1-10. A “turn on” fluorescence sensor for avidin. Figure was reprinted with permission from Whitten¹⁰ and Swager et al.³⁶

Dye-sensitized solar cells

The dye-sensitized solar cell (DSSC) is one of the major inventions towards utilizing solar energy. Since they were introduced by Gratzel in 1991⁵⁰, DSSCs have evoked increasing research interest both from the fundamental viewpoints and exploration of the commercialization opportunities.⁵¹ Compared to the traditional solid-state solar cells, the advantages of this photovoltaic device format include the use of

relatively inexpensive materials and the possibility that mechanically flexible modules can be deployed on a large scale for low overall cost.^{50,52} A schematic presentation of the operating mechanism of the DSSCs⁵² is illustrated in Figure 1-11. On the top of a thin film of fluorine-doped tin oxide glass plate, a mesoporous layer of TiO₂ is placed. A monolayer of dye (sensitizer) is adsorbed to the surface of the nanocrystalline film. Excitons are generated when the dye is irradiated with photons, and electrons are injected to the conduction band of the semiconductor from the dye's excited state. The sensitizer is restored to its ground state by electron donation from the mediator, usually a redox couple such as iodide/triiodide. The reducing species is then regenerated by reduction of the oxidizing species at the electrode. Overall, the cell converts light to electric power without chemical transformation.

To date, great success has been achieved on DSSCs with transition metal complex-based sensitizers. A few specific metal (eg. Ru, Pt and Zn) complex sensitizers exhibit broad absorption throughout the UV-vis and near-IR regions with high (> 85%) incident photon to current efficiency (IPCE). With careful engineering, these devices achieve up to 13% power conversion efficiency (PCE).^{53,54} In addition, metal-free small molecule dyes as alternatives also have attracted attention with the concerns that the source of transition metals is limited.⁵⁵ Moderate PCEs (6-9%) have been reported for these devices.^{55,56}

Conjugated polyelectrolytes are also important sensitizers utilized in DSSCs.^{14,57-59} Motivation to apply CPEs as sensitizers in DSSC comes from their capacity to offer effective light-harvesting efficiency due to large absorption coefficients and tunable optical band gaps.²² Most recently, donor-acceptor approach was employed to engineer

the energy levels of the CPE so that high light-harvesting efficiency and charge injection efficiency was realized.^{60,61} Several research cases conducted in the Schanze group will be discussed here to illustrate the CPE-based DSSCs.

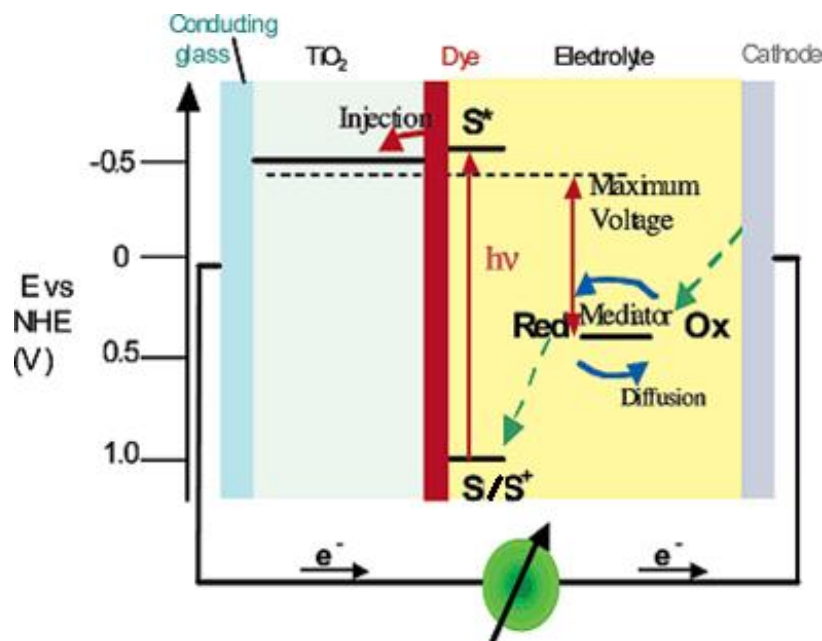


Figure 1-11. Principle of operation of DSSCs. Figure was taken from Gratzel et al.⁵²

In 2006, Schanze, Reynolds and co-workers demonstrated the concept of “spectral broadening” by using a dual-CPE sensitizer in a TiO_2 DSSC format.¹⁴ As shown in Figure 1-12, the authors combined poly(phenylene ethynylene) (PPE) and polythiophene (PT) types of CPEs in one cell, and the performance of the hybrid cell was compared to the individual cells based on one CPE. Transient absorption studies indicated that the electron injection from each CPE to TiO_2 was favored, and the photocurrent and PCE obtained for the dual-CPE cell were the sum of the corresponding responses from each individual CPE.

As part of their ongoing interest in constructing low bandgap CPE sensitizers, Schanze et al. reported a series of poly(arylene-ethynylene) CPEs with carboxylic acid

side groups (Figure 1-13).⁵⁸ The HOMO-LUMO gap of the CPEs varied with absorption maxima ranging from 400 nm to 500 nm. The CPEs were assembled with TiO₂ films and the cell performances were tested under AM1.5 illumination. The photocurrent and PCE increased in the order PPE < TH-PPE < EDOT-PPE, indicating that the lower bandgap CPE is able to accomplish more efficient solar energy conversion. Interestingly, the IPCE and PCE for the BTD-PPE (Figure 1-13), which bears the longest absorption wavelength, were substantially less than those for the other CPEs. The authors attributed this decrease in efficiency to exciton trapping in polymer aggregates. In other words, instead of injecting into TiO₂, the excitons were hopping in the CPE aggregates far from the CPE/TiO₂ interfaces. This argument emphasized the importance of subtle changes in device morphology on performance of the solar cells.

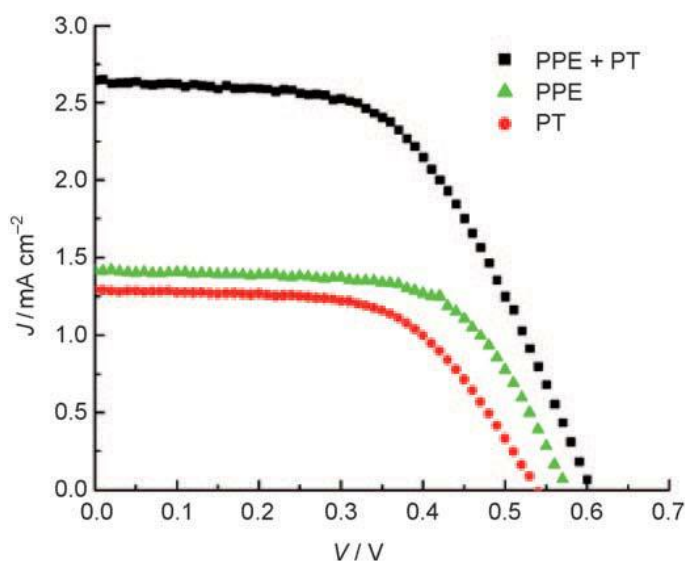


Figure 1-12. J–V characteristics under AM1.5 conditions for solar cells sensitized with PPE, PT, and PPE/PT mixture. Figure was taken from Schanze et al.¹⁴

Recently, the Schanze group used the donor-acceptor approach to achieve low bandgap CPE sensitizers for DSSCs.⁶¹ In this work, electron-poor 1,2,3-benzothiadiazole (BTD) was incorporated with electron donor terthiophene segment to

yield a polymer exhibiting an absorption onset at 625 nm corresponding to a ~ 1.9 eV bandgap. The polymers were modified with carboxylic acid groups which were able to attach to the TiO_2 surface. The CPE turned out to be a promising candidate for DSSC sensitizer by offering $\sim 3\%$ PCE. The best result was $\sim 65\%$ peak IPCE with $J_{sc} \sim 12.6 \text{ mA cm}^{-2}$ under AM1.5 illumination, which is the record for CPE based DSSCs.

Furthermore, the authors also investigated the relationship between the CPE molecular weight and the cell performance. It was observed in this study that CPEs with lower molecular weight (~ 4 kD) yield better cell performance than those with higher molecular weight (~ 10 kD), and the difference was believed to come from the different extent of adsorption of the dyes on the TiO_2 . The shorter CPE chains are able to access a greater fraction of the TiO_2 surface for adsorption due to effective penetration into smaller pores, leading to the observed greater surface coverage. By contrast, the longer chains are excluded from a substantial fraction of the surface and thus are not able to give rise to as much surface coverage.⁶¹

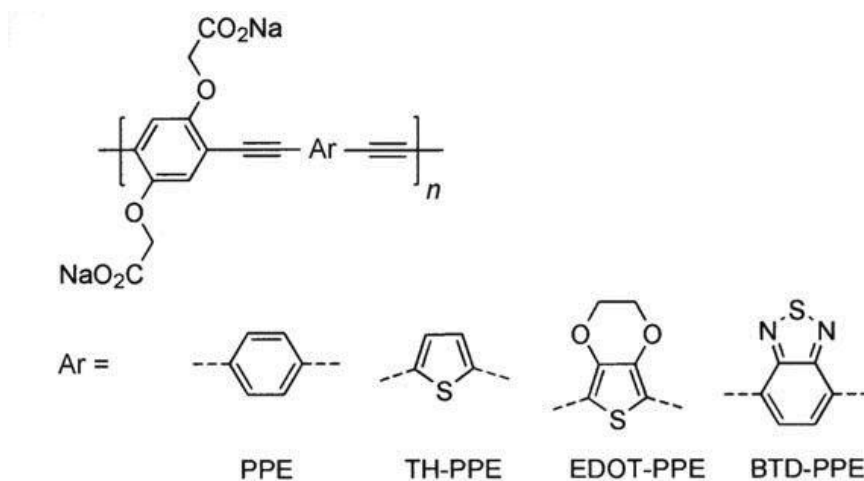


Figure 1-13. Structures of the repeat units for variable-gap PPE-based CPEs used in TiO_2 -sensitized photovoltaic devices. Figure was taken from Schanze et al.⁵⁸

Summary for CPEs

In this section, we reviewed the synthesis, photophysical properties and applications of conjugated polyelectrolytes.

Synthetically, the CPEs are readily accessible thanks to the development of transition metal-catalyzed organic reactions, albeit other synthetic methodologies also share the credit for the vast variety of CPEs bearing different properties.

The photophysical properties of the CPEs are dependent on several factors. 1) Conjugated backbones allow excitons to delocalize and migrate, which is the inherent character of CPE. 2) The amphiphilic nature of CPE chains gives rise to aggregation and self-assembly properties in water or polar organic solvents, thereby producing dramatic changes in the photophysical properties.

The application of CPEs in highly sensitive bio/chemo sensors directly results from their amplified quenching capability. Based on how the sensory systems are designed, both fluorescence “turn off” and “turn on” of the CPEs could be used as signs to detect the presence of analytes.

The application of CPEs in DSSCs was also reviewed. Examples were discussed to show the importance of engineering the bandgaps of CPEs in these photovoltaic devices. Additionally, it is also critical to optimize the morphology and structures on the nanometer scale for optimum device performance.

Conjugated Polymer/Oligomer-Semiconductor Nanocrystal Hybrid Materials

The study of conjugated polymer/oligomer and inorganic semiconductor nanocrystals (NCs) had little overlap until early 1990s.⁶² The investigation into the interfaces between the two types of functional materials with different chemistry was fueled by Alivisatos and co-workers' early works on optoelectronic devices based on

poly(phenylene vinylene) (PPV)/CdSe NCs hybrids⁶³ and polythiophene (PT)/CdSe NCs hybrids.⁶⁴ It was found in these works that a combination of two conventional materials would give rise to novel properties that are unmatched by their components. To date, several research areas such as light emitting diodes, photodiodes, and photovoltaic cells have witnessed the promising applications of these hybrid materials.⁶⁵⁻⁷⁶ In this review, the materials will be organized to elucidate three aspects regarding the hybrid materials. First, the synthetic strategies of the hybrids are categorized into two classes. Second, the means of characterizing the physical process at the interface of the hybrids are to be introduced. Third, a few examples will be exhibited to illustrate the application of the hybrids in the optoelectronic devices.

Synthetic Strategies

The syntheses of hybrids are generally in the order of “obtaining the core inorganic NCs” and “incorporating with organic semiconductors to yield the hybrids”. The preparations of inorganic NCs have been reviewed by a number of recent articles in details.⁷⁷⁻⁷⁹ Concerning the scope of this dissertation, we are not going into this topic any further.

Depending on how the inorganic NCs are incorporated with organic semiconductors, the synthetic strategies can be categorized into two classes, namely the “graft to” and “graft from” methods. In the “graft to” mode, the organic oligomer/polymers are synthesized before they are mixed with NCs, while in the “graft from” mode, the precursors of one component are first modified on the other complete components, and then the precursors are allowed to grow with more building blocks into a new phase. Details are exhibited to compare the two methodologies.

“Graft to” method

The “graft to” method involves syntheses of each component prior to mixing them together. The construction of conjugated polymer/oligomer backbones are similar to those of CPEs (as reviewed in the first section), which largely benefit from the development of Pd-catalyzed cross coupling reactions.

The simplest form of hybrid material using the “graft to” method is a composite directly resulting from blending inorganic NCs with unfunctionalized polymers/oligomers.⁶⁴ However, simple casting from a common solvent leads to hybrid films with phase separation of the components on a micrometer scale.⁸⁰ This phenomenon is originated from the tendency of the inherent ligands on the surface of NCs to pack upon removal of solvents,^{81,82} a major impediment for interaction between organic SCs and inorganic NCs.

Modifying the conjugated polymer/oligomer with anchoring groups that are capable of binding to the NC surface is a solution towards monodispersity of the hybrid materials.⁶⁸ Upon mixing, the anchoring group functionalized macromolecules undergo a so-called “ligand exchange process” with the inherent ligands, such as trioctylphosphine oxide (TOPO) and oleic acid, at the NC surfaces. The driving force for ligand exchange is that anchoring groups usually have a larger affinity to the NCs, or that anchoring groups are in relatively higher concentrations. To date, a series of anchoring groups has been reported which include phosphine oxide,^{75,76} thiol groups,^{83,84} carbodithioic acid,^{85,86} carboxylic acid,⁸⁷⁻⁸⁹ phosphonic acid,^{67,90} amines,⁶⁸ and anilines.⁷³ These anchoring groups attach to the NC surfaces via covalent bonds. Nonetheless, interaction between conjugated polymers/oligomers and inorganic NCs is not limited to the covalent bonding. The molecular recognition approach via hydrogen

bonding, for example, has been utilized to connect the NCs with conjugated polymers.⁹¹ In a work reported by Pron and co-workers, regioregular poly(3-hexylthiophene-2,5-diyl) (P3HT) that bears diaminopyrimidine (DAP) side groups are able to molecular recognize 1-(6-mercaptohexyl) thymine (MHT) capped CdSe NCs via three hydrogen bonds (depicted in Figure 1-14), and as a result, hybrid film with uniform distribution of the NCs in the polymer matrix is achieved.

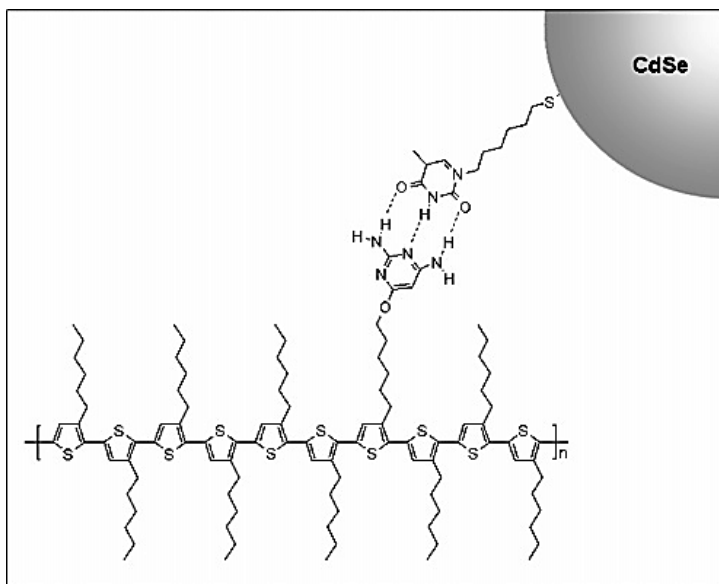


Figure 1-14. Schematic presentation of molecular recognition between MHT functionalized CdSe NCs and DAP modified P3HT. Figure was taken from Pron et al.⁹¹

Regarding the pattern of how the polymers/oligomers are attached to the NCs, there are mainly five circumstances. Figure 1-15 shows a schematic presentation of the five different routes through which the hybrids are synthesized.

For oligomers or polymers with low molecular weight, the anchoring groups can reach the NC surface either as terminal or side functionalities (Figure 1-15, routes 1 and 2).⁶⁷ For higher molecular mass polymers, the terminal anchoring groups are less available for binding to the NCs due to the fact that the ratio of the end groups to the polymer chain length decreases (Figure 1-15, route 4). In this case direct ligand

exchange process is harder to realize. Frechet and co-workers addressed this problem by applying a two-step procedure. First, pyridine was used to replace the initial ligands on CdSe NCs, and then the temporary pyridine ligands were exchanged with the polymer functional groups.⁶⁸ By contrast, introducing the anchoring functionalities as side groups is more favorable for the NC connection (Figure 1-15, route 5). For example, Reiss and co-workers synthesized polythiophenes that are side-functionalized with carbodithioic groups. These polymers are attached to the CdSe surfaces under relatively mild conditions.⁸⁶ Finally, dendritic oligomer/polymer has also been reported to incorporate with NCs (Figure 1-15, route 3). For example, Advincula and co-workers demonstrated the connection between CdSe NCs and dendritic polythiophenes containing phosphonic acid groups.⁹⁰

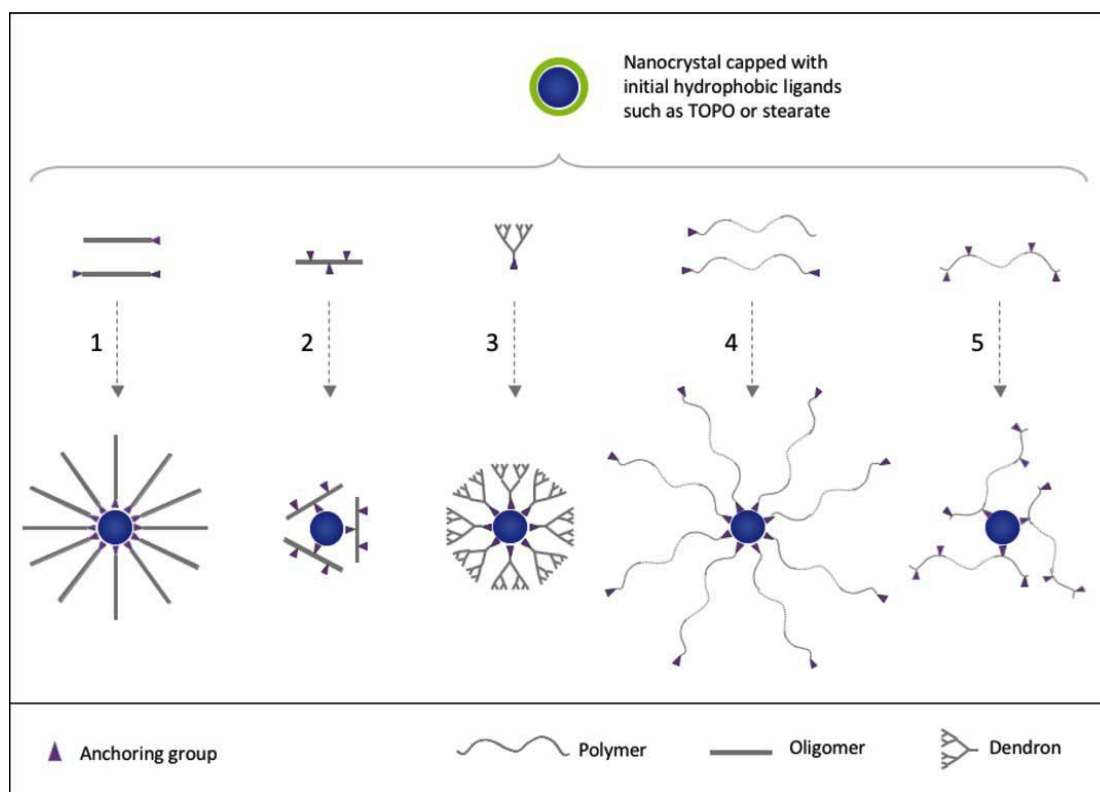


Figure 1-15. Schematic presentations of different routes the oligomers/polymers are attached to the NC surfaces. Figure taken from Pron et al.⁶²

In all, functionalized oligomers/polymers have been proven to attach to the NC surfaces in different patterns via either covalent or other specific interactions between anchoring groups on the oligomers/polymers and inorganic NCs. Such design helps to diminish the phase separation, and thus facilitates the communication between different components at molecular level. Better device performances based on the hybrids are expected.

“Graft from” method

The “graft from” method is another way to obtaining intimate blends of NCs and conjugated polymers. This method is, so to speak, to grow one component on the other. Both means that “grafting polymer from NCs” and “grafting NCs from polymers” have been used to synthesize hybrid nanocomposites.^{69,75,92}

Grafting polymer from NCs. This strategy was first introduced by Emrick and co-workers.⁶⁹ In that work, the authors first synthesized a bromide functionalized surfactant DOPO-Br (compound 1, Figure 1-16) which mimics the role of TOPO (which caps with CdSe since its nucleation and growth process). After the surfactant was modified on the CdSe NCs, a PPV shell was allowed to grow *in-situ* on the surface of CdSe by copolymerizing 1,4-divinylbenzene and 1,4-dibromobenzene derivatives (Figure 1-16). The advantage of this method is that it reduces the preparation steps of hybrid materials since no “ligand exchange” is needed. However, compared to the “graft to” method, it is inevitable for this approach to weaken the control of the hybrids dispersity, due to the fact that the chain lengths of the polymers on the CdSe NCs are varying. Based on this argument, the “graft from” strategy is not quite helpful to the well-defined oligomer/NC systems.

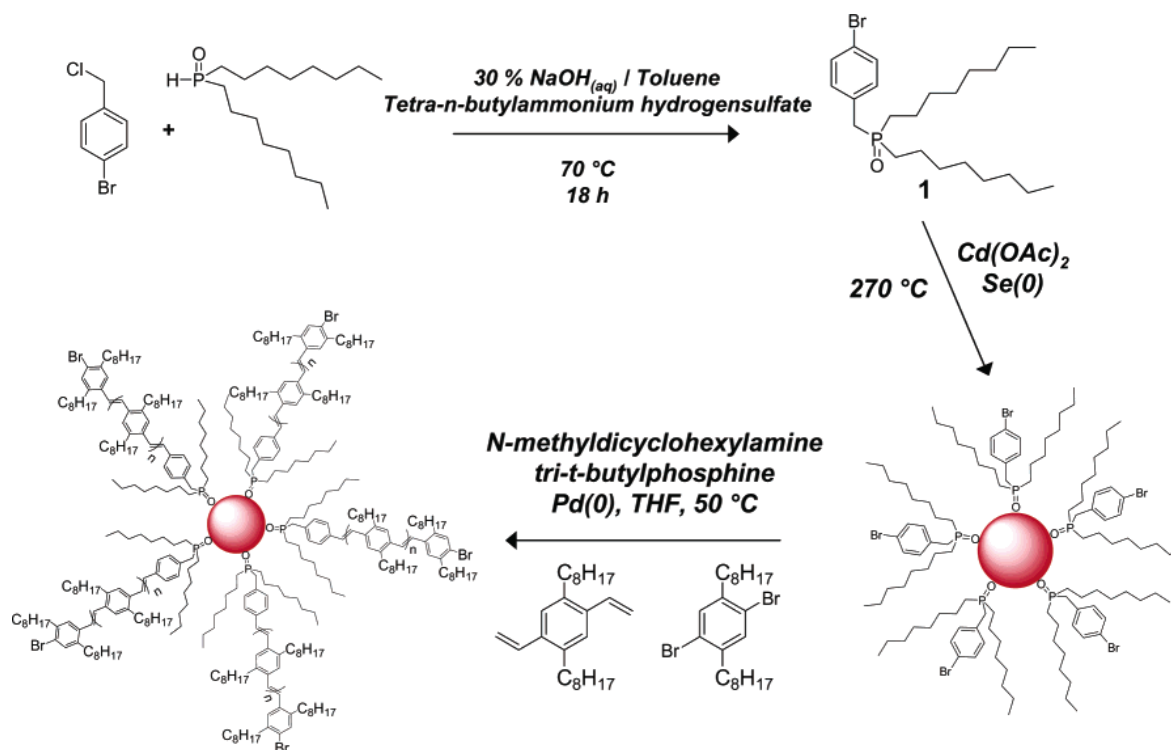


Figure 1-16. “Graft from” synthetic scheme for PPV/CdSe hybrids. Figure was taken from Emrick et al.⁶⁹

Grafting NCs from polymer. This method is to *in-situ* grow NCs in the polymer matrix. By coordinating with the NC precursors, the polymers can not only form uniform hybrids with the NCs, but also act as templates to control the shape of the NCs. This method was employed by Liu and co-workers to synthesize a P3HT/CdS hybrid system.⁹² Specifically, the authors used the sulfur atoms in the polythiophenes as the coordinating site for Cd²⁺ cations. As CdS NCs nucleated and grew, the backbone of the polythiophene oriented the NCs to form the nano-rod shaped crystals (Figure 1-17). The as-prepared hybrids were applied to the solar cells, and promising power conversion efficiency (~3%) was reported.

In a separate research, Zhou and co-workers prepared a PT and zinc methacrylate based copolymer by means of atom-transfer radical polymerization (ATRP). Subsequent hydrolysis of zinc methacrylate groups gave rise to a hybrid

nanocomposite based on the PT/ZnO. Photoluminescence quenching of PT was observed, which provided evidence for efficient interaction between the two components.⁹³

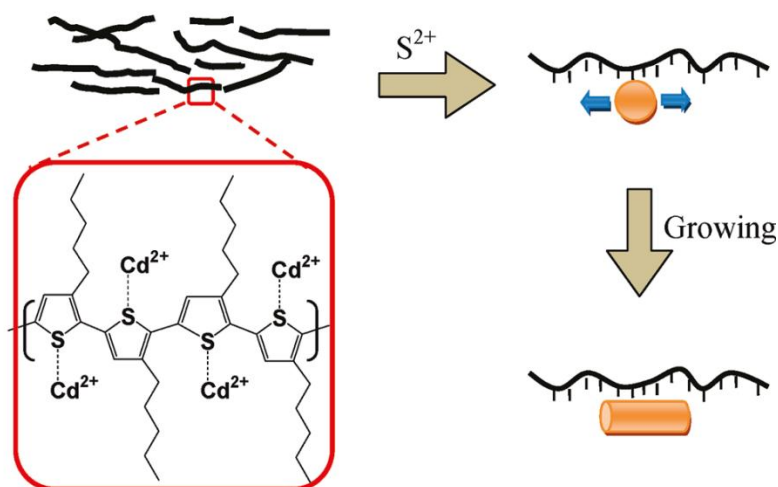


Figure 1-17. *In situ* synthesis of CdS nanorods template by P3HT. Figure was taken from Liu et al.⁹²

Characterization-Interfaces of the Hybrids

Many techniques have been employed to analyze the properties of hybrids for the reason that they are relatively complex systems and the numbers of parameters are large.⁶² The characterization can be generally sorted into two categories: compositional analysis and photophysical/electrochemical analysis. In this review, several most used characterizations of the hybrids will be discussed by exhibiting research cases.

Compositional analysis

When a hybrid system is prepared, it is necessary to decipher the stoichiometry, distribution, and morphology of each component, and the nature of interaction at the components interface.

First, FTIR spectroscopy usually provides qualitative information on establishment of communication between the conjugated oligomers/polymers and the inorganic NCs.

Comparing the IR spectra of the NCs before and after the “ligand exchange” process unveils replacement of the initial ligands by anchoring groups from the oligomers/polymers given that the initial and latter ligands have separable diagnostic signals.⁸⁹

Second, NMR spectroscopy also provides evidence for success of anchoring from oligomers/polymers to NCs. For example, in Frechet and co-workers’ report on oligothiophene/CdSe NCs hybrids,⁶⁷ the ¹H NMR of the hybrid’s colloidal solutions and the free oligothiophene ligands were registered (Figure 1-18). Compared to the free oligothiophene ligands, the lines of aromatic region ¹H NMR for the hybrids were broadened and shifted. The authors attributed this phenomenon to the limited molecular mobility of the molecules coordinated to the NC surfaces. Other works also use NMR as a semi-quantitative approach to estimate the ligands’ relative ratios.^{94,95}

Third, elemental analysis is another technique to determine the composition of the hybrids. It is especially helpful in cases where a specific element is present in the anchoring groups and absent in the initial ligands, or *vice versa*.

Forth, thermogravimetric analysis (TGA) can provide information of the mass ratios of organic and inorganic component. Generally, the organic species should have much less tolerance to high temperature than the inorganic ones, thus the relative mass percentage of the organic component can be readily accessible at the plateau where the ligands are fully decomposed while the inorganic NCs remain intact.

Fifth, the most direct image of the hybrid materials can be exhibited by electron and atomic force microscopy (EM and AFM, respectively). Taking advantage of these techniques, one can “see” the shape, size and dispersion of the hybrid materials on

nanometer scale. Figure 1-19 shows an example of a morphology study of P3HT/CdSe NCs conducted by Frechet and co-workers.⁶⁸ In this work, the authors synthesized two types of P3HT polymers, one with amine anchoring groups and the other without. The polymers were blended with CdSe NCs to make hybrid films. Using transmission electron microscopy (TEM), it was shown unambiguously that the films with functionalized P3HT polymers had a much more uniform dispersity than those with unfunctionalized P3HT polymers. Accordingly, the hybrid film with better dispersity offered better device performance when solar cells were assembled.

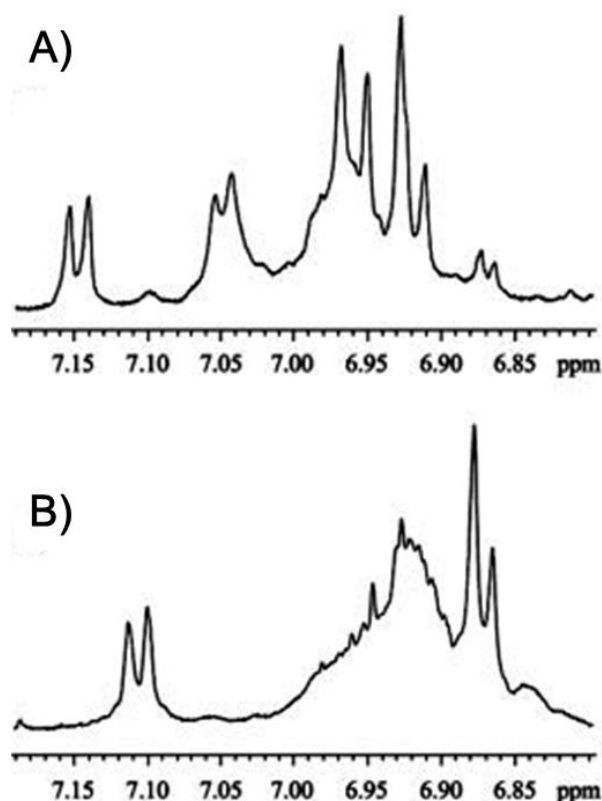


Figure 1-18. ¹H NMR broadening as free oligothiophenes bind to CdSe NCs. A) ¹H NMR of free oligothiophene. B) ¹H NMR of oligothiophene/CdSe hybrids. Figure was taken from Frechet et al.⁶⁷

Finally, it is necessary to point out that the above methods are usually applied in a combining manner so that the most accurate compositional information of hybrid materials can be obtained.

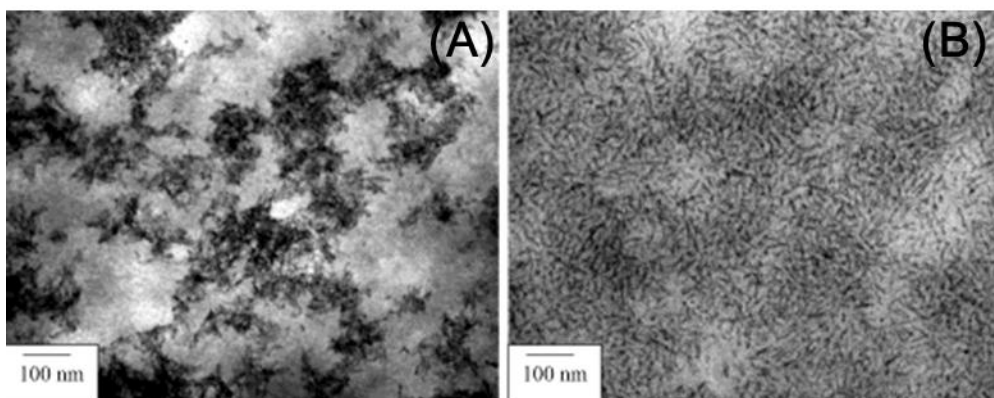


Figure 1-19. TEM characterizations of the hybrid films. A) image of unfunctionalized P3HT/CdSe (wt% 40%) film and B) functionalized P3HT/CdSe (wt% 40%) film. Figure was taken from Frechet et al.⁶⁸

Photophysical and electrochemical analysis

The applications of the conjugated oligomer/polymer and semiconductor NC hybrids in electronic devices are solely dependent on their photophysical and electrochemical properties. These properties are determined by the electrochemical/photochemical nature of the corresponding parental components. For example, in a photovoltaic device with conjugated polymers as donors and CdSe NCs as acceptors, the energy levels of the species should be staggered (as depicted in Figure 1-20) for the photo-induced electrons/holes to move to the electrodes for electric currents generation. So before hybrid materials are synthesized and applied to devices, it is necessary to conduct clear characterization on the individual components and carefully design the combination of the two. In this review, we selectively discuss the characterizations that are applied in our researches (Chapter 4), and more complete

introductions on the methods characterizing hybrid materials can be found in Pron's recent review article.⁶²

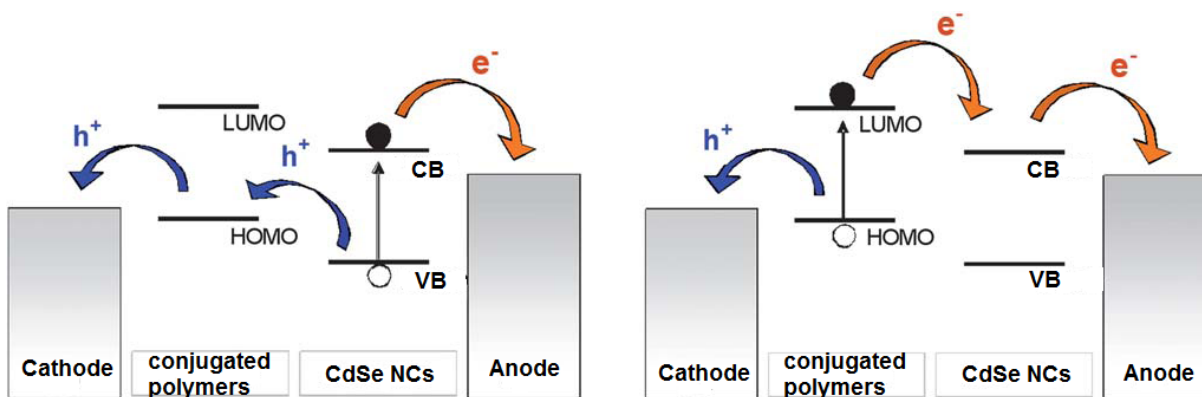


Figure 1-20. Energy level alignment in a conjugated polymer (donor)/CdSe NC (acceptor) hybrid film facilitating charge separations.

UV-vis absorption and cyclic voltammetry (CV) study. The energy levels of the conjugated oligomers/polymers and inorganic NCs can be determined by UV-vis absorption spectroscopy and electrochemical analysis. The onset of the UV-vis spectra deciphers the HOMO-LUMO energy difference of the study system. However, in this spectrum, the absolute position of the energy levels is not accessible. Detailed information is given by electrochemical studies. In CV measurement, the HOMO and LUMO positions can be estimated by measure of the onset of the oxidation and reduction wave onsets, respectively. In the systems that require higher sensitivity and resolution, differential-pulse-voltammetry (DPV) can be applied.⁹⁶ Generally, the HOMO-LUMO energy difference from electrochemical studies agrees with that is calculated from optically measured one, albeit exceptions do exist where the lowest-energy optical transition does not reflect the HOMO-LUMO transition. A typical example is given by donor-acceptor type of polymers where the HOMO and the LUMO orbitals are located on different moieties.⁹⁷

Photoluminescence quenching studies. Most conjugated oligomers/polymers and inorganic semiconductor NCs are photoluminescent. Depending on the energy levels of the components, charge or/and energy transfer process can happen when attached together.^{67,98} One direct indication for these physical processes to happen is photoluminescence quenching. For example, an early work conducted by Frechet and co-workers used photoluminescence quenching as an indicator to deduct the physical process occurring at the interface of oligothiophenes and CdSe NCs.⁶⁷ In this work, terthiophene (T3) and pentathiophene (T5) that contained phosphonic acid groups as anchoring groups were allowed to interact with CdSe NCs in solution. Both fluorescence of T3 and T5 were quenched upon addition of CdSe, but when the fluorescence of the CdSe was studied, the CdSe NC fluorescence increased after complexing with T3, while it decrease with T5. From these observations, a plausible proposal of the energy level alignment between the species was proposed (Figure 1-21).

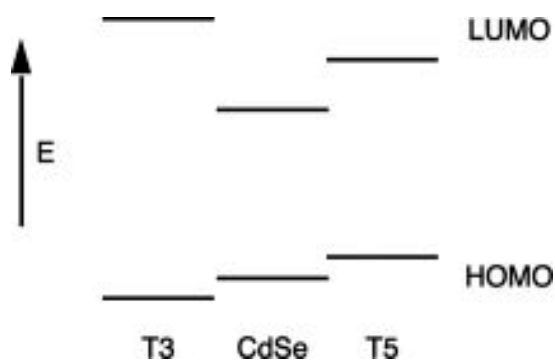


Figure 1-21. Schematic presentation of the proposed energy level alignment in CdSe-oligothiophene complexes.⁶⁷

The Hybrids' Applications in Solar Cells

The application of the conjugated oligomer/polymer- inorganic NCs in solar cells is originated from Alivisatos and co-workers' work on unfunctionalized PPV⁹⁹ and PT⁶⁴ polymers with CdSe NCs. Although the early record was fairly low, they did arouse a

great deal of research interest on this solar cell format. Optimizing the device performance involve engineering both conjugated polymers and semiconductor NCs.

As the aspect of polymer engineering, Frechet and co-workers demonstrated the role of functionality (the “anchoring groups”) on the polythiophenes in optimizing the morphology of the resulting hybrid films. The more uniform hybrid films turned out to exhibit higher power conversion efficiency.⁶⁸ Besides increasing affinity to semiconductor NCs, fine-tuning the energy levels of the polymers towards harvesting more solar energy has been pursued consistently. Recently, Dayal and co-workers applied a low-bandgap thiophene benzothiadiazole base copolymer in the CdSe NC hybrid films, and a efficiency ~3% was achieved.¹⁰⁰

Regarding the optimization of NCs, works have been focused on tailoring the shape of the NCs. The morphology of the inorganic component is important because the inorganic component is the main contributor to charge transport in the hybrid cells (the charge mobility for conjugated polymers is usually low¹⁰¹). For example, rod-shaped CdSe NCs were incorporated with P3HT and improved the power conversion efficiency compared to the devices based on spherical CdSe NCs,⁶⁴ which was attributed to the fact that rod-shaped NCs facilitates charge transport better than spherical ones. However, as the nanorods become longer, improvement in device performance is limited, since the increasing charge transport characteristics are trade-off with decreasing solubility of NCs in the processing solution, which give rise to phase separation. In another work, tetra-pod shaped CdSe NCs and PPV hybrids offered an efficiency close to 3%.¹⁰² Finally, it should be mentioned that the engineering on NC

shapes were initiated from the synthetic work by Peng et al., who first introduced the concept of shape anisotropy to inorganic NCs.¹⁰³

To sum up, the application of conjugated polymer/semiconductor NC hybrids in solar cells are widely investigated. Abundant improvement has been achieved from both the organic molecular design and the inorganic NC engineering aspects. And of course, the state-of-art hybrid cells are yet to be developed.

Summary for Polymer/Oligomer-Semiconductor Nanoparticle Hybrids

In this section, we provided an overview of synthesis, characterization, and application of a class of hybrid materials based on conjugated polymer/oligomer and inorganic semiconductor NCs.

First, synthetically, the development of the hybrid materials involves both engineering conjugated polymers/oligomers and inorganic semiconductors. The construction of conjugated polymer/oligomer backbone is similar to that for conjugated polyelectrolytes (described in the previous section), which are fueled by the transition metal-catalyzed cross-coupling reactions. The synthetic method of inorganic NCs was not reviewed in this dissertation. Regarding incorporating the two components, there are two methods to consider. The “graft to” method is to obtain both components prior to mixing them together, while the “graft from” method involves modifying the precursor of one component on the prepared other species, followed by *in-situ* growing of the precursors. Compared to “graft from” approach, the “graft to” approach requires more steps synthetically, but it keeps the advantage of the capability to offer well-defined oligomer-NC hybrids.

Second, the hybrid materials are usually complicated systems. Characterization of the materials includes compositional analysis and electrochemical/photophysical

analysis. In the compositional analysis, the stoichiometry, distribution, and morphology of each component and the nature of interaction at the component interfaces are deciphered. While in the electrochemical/photophysical analysis, the energy level alignment of the organic and inorganic phase and the physical process in terms of the components interactions are determined, which are the basis of their practical application in electronic devices.

Finally, the application of the hybrid materials in solar cells was discussed. A few examples were shown to elucidate the effects of engineering both conjugated polymers and inorganic NCs.

CHAPTER 2

AGGREGATION INDUCED AMPLIFIED QUENCHING IN CONJUGATED POLYELECTROLYTES WITH INTERRUPTED CONJUGATION

Conjugated Polyelectrolytes

Conjugated polyelectrolytes (CPEs) are a class of polymers that contain π -conjugated backbones and ionic side chains.¹ Since Wudl and co-workers' pioneering work on water soluble polythiophene and poly(phenylene vinylene)s,^{2,3} the field of CPEs has experienced phenomenal growth leading to development of new polymers that have broad applications in optoelectronic devices and bio/chemo sensory materials.^{4-10,12,104} Specifically, the strong fluorescence of poly(phenylene ethynylene) (PPE) based CPEs coupled with their high quenching response to biomolecules and metal ions have attracted significant research interest in their photophysical properties both from fundamental and application viewpoints.^{1,5,7,105-107}

Studies have shown that CPEs self-assemble into a variety of supramolecular architectures in aqueous solution.^{1,21,30,108,109} In addition, it has been demonstrated that the photophysical properties of CPEs are very sensitive to the solvent environment.^{1,21} For instance, CPEs form π -stacked aggregates in water²⁴ and divalent cations²³ induce aggregation in polar organic solvents which results in a dramatic change in the photophysical properties of the CPEs.¹¹⁰

Another property that is characteristic of CPEs is amplified quenching.^{10,21,24,35} The fluorescence of CPEs is efficiently quenched by low concentration of oppositely charged quencher ions. This amplified quenching is attributed to delocalization and migration of the excitons along the polymer backbone which is often referred to as the "molecular wire effect".¹¹¹ Evidence shows that aggregation of CPEs further enhances the amplified

quenching effect by enabling exciton transport between polymer chains.²⁴ In the case where a meta-linked poly(phenylene ethylene) with sulfonate side chains (m-PPESO₃) was studied, the fluorescence quenching behavior indicated that the quenching efficiency for aggregates present in the helical conformation of the polymer was higher than for the random coil conformation,³⁰ once again demonstrating the role of inter-chain exciton transfer. It is with such properties like efficient fluorescence and amplified quenching that the applications of the CPEs to ultra-sensitive chemo-/bio- sensors were developed.

Now that the amplified quenching effect has been well established in CPE systems, we consider the question: Is amplified quenching limited to fully conjugated polyelectrolytes, or can it also occur in systems that are not fully π -conjugated? We note that previous studies have explored this concept. In particular, Whitten and coworkers synthesized a series of poly(L-lysines) with varying chain length that contained cationic cyanine dye units on every repeat.¹¹² These polymers exhibited amplified quenching to an extent that varied with the poly(lysine) chain length, and they attributed it to J-aggregate formation and exciton transport among the pendant cyanine dyes. In a separate study, Heeger, Bazan and co-workers reported amplified quenching in supramolecular aggregates formed from a sulfonate substituted (phenylene vinylene) oligomer.¹¹³ In the present chapter we describe an investigation of two anionic polyelectrolytes that contain discrete oligo(phenylene ethynylene) chromophore units that are tethered into linear chains by weakly or non-conjugated linker groups. These “interrupted conjugation” CPEs exhibit distinctly different amplified quenching behavior,

and we find that the difference is closely related to the ability of the chromophores to self-assemble into fluorescent aggregates.

Results and Discussion

Synthesis and Structural Characterization

The chemical structures of the CPEs investigated are shown in Figure 2-1. These polymers feature chromophores consisting of three ring phenylene ethynylene segments functionalized with two propylene sulfonate side groups. The units are linked into a polymeric array via a $-(CH_2)-$ or $-O-$ link (**C-PPE** and **O-PPE**, respectively). Both polymers were synthesized by Sonogashira coupling and characterized by 1H NMR spectroscopy.

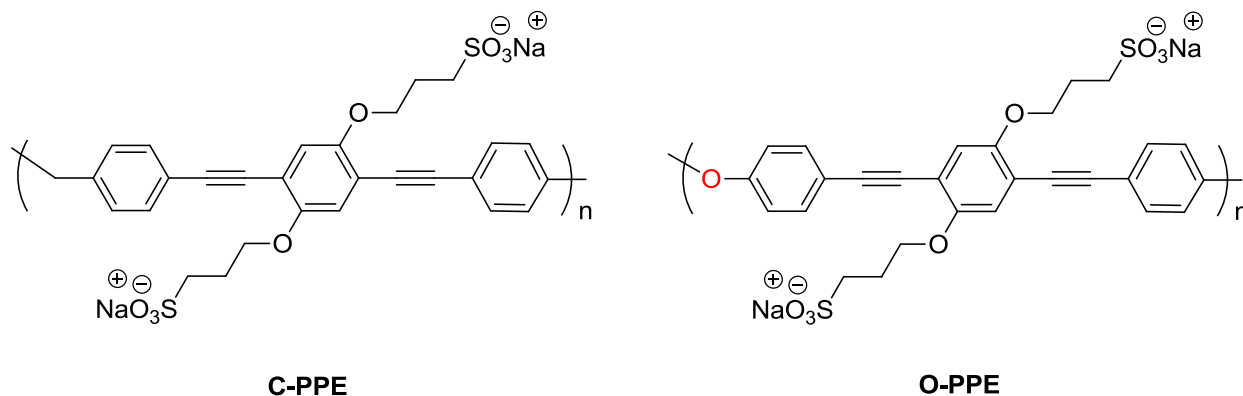


Figure 2-1. Structures of **C-PPE** and **O-PPE**

The syntheses of the two CPEs are presented in Figure 2-2. First, the starting material diphenylmethane or diphenyl ether was iodinated at para-position relative to the linkers. The reaction condition for diphenyl ether was milder compared to that for diphenylmethane, presumably due to stronger electron donating ability of “O” linker than that of “CH₂” linker. Second, the iodine was transformed into trimethylsilyl (TMS) protected alkynes via Sonogashira coupling in high yield, and removal of TMS group by Na₂CO₃ in methanol/ dichloromethane solution provided monomer **5** or **6**. Third, the

monomer **7** was synthesized following a reported procedure²¹. Finally, the polymerization of the monomers was carried out in H₂O/DMF mixed solvent at 70°C via Sonogashira coupling. Precipitation and dialysis were conducted to purify the polymers.

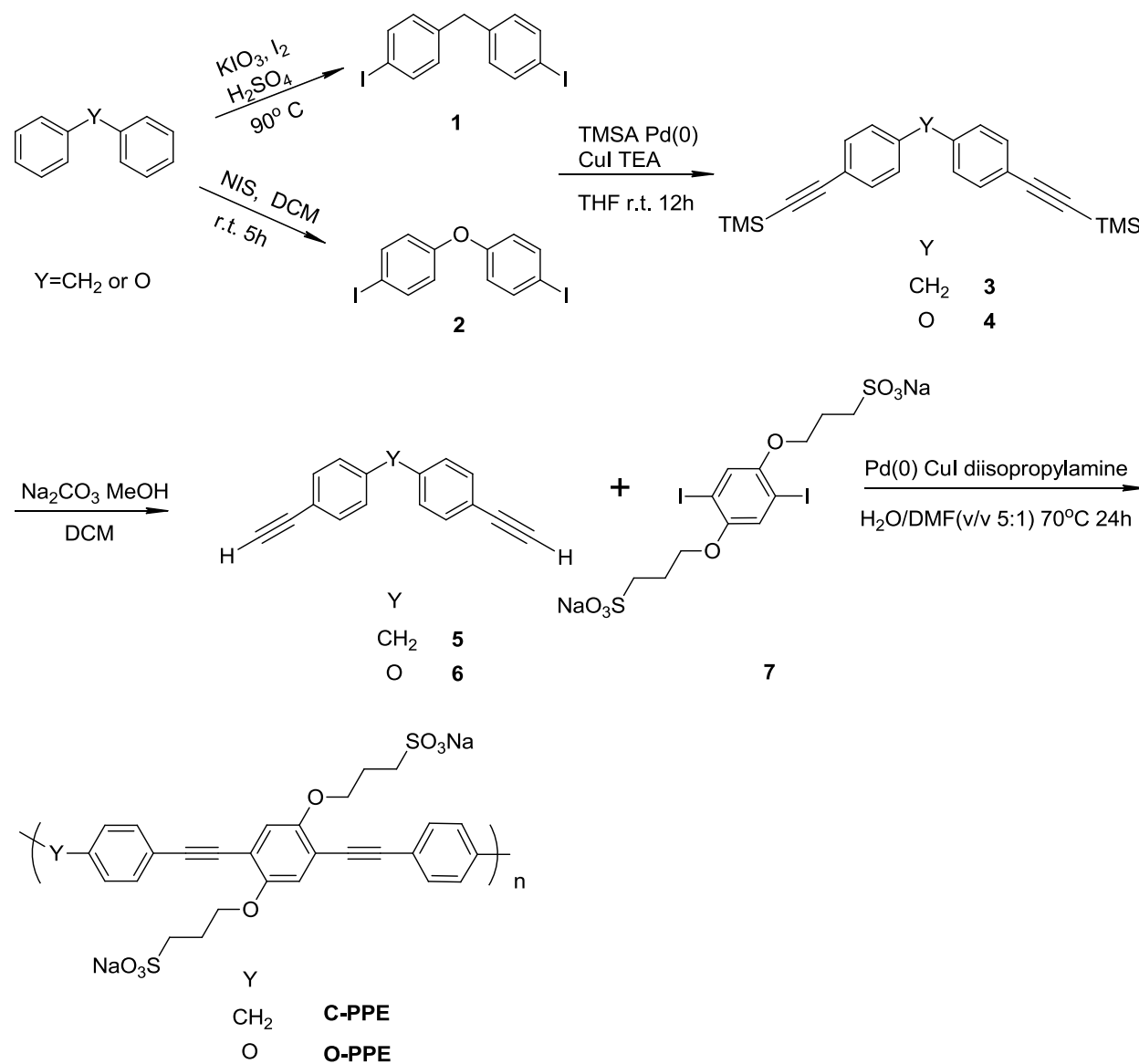


Figure 2-2. Synthetic scheme of **C-PPE** and **O-PPE**

After purification, the ¹H NMR spectra of **C-PPE** and **O-PPE** were recorded in DMSO-*d*₆, which are shown in Figure 2-3. All peaks are clearly assigned, indicating purity of the samples.

The purified CPEs were stored in “stock solutions” at 0°C under dark in DI water (Millipore Nanopure™) with pH 8.5, and the concentrations were ca. 1 mg/ml. The stock solutions were diluted for spectroscopy studies.

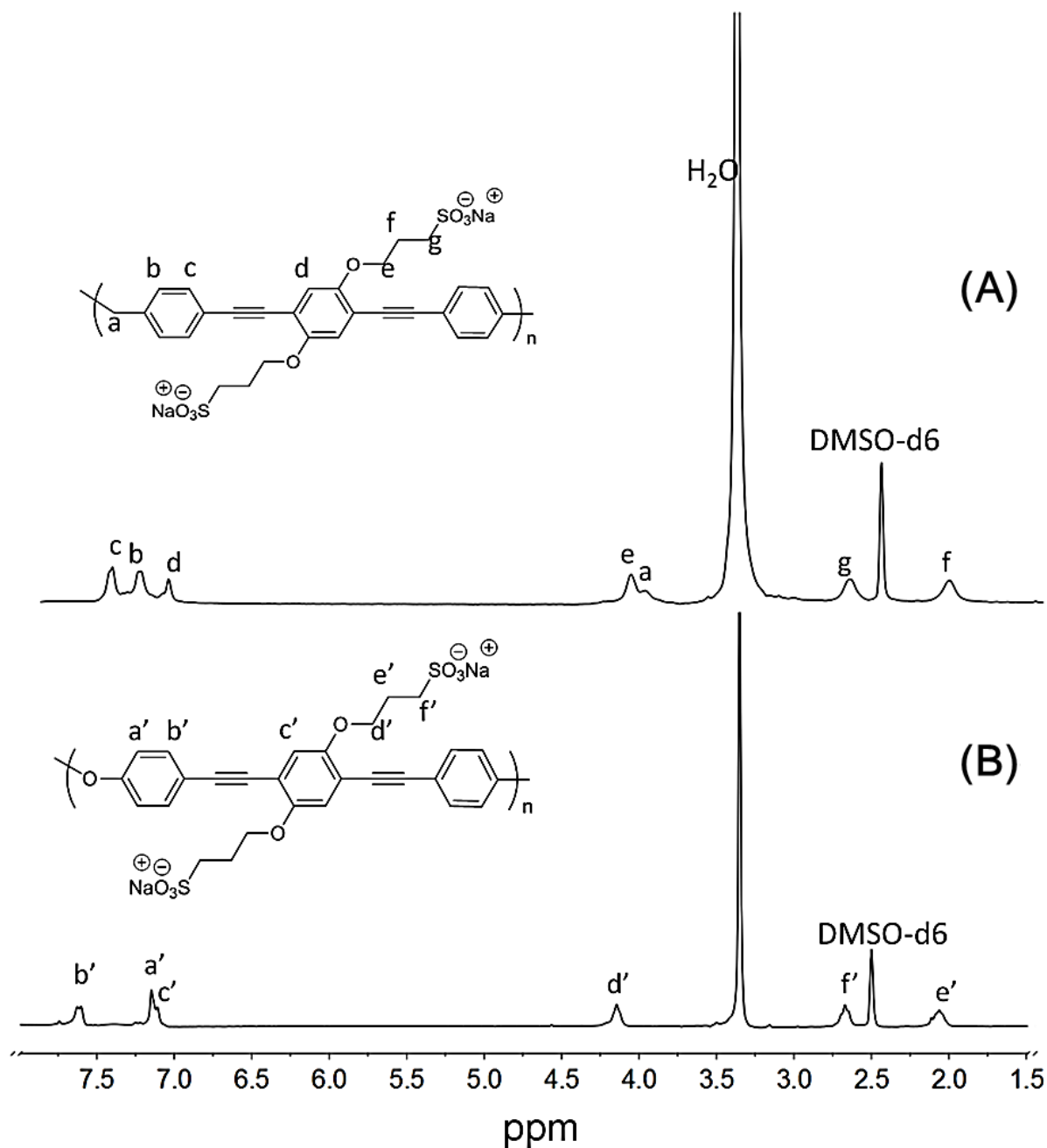


Figure 2-3. ^1H NMR and peak assignment for A) **C-PPE** and B) **O-PPE**.

Photophysics

The absorption and fluorescence spectra of **C-PPE** and **O-PPE** in methanol are shown in Figure 2-4. Methanol is typically considered to be a “good solvent” for CPEs as aggregation is minimal in this solvent.²¹ The absorption spectra of the polymers show a very similar pattern; their band maxima are in the near UV region, which is typical for 3-ring OPEs,¹¹⁴ indicating the two chromophores are very similar. The shorter wavelength for the absorption maximum in **C-PPE** and **O-PPE** in comparison to fully conjugated PPE-type polymer is attributed to the interruption of conjugation enforced due to the presence of the “CH₂” or “O” linkers. While the absorption spectra are very similar, the fluorescence spectra of **C-PPE** and **O-PPE** exhibit an interesting difference. The fluorescence emission of **C-PPE** and **O-PPE** show a similar structured band at short wavelength ($\lambda \sim 400$ nm); however, in addition to showing a well resolved 0-0 band at short wavelength, **O-PPE** exhibits a second broad band at longer wavelength ($\lambda \sim 450$ -500 nm) suggesting the formation of emissive aggregates in pure methanol.^{21,24} Such aggregate emission is not observed for **C-PPE** in methanol.

More insight into the influence of solvent environment on the aggregation of the polymers comes from the solvent dependence of fluorescence. To understand the role of solvent medium on the aggregation behavior of **C-PPE** and **O-PPE**, their fluorescence was investigated in a mixture of methanol and water by systematically varying the solvent ratio (Figure 2-5).

As the volume percent of water increases in the medium, the fluorescence of **C-PPE** decreases significantly in intensity; however, no clear evidence for a separate aggregate emission at longer wavelength can be seen (Figure 2-5a). By contrast, **O-**

PPE exhibits complex behavior as the solvent composition is changed. Importantly, it is obvious from the dual emission of **O-PPE** (i.e., the appearance two emission bands, Figure 2-5b, black solid line) that it forms aggregates in pure MeOH. Interestingly, as the fraction of water is increased to 20%, the aggregate band almost disappears, and the monomer emission intensity increases significantly (5 - fold increase). With further increase in the volume percent of water in the medium, the monomer fluorescence gradually disappears and is replaced by the aggregate emission at longer wavelength. The 80% methanol-water mixture appears to be the best solvent as the least polymer aggregation is seen in this mixture. Similarly, methanol is an intermediate solvent and water could be considered as a poor solvent as **O-PPE** is present in an entirely aggregated state in this medium. Similar solvent-dependent aggregation behavior has been observed for other CPE systems.^{1,19} Table 2-1 consolidates the photophysical data of **C-PPE** and **O-PPE** in H₂O and MeOH.

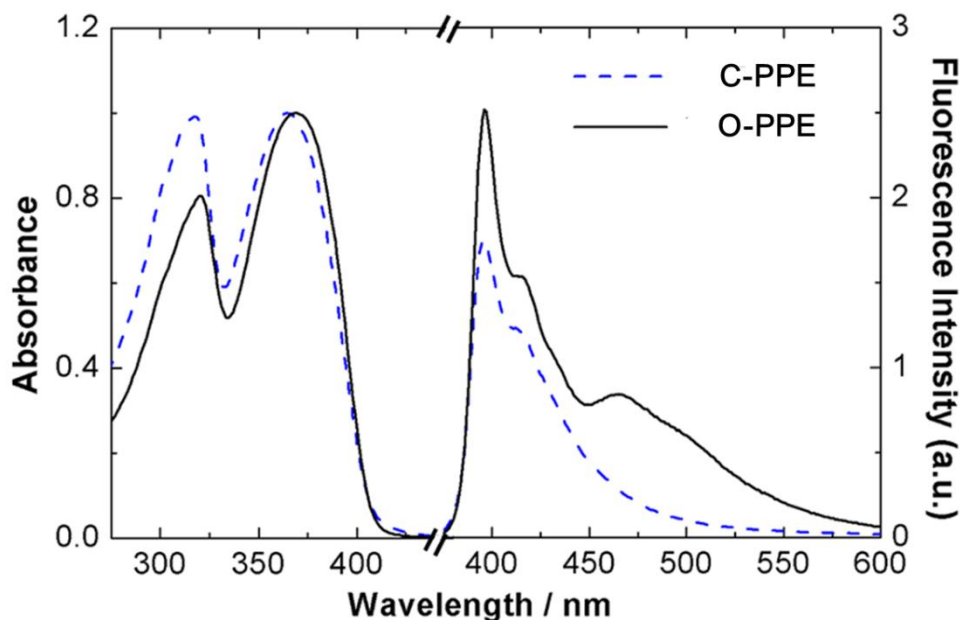


Figure 2-4. Absorption and fluorescence spectra of **C-PPE** (dashed) and **O-PPE** (solid) in MeOH. Fluorescence spectra are area normalized to reflect relative quantum yields.

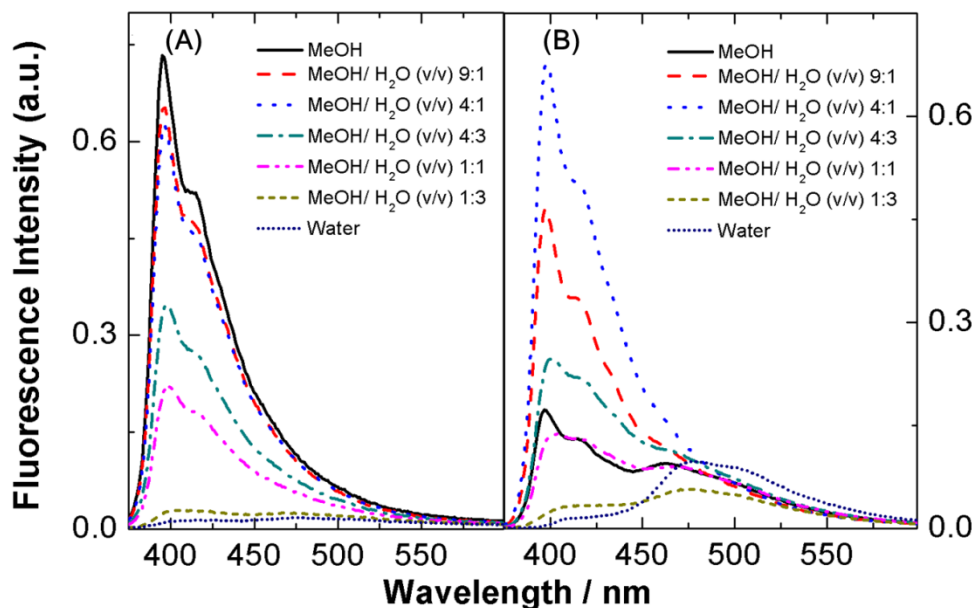


Figure 2-5. Fluorescence spectra of A) **C-PPE**, and B) **O-PPE** in a mixture of methanol and water (Intensities reflect relative quantum yields).

Table 2-1. Photophysical data of **C-PPE** and **O-PPE**

Polymer /Solvent	$\lambda_{\text{max}}^{\text{abs}}$ (nm)	ϵ_{max} ($\text{M}^{-1}\text{cm}^{-1}$)	$\lambda_{\text{max}}^{\text{Fl}}$ (nm)	$\Phi_{\text{Fl}}^{\text{a}}$	τ_{fl} (ns)	
					400 nm	500nm
C-PPE /MeOH	365	24500	396	0.075	0.85	1.01
C-PPE /H ₂ O	365	22800	473	0.005	1.45	1.50
O-PPE /MeOH	370	69000	396	0.10	0.73	1.36
O-PPE /H ₂ O	371	67400	480	0.02	0.24	1.30

^a Measured using quinine sulfate in 0.1 M sulfuric acid ($\Phi_{\text{F}} = 0.54$) as standard.

The fluorescence quenching behavior of the two polyelectrolytes in MeOH and H₂O was investigated. The electron acceptor N,N'-dimethyl-4,4'-bipyridinium (MV^{2+}) was chosen as a quencher to examine whether the amplified quenching effect could be observed. In MeOH solution, **C-PPE** is quenched with moderate efficiency, with a Stern-Vomer constant (K_{SV}) of $\sim 10^5 \text{ M}^{-1}$, which is slightly higher than reported for an anionic 3-ring phenylene ethynylene oligomer ($\sim 10^4 \text{ M}^{-1}$),²¹ but much lower than typical for fully conjugated polyelectrolytes ($\sim 10^6 - 10^7 \text{ M}^{-1}$). This result suggests that exciton migration

is not as effective in **C-PPE** compared to typical CPEs, presumably due to the interrupted conjugation.

However, the quenching behavior for **O-PPE** is quite unusual. As shown in Figure 2-6a, in MeOH where the emission of **O-PPE** consists of both aggregate and monomer fluorescence, quenching of the aggregate is seen at very low quencher concentration ($\ll 1 \mu\text{M}$), with $K_{\text{SV}} \sim 10^7 \text{ M}^{-1}$; such a large quenching efficiency is similar to that of typical CPEs.

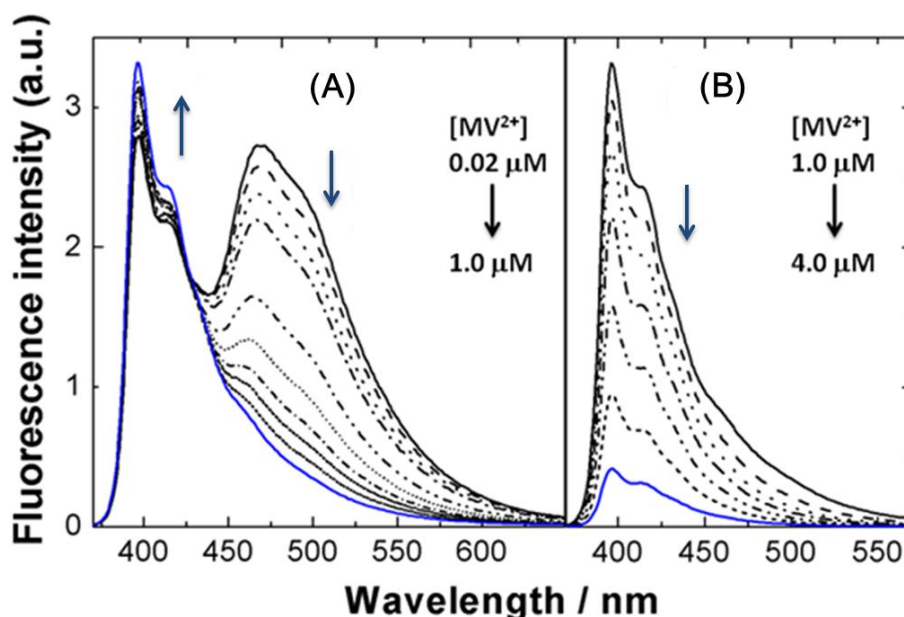


Figure 2-6. Fluorescence spectra of **O-PPE** with added MV^{2+} . $[\text{O-PPE}] = 10 \mu\text{M}$. Note that A) at lower concentrations ($[\text{MV}^{2+}] = \text{from } 0.02 \text{ to } 1.0 \mu\text{M}$) the aggregate emission is quenched first and B) with increasing concentrations of MV^{2+} ($[\text{MV}^{2+}] = \text{from } 1.0 \text{ to } 4.0 \mu\text{M}$) further quenching of monomer emission was observed.

Interestingly, while the emission of the aggregates is quenched by MV^{2+} , the intensity of the monomer emission increases slightly with increasing quencher concentration, suggesting that interaction of the divalent quencher cation with the anionic polymer affects the balance between monomer and aggregate state. Notably, quenching of the monomer emission does not begin until the aggregate emission is

entirely quenched (Figure 2-6b); monomer emission is quenched only at much higher concentration of the quencher, with a quenching efficiency ~ 200 times less than quenching of the aggregate emission ($K_{SV} \sim 10^5 \text{ M}^{-1}$). This selective fluorescence quenching of the aggregate state in CPEs has been reported previously,³⁰ but the highly selective aggregate quenching exhibited by **O-PPE** is unprecedented, and clearly underscores the importance of exciton delocalization and diffusion in the aggregates of π -conjugated chromophores.^{1,106,111} Importantly, the unusual quenching effects seen for **O-PPE** are not limited to MV^{2+} . Indeed, the cationic dyes 3,3'-diethyloxacarbocyanine iodide (DOC) and 3,3'-diethyloxadiazocarbocyanine iodide (DODC) quench the fluorescence of **O-PPE** via energy transfer, and a quenching trend similar to MV^{2+} is observed, i.e. quenching of aggregate emission is much more efficient compared to the monomer quenching (Figure 2-7 and 2-8).

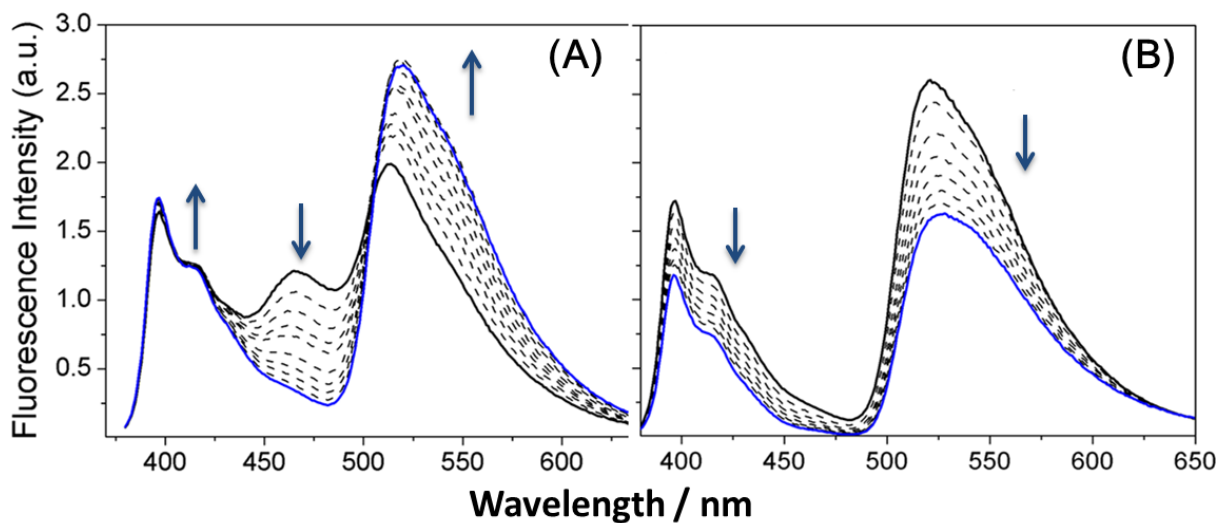


Figure 2-7. Fluorescence quenching of **O-PPE** ($10 \mu\text{M}$) by adding DOC. A) At a lower DOC concentration [$0.1 \mu\text{M} - 1.0 \mu\text{M}$] and B) at a higher DOC concentration [$1.0 \mu\text{M} - 5.0 \mu\text{M}$].

Comparison of the Stern-Volmer plots for **C-PPE** and **O-PPE** quenching by MV^{2+} in MeOH and H_2O is illustrated in Figure 2-9. This presentation makes it very clear the

considerably higher efficiency for aggregate vs. monomer quenching of **O-PPE** in MeOH and the intermediate efficiency exhibited by **C-PPE**. In water, the quenching of **C-PPE** is slightly more efficient than in MeOH; however, for **O-PPE** the quenching efficiency is very similar to that for the aggregate state of the polymer in MeOH. This is not surprising, given that the emission of **O-PPE** in water is dominated by the aggregate band (Figure 2-5b).

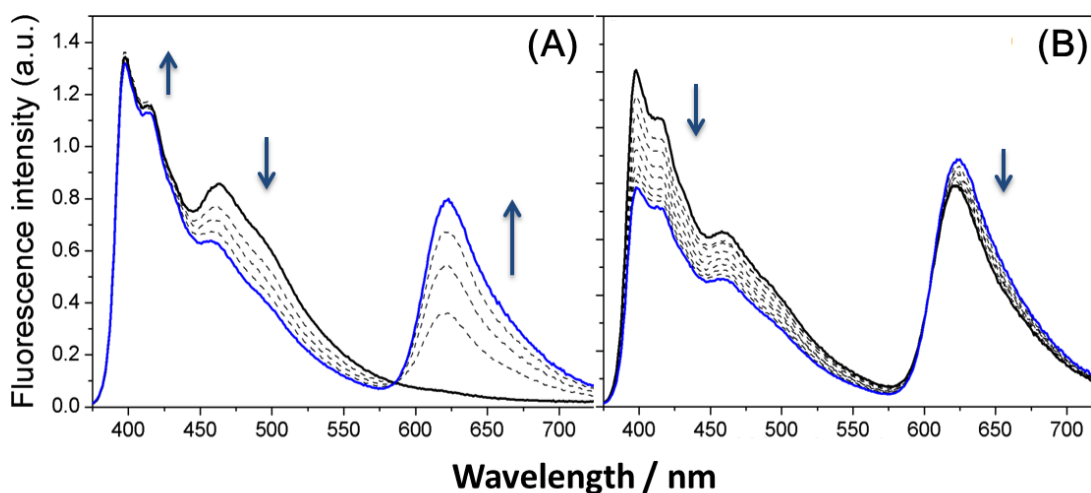


Figure 2-8. Fluorescence quenching of **O-PPE** (10 μM) by DODC. A) At a lower DODC concentration [0.1 μM - 1.0 μM] and B) at a higher DODC concentration [1.0 μM - 5.0 μM].

The dramatically different quenching behavior of **C-PPE** and **O-PPE** is clearly tied to the difference in ability of the chromophore units to assemble into aggregate structures that give rise to a distinct aggregate fluorescence coupled with exciton delocalization and migration in the aggregate. The difference in aggregate structures is reflected by dynamic light scattering data obtained on the polymers in methanol and water (Figure 2-10). Specifically the two polymers exhibit a similar hydrodynamic radius in methanol (~ 10 nm); however, in water the radius of **C-PPE** is considerably larger than that of **O-PPE** (55 vs. 18 nm), indicating a much more compact aggregate for the latter

polymer in the aqueous environment. The difference in aggregate structures must be related the structural or electronic differences imparted by the $-\text{CH}_2-$ linker in **C-PPE** and the $-\text{O}-$ linker in **O-PPE**.

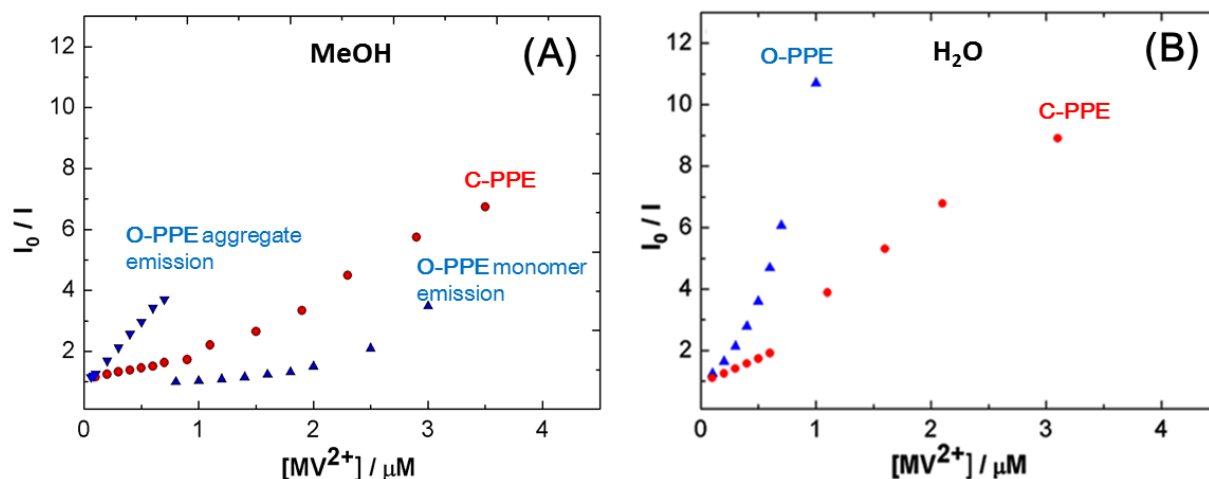


Figure 2-9. Stern-Volmer plots of **C-PPE** and **O-PPE** with MV^{2+} in A) MeOH and B) Water. (Polymer concentration = $10 \mu\text{M}$ in each case).

The linker difference could manifest in two possible ways: 1) the electron donating effects of the oxygen linker may favor formation of compact emissive aggregate structures; or 2) the difference in linker structure may induce differences in secondary structure as the polymers fold in solution. Molecular modeling studies do not suggest that there is a significant difference in conformation induced by the two linkers. However, we believe that in solution the polymers likely fold into a “helical like” coiled secondary structure, and the propensity of the π -conjugated chromophore segments to form a compact π -stacked aggregate structure is stronger for the oxygen linked system (**O-PPE**), either due to steric or electronic factors.

Seeking evidence for a difference in the secondary structures of the two CPEs, we explored their interaction with the cationic luminescent metallointercalator

$\text{Ru}(\text{bpy})_2(\text{dppz})^{2+}$ (Ru-dppz , where bpy = 2,2'-bipyridine and dppz = dipyrido[3,2-a:2',3'-

c]phenazine).¹¹⁵ In previous work we have shown that this complex intercalates into the π -stacked aromatic residues in the helical conformation of anionic meta-linked poly(phenylene ethynylene) CPEs.^{30,31} Intercalation of Ru-dppz is signaled by the appearance of its strong metal-to-ligand charge transfer (MLCT) luminescence, which is quenched when the complex is in water in the absence of a host. Interestingly, in support of the hypothesis of a π -stacked helical conformation for **O-PPE**, we find that addition of the polymer to a solution of the Ru-dppz gives rise to significant enhancement in the MLCT emission of the metal complex (Figure 2-11). A similar effect is not seen concomitant with addition of **C-PPE** to the metal complex. This result suggests that there is a stronger degree of π -stacking (and possibly helix formation) within the aggregate state of **O-PPE**, which is consistent with the observation of significant aggregate emission and enhanced amplified quenching.

It is believed that the fluorescence lifetime of $\text{Ru}(\text{bpy})_2(\text{dppz})^{2+}$ MLCT emission is positively correlated to how well they are shielded from water¹¹⁶. In this sense, it is interesting to investigate the fluorescence lifetime of $\text{Ru}(\text{bpy})_2(\text{dppz})^{2+}/\text{O-PPE}$ complex and compare it with the established $\text{Ru}(\text{bpy})_2(\text{dppz})^{2+}/\text{DNA}$ ¹¹⁶ systems. The fluorescence decay of $\text{Ru}(\text{bpy})_2(\text{dppz})^{2+}/\text{O-PPE}$ complex was recorded on time correlated single-photon counting (TCSPC) instrument, and the result is shown in Figure 2-11d. The multi-exponential decay consists of two shorter components at 5 ns and 25 ns, and a longer component at 150 ns. Since free $\text{Ru}(\text{bpy})_2(\text{dppz})^{2+}$ is non-emissive in water, all decays come from the interaction of $\text{Ru}(\text{bpy})_2(\text{dppz})^{2+}$ and **O-PPE**. The shorter decay may be due to external binding, while the longer one should be the result of intercalation of $\text{Ru}(\text{bpy})_2(\text{dppz})^{2+}$ into **O-PPE** secondary structure. It is

necessary to point out that the average fluorescence lifetime of $\text{Ru}(\text{bpy})_2(\text{dppz})^{2+}/\mathbf{O}\text{-PPE}$ complex is shorter than that of $\text{Ru}(\text{bpy})_2(\text{dppz})^{2+}/\text{DNA}^{116}$ (121 ns) complex, indicating that the secondary structure of **O-PPE** is “loose” packed comparing to DNAs and thus not able to shield $\text{Ru}(\text{bpy})_2(\text{dppz})^{2+}$ from water as well.

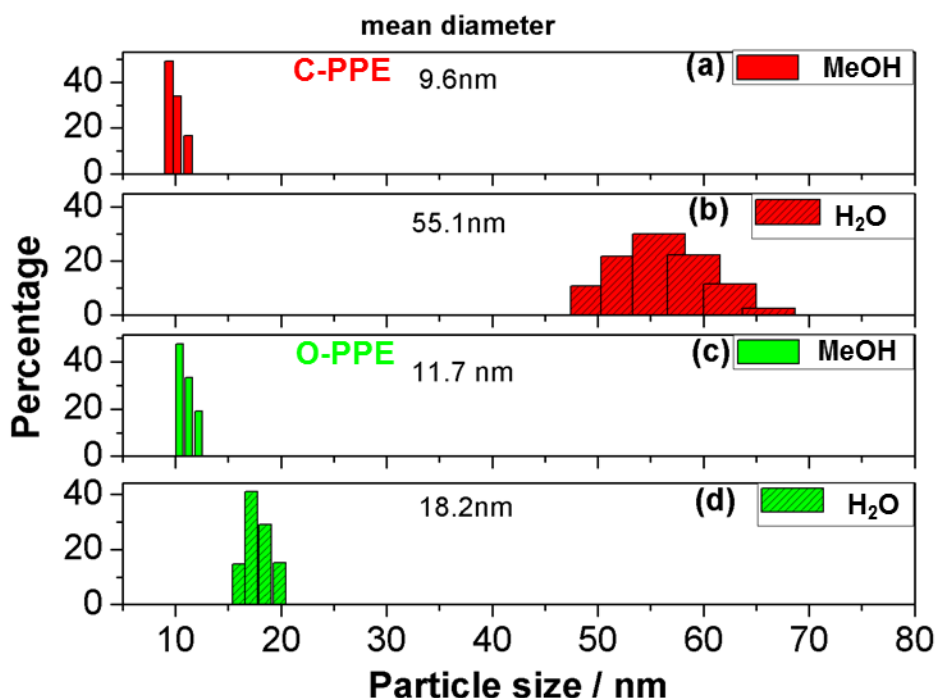


Figure 2-10. Distribution of particle sizes of **C-PPE** and **O-PPE** in MeOH and H_2O (concentration at $20\ \mu\text{M}$) measured by dynamic light scattering. All samples were passed through a $0.2\ \mu\text{m}$ PTFE membrane, and measured under 25°C

Indeed, the aggregate state of **O-PPE** is in equilibrium with its monomer state. We have shown above that the emission ratio of aggregate band to monomer band varies in solvents that contain different amounts of MeOH and H_2O . Furthermore, the concentration and temperature dependent photophysics was studied. 1) Figure 2-12 presents the absorption and fluorescence spectra of **O-PPE** at different concentrations. While the concentration of the CPE increases, the ratio of monomer to aggregate emission decreased, presumably because higher concentration favors the formation of aggregates. 2) Figure 2-13 records the emission spectra of **O-PPE**. As the temperature

increases, the absorption is almost identical. While both monomer and aggregate emissions decrease, the ratio of monomer emission to aggregate emission changes. It turns out that the monomer emission is more sensitive to temperature change than that of the aggregates. One plausible reason for this phenomenon is that the monomers tend to aggregate at higher temperatures. Taken together, the equilibrium between aggregate and monomer of **O-PPE** is sensitive to concentration, solvent, and temperature, which is consistent with our conclusion that the **O-PPE** forms “loose” secondary structures.

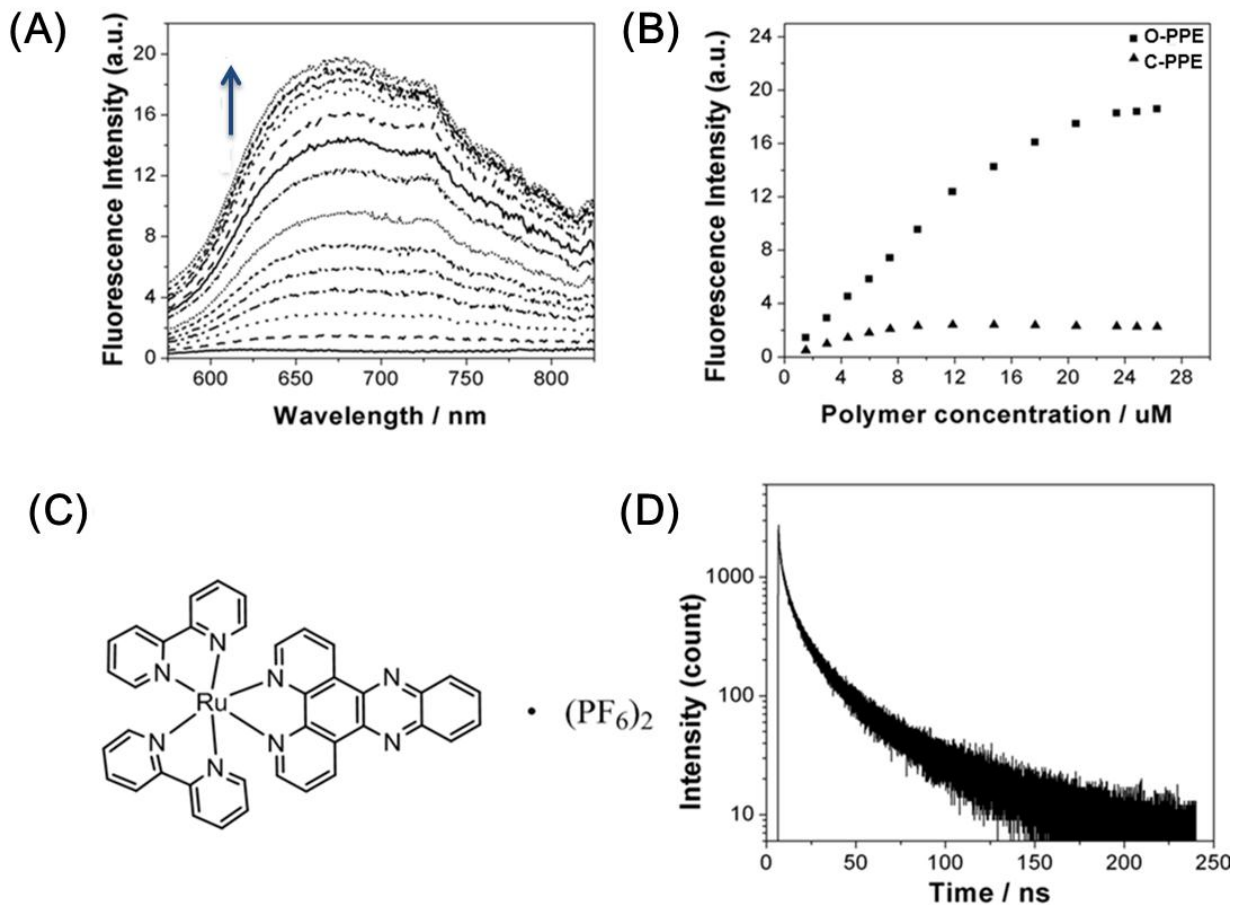


Figure 2-11. Interaction between $\text{Ru}(\text{bpy})_2(\text{dppz})^{2+}$ and **O-PPE**. A) The enhancement of $\text{Ru}(\text{bpy})_2(\text{dppz})^{2+}$ (concentration 5 μM) emission in water upon adding **O-PPE**, B) plot showing variation of the emission intensity of $\text{Ru}(\text{bpy})_2(\text{dppz})^{2+}$ with the concentration of **C-PPE** and **O-PPE**, C) the structure of $\text{Ru}(\text{bpy})_2(\text{dppz})^{2+}$ and D) the decay curve of $\text{Ru}(\text{bpy})_2(\text{dppz})^{2+}$ with 20 μM **O-PPE** in H_2O .

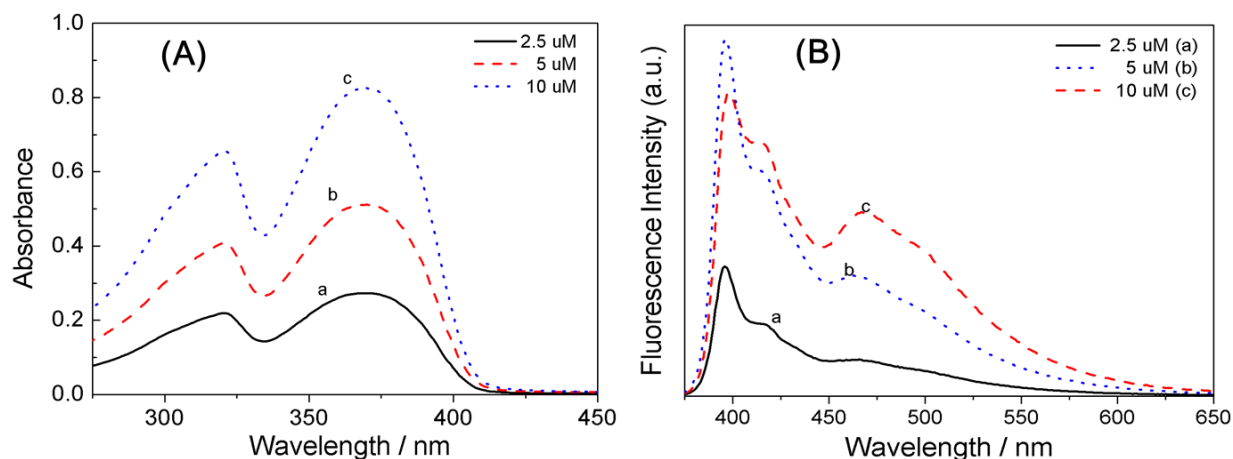


Figure 2-12. Photophysics of **O-PPE** at different concentrations. A) Absorption and B) fluorescence spectra of **O-PPE** at various concentrations in MeOH. (a) 2.5 μM (solid line), (b) 5.0 μM (dashed line) and (c) 10 μM (dotted line).

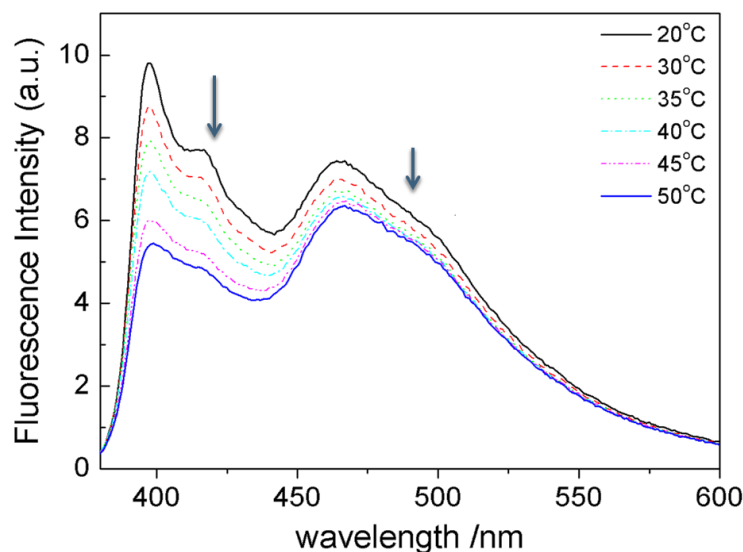


Figure 2-13. Fluorescence spectra of **O-PPE** at different temperatures in MeOH.

Summary and Conclusions

In summary, this study provides insight concerning the effect of “interrupted conjugation” on the photophysical properties and amplified quenching of conjugated polyelectrolytes. Polymer **C-PPE** does not exhibit emission from an aggregate state in either MeOH or H_2O , and while the quenching of this polymer is enhanced slightly compared that of a monomeric chromophore, the polymer exhibits only a modest amplified quenching effect. By contrast, polymer **O-PPE** exhibits both monomer and

aggregate emission, and the aggregate state is quenched 200-fold more efficiently compared to the monomer state with a K_{SV} value rivaling the maximum efficiency seen for fully conjugated polyelectrolytes. The results underscore the important role played by chromophore aggregation in promoting efficient exciton transport which is key to the amplified quenching effect.

Experimental

Materials and Methods

All chemicals were purchased from either Acros or Aldrich and used as received without further purification. NMR spectra were recorded on a VarianVXR-300 or a Varian Gemini-300. UV-visible absorption spectra were obtained either on a Varian Cary 100 or a PerkinElmer Lambda 25 dual beam absorption spectrometer using 1-cm quartz cells, and corrected for background due to solvent (HPLC grade). Fluorescence spectra were recorded on a PTI fluorimeter. Fluorescence lifetime data was recorded on a PicoQuant Picoharp-300 TCSPC instrument. Dynamic light scattering results were obtained from Brookhaven ZetaPlus.

The reported concentrations refer to the concentration of polymer repeat units (PRU). Solutions for spectroscopic studies were prepared by dilution of stock solutions. The **C-PPE** stock concentration was 0.72 mg/mL, which corresponds to 1.2 mM and **O-PPE** stock concentration was 0.89 mg/mL, which corresponds to 1.4 mM.

Synthetic Procedures

bis(4-iodophenyl)methane (1). To a stirring mixture of 8.4 g (0.05 mol) diphenylmethane, 100 mL acetic acid and 10 mL deionized water, 10.5 g iodine and 4.3 g KIO_3 were added. The resulting mixture was heated to above 90°C before 5 mL concentrated H_2SO_4 were charged dropwise. The reaction was allowed 12 hr under

reflux. Saturated $\text{Na}_2\text{S}_2\text{O}_3$ solution was added to quench the excess I_2 , the color of the solution turned from dark brown to light yellow. After cooling, the reaction mixture was poured into 1 L ice cold water and then further cooled at 0°C for 1 hr. The precipitates were isolated and the crude product was recrystallized by Hexane. **1** was obtained as white crystals. Yield 6g (30%). ^1H NMR (300 MHz, CDCl_3 , ppm) 3.96 (s, 2H), 7.07 (d, 4H), 7.39 (d, 4H). ^{13}C NMR (75 MHz, CDCl_3 , ppm) 41.81, 94.03, 129.08, 132.20, 140.91.

4,4'-oxybis(iodobenzene) (2). To a 100-mL round-bottom flask, 5.6 g of N-iodosuccinimide was dissolved in 40 mL of acetonitrile. 2 g diphenyl ether (11.7 mmol) was charged before 5 drops of CF_3COOH was added to the solution. The reaction was allowed to run for 5 hr under room temperature and the process was monitored by TLC plate. After reaction was done, the solvent was evaporated and the solid was redissolved in DCM, the solution was washed with saturated $\text{Na}_2\text{S}_2\text{O}_3$ solution twice, and then brine. Organic layers were combined and evaporated. The crude product was recrystallized by acetone. **2** was obtained as white crystals. Yield 3 g (60%). ^1H NMR (300 MHz, CDCl_3 , ppm) 6.91 (d, 4H), 7.43 (d, 4H). ^{13}C NMR (75 MHz, CDCl_3 , ppm) 84.32, 120.04, 137.24, 153.86.

bis(4-((trimethylsilyl)ethynyl)phenyl)methane (3). To a 200-mL round-bottom flask, 3 g of compound **1** (7.2 mmol) was charged. A mixture of 50 mL dry THF and 20 mL tri-ethylamine (TEA) was used to dissolve the solid. The solution was degassed by argon flow for 20 min before 80 mg $\text{Pd}(\text{PPh}_3)_4$ and 60 mg CuI were added quickly to the stirring solution. After 5 min, 1.67 mL (16 mmol) trimethylsilyl acetylene was added to the reaction mixture by syringe. Precipitates formed immediately. The reaction was allowed to run for overnight under room temperature. After reaction was done, the

precipitates were filtered. The filtrate was evaporated and the solid was redissolved in DCM. The solution was washed by diluted HCl (30 mL x2), brine (30 mL x2) and water (30 mL). The organic layers were combined and dried over anhydrous Na₂SO₄. After DCM was evaporated, the crude product was purified by flash chromatography (eluent Hexanes). **3** was obtained as white solid. Yield 2.3 g (90%). ¹H NMR (300 MHz, CDCl₃, ppm) 0.24 (s, 18H), 3.96 (s, 2H), 7.07 (d, 4H), 7.39 (d, 4H). ¹³C NMR (75 MHz, CDCl₃, ppm) 0.22, 41.87, 94.78, 124.05, 129.06, 132.36, 141.32.

((oxybis (4,1-phenylene))bis(ethyne-2,1-diyl))bis(trimethylsilane) (4). This compound was synthesized by the same procedure used to prepare **3**, except that the amounts of reagents used were: **2** (1.5 g, 3.55 mmol), trimethylsilyl acetylene (0.88 mL, 8.0 mmol), Pd(PPh₃)₄ (40 mg) and CuI (30 mg). The product was purified by elution through a plug of silica gel with a mix solvent of Hexanes and DCM (10:1 v/v). Yield 1 g (78%). ¹H NMR (300 MHz, CDCl₃, ppm) 0.25 (s, 18H), 6.91 (d, 4H), 7.43 (d, 4H). ¹³C NMR (75 MHz, CDCl₃, ppm) 0.28, 114.95, 117.54, 132.21, 156.03.

bis(4-ethynylphenyl)methane (5). To a 200-mL round-bottom flask, 1.0 g of **3** (2.77 mmol) was charged. A mixture of 15 mL DCM, 10 mL Hexane, and 15 mL CH₃OH were added to dissolve the reactant. The solution was degassed by argon for 15 min before 2.21 g of K₂CO₃ (16 mmol) was added portion-wise to the solution. The reaction was done in 2 hr (monitored by TLC plate). After filtration, the filtrate was concentrated. The solid was purified by flash chromatography (Hexane/DCM 1/1 v/v) and **5** was obtained as a white solid. Yield 0.52 g (87%). ¹H NMR (300 MHz, CDCl₃, ppm) 3.04 (s, 2H), 3.97 (s, 2H), 7.12 (d, 4H), 7.43 (d, 4H). ¹³C NMR (75 MHz, CDCl₃, ppm) 41.89, 83.77, 120.30, 129.15, 132.57, 141.57.

4,4'-oxybis(ethynylbenzene) (6). This compound was synthesized by the same procedure used to prepare **5**, except that the reagent used was **4** (1.02 g 2.8 mmol). Yield 0.45 g (75%). ¹H NMR (300MHz, CDCl₃, ppm) 3.15 (s, 2H) 6.92 (d, 4H), 7.42 (d, 4H). ¹³C NMR (75MHz, CDCl₃, ppm) 81.23, 115.78, 117.32, 132.21, 152.56.

Sodium 3,3'-((2,5-diiodo-1,4-phenylene)bis(oxy))bis(propane-1-sulfonate) (7). 7.24 g (20.0 mmol) 2,5-diiodohydroquinone was dissolved in a solution that contained 2.0 g (50.0 mmol) sodium hydroxide in 200 mL water in a Erlenmeyer flask under argon. A solution of 6.1 g (50.0 mmol) of 1,3-propanesultone in 40 mL of dioxane was added to the former solution at once. The resulting mixture was then stirred at room temperature for overnight, during which time a thick pink slurry formed. The reaction mixture was then stirred at 80-100°C for another 30 min and then cooled in a water/ice bath. The suspension obtained was vacuum filtered, and the retained solid was washed with cold water followed by acetone, and crystallized twice from water. Yield 8.7 g (66%). ¹H NMR (300MHz, DMSO-d₆, ppm) 2.00 (t, 4H); 2.64 (t, 4H); 4.05 (t, 4H); 7.30 (s, 2H). ¹³C NMR (75MHz, DMSO-d₆, ppm) 25.37, 48.14, 68.99, 86.99, 122.44, 152.32.

C-PPE was synthesized by a modified literature procedure.²¹ 0.735 g (1.16 mmol) monomer **7** and 0.250 g (1.16 mmol) monomer **5** were dissolved in a mixture of 10 mL water and 10 mL DMF in a Schlenk flask with a gentle flow of argon with stirring. The resulting clear solution was deoxygenated by several cycles of vacuum-argon cycling. Another solution comprised of 60.0 mg of Pd(PPh₃)₄ and 50.0 mg CuI in a mixture of 10 mL triethylamine and 10 mL of DMF was likewise deoxygenated and was subsequently added to the former solution by means of a syringe. The final mixture was again deoxygenated by vacuum-argon cycling and was then warmed to 70°C and stirred

under a positive pressure of argon for 24 h. The solution was cooled and then slowly added to 1 L of a methanol/ether mixture (30:70 v/v). The polymer precipitated as greenish fibers. It was redissolved in 200 mL of water/DMSO (98:2 v/v), treated with 0.08 g of sodium sulfide (Na_2S), and then the solution was filtered through quantitative filter paper, followed by a 10-20 μm fritted glass filter, and finally through a 0.8 μm nylon membrane. The polymer was precipitated by addition to a large volume of methanol/ether (30:70). The polymer was dissolved in water/DMSO and reprecipitated from methanol/ether two more times. Finally, the polymer was dissolved in 200 mL of water with 1 mL DMSO, and the resulting solution was dialyzed against water (Millipore NanopureTM) using a 10-12 kD MWCO cellulose membrane. After the dialysis, the polymer concentration was 1.0 mg/mL (or 1.67 mM for polymer repeat unit). The polymer was stored in this format and diluted as appropriate for spectroscopic studies. 30 mL polymer solution was dried by means of freeze drying and redissolved in DMSO- d_6 for NMR characterization. ^1H NMR (300 MHz, DMSO- d_6 , ppm) 2.04(broad 4H), 2.72(broad 4H), 4.00-4.18 (broad 6H), 7.09 (broad 2H), 7.31(broad 4H), 7.50 (broad 4H).

O-PPE was synthesized under exactly the same condition with that of **C-PPE**, except that the monomer used were **6** and **7**. After dialysis, the polymer concentration was 0.9 mg/mL (or 1.50 mM for polymer repeat unit). ^1H NMR (300 MHz, DMSO- d_6 , ppm) 2.04 (broad 4H), 2.70 (broad 4H), 4.13(broad 4H), 7.06-7.17 (broad 6H), 7.62 (broad 4H).

CHAPTER 3

SYNTHESIS AND CHARACTERIZATION OF BODIPY BASED POLYELECTROLYTES AND THEIR INTERACTIONS WITH QUENCHERS

Incorporating BODIPY into Polymer Backbones

4,4'-Difluoro-4-bora-3a,4a-diaza-s-indacene (BODIPY) dyes (structure shown in Figure 3-1) and their derivatives have been receiving continuous research interest since first introduced by Treibs and Kreuzer¹¹⁷ for many reasons. First, their molar extinction coefficients are very high (usually around 70,000-80,000 M⁻¹ cm⁻¹).¹¹⁸ Second, they feature relatively sharp emission and high photoluminescence quantum yields. Third, their excellent photochemical and thermal stability, and good solubility in many solvents offer them great potentials as functional materials.¹¹⁹ Most important, their photophysical properties are easily tuned as desired upon modification of chemical structures.¹²⁰ Based on these properties, the applications of BODIPYs in many fields that include biological labeling,¹²¹ ion sensing,¹²² light harvesting,¹²³ and solar cells^{118,124} have been explored. While there is a good amount of research that succeeds in fine-tuning the optical properties of BODIPYs by chemical structure modifications,^{117,125} most work is engaged in small molecules, and only a few reports have been presented in which the dyes are incorporated into conjugated polymer backbones.^{120,124,126} In 2008, Nagai et al. reported a novel set of polymers that included BODIPY into poly(phenylene ethynylene) or poly(fluorene ethynylene) back bones (Figure 3-2a),¹²⁰ achieving better processability comparing to the small molecules. These polymers, however, bear almost identical absorption and emission spectra as those of typical BODIPY dyes.¹²⁰ This is because that the p-arylene ethynylenes were attached to the 4,4' positions (Figure 3-1) on the BODIPYs, which does not offer efficient conjugation between the arylene-

ethynylene units and the BODIPY cores. Similar phenomena were also observed in other researches.¹²⁷⁻¹²⁹ In 2009, Liu and co-workers modified the co-polymer patterns by connecting BODIPYs at 2,6 positions (Figure 3-1) with a series of aromatic units featuring different band gaps (Figure 3-2b).¹²⁶ As a result, polymeric BODIPY dyes that emits at deep red and near-IR regions were developed, due to significant extension of π -conjugation between BODIPYs and other aromatic units. In parallel, their cooperating group (Frechet et al.) explored the potential of these BODIPY containing polymers in bulk heterojunction solar cells and achieved about 2% power conversion efficiency.¹²⁴ In a separate study, Thayumanavan and co-works synthesized a series of alternating π -conjugated donor-acceptor polymers based on the BODIPYs core and acceptors with different HOMO and LUMO levels such as quinoxaline, benzothiadiazole, and rylene acceptors.¹³⁰ The electrochemistry of the polymers was carefully investigated, and preliminary results revealed the strong potential for such BODIPY based polymers to function as either p-type or n-type semiconductors, depending on the electrochemical nature of the comonomers.¹³⁰

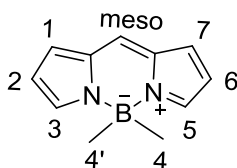


Figure 3-1. Chemical structure of BODIPY

Now that it has been established that conjugated polymers with BODIPYs in the conjugated backbone combine the unique properties of both BODIPY and conjugated polymers,^{120,124,126,130} we propose that the scope of the application of such polymers would be further expanded if they could be rendered with water solubility. In fact, several fields such as ion sensing, bio-labeling, and the study of amplified quenching

behavior require good solubility in water or protic organic solvents. Although there are a few cases in which the water-soluble BODIPY dyes were introduced,¹³¹⁻¹³⁶ the studies were all limited to small molecules. To the best of our knowledge, the water-soluble polymeric BODIPY electrolytes have not been reported. Previously, we reported a series of conjugated polyelectrolytes (CPEs) with different band gaps that feature sterically congested, branched polyionic side groups.¹³⁷ It was found that highly charged ionic functional groups serve to enhance the solubility of the CPEs in aqueous solution by increasing electrostatic repulsion between polymer chains, and thus reducing the hydrophobic interchain interactions.¹³⁷ Following the same method, we have synthesized the BODIPY and phenylene-ethynylene based CPEs that bear branched polyionic side groups. In this chapter, we will first introduce the synthesis of the CPE that features BODIPY and phenylene ethynylene backbones and dendritic side groups; then the photophysical character and the amplified quenching behavior of the CPE will be discussed. Finally, the preliminary results of its application in dye-sensitized solar cells will be described.

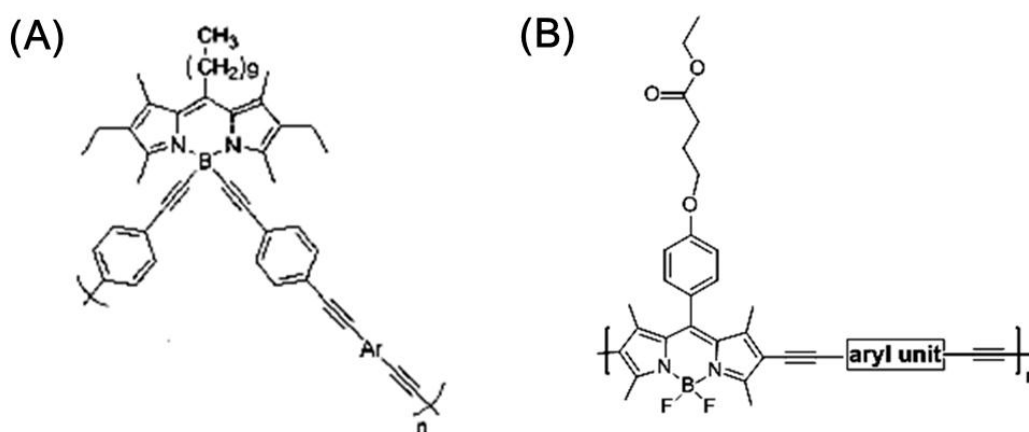


Figure 3-2. Two examples of conjugated polymers incorporating BODIPY. A) attaching BODIPY at 4,4' positions¹²⁰ and B) attaching BODIPY at 2,6 positions¹²⁶

Results and Discussion

Synthesis and Structural Characterization

In this section, we introduce the synthesis of BODIPY-phenylene-ethynylene type of CPE carrying polyionic side chains using the “precursor strategy”, namely, the precursor polymers are synthesized and purified in organic solvents before the protecting groups (t-butyl in this case) are hydrolyzed to yield the corresponding CPEs. The synthesis of compound **5** was carried out following literature procedures.¹³⁸ As shown in Figure 3-3, the diiodobenzene with dendritic side chains (**5**) was prepared from 4 step reactions with an overall yield of 50%. Compound **5** was then reacted with trimethylsilyl (TMS) acetylene under Sonogashira coupling condition and transformed into TMS protected diethynylene benzene, which was subsequently deprotected by tetra-n-butylammonium fluoride (TBAF) to give monomer **6**.

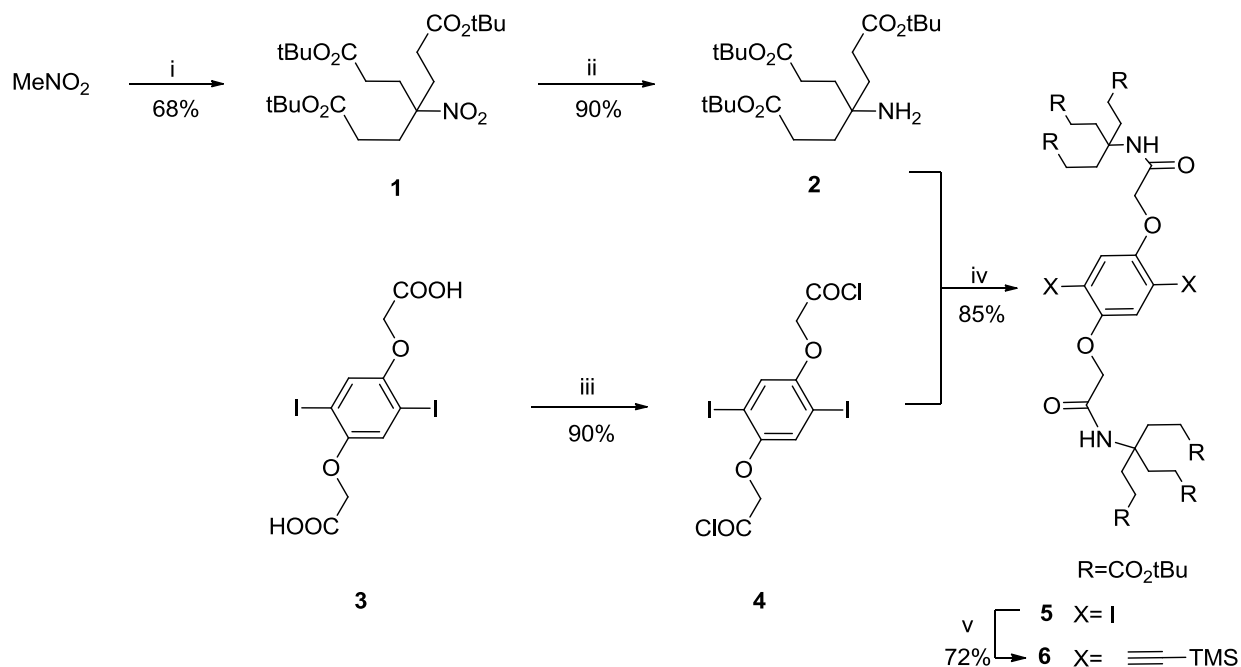


Figure 3-3. Synthesis of monomer **6**. (i) DME, Triton-B, t-butyl acrylate 80°C; (ii) Raney nickel, EtOH, H₂, 48hr; (iii) SOCl₂, DMF, 90°C, 2hr; (iv) TEA, DCM, 0°C to r.t. overnight; (v-1) TMSA, Pd(0), CuI, THF r.t. 13hr; (v-2) TBAF 30 min.

On the other hand, the BODIPY monomer was synthesized following the scheme presented in Figure 3-4. Triethylene glycol monomethyl ether was tosylated to give compound **7**, which underwent an S_N2 reaction attacked by deprotonated 4-hydroxybenzaldehyde under basic condition to yield compound **8**. The BODIPY core (**9**) was obtained from **8** in a three-step one-pot synthesis: condensation of benzylaldehyde with 2,4-dimethylpyrrole to give dipyrro-monophenyl-methane, followed by oxidation by 2,3-Dichloro-5,6-dicyano-1,4-benzoquinone (DDQ) and complexation with trifluoro boron (BF_3). The overall yield for three steps was around 20%, which is consistent with similar reactions reported.¹¹⁷ The iodination at 2,6 positions of compound **9** by I_2/HIO_3 system was done under fairly mild condition with considerable yield (64%). The purity of monomer **6** and **10** was proven by NMR (1H and ^{13}C) and MS spectroscopy before they were polymerized.

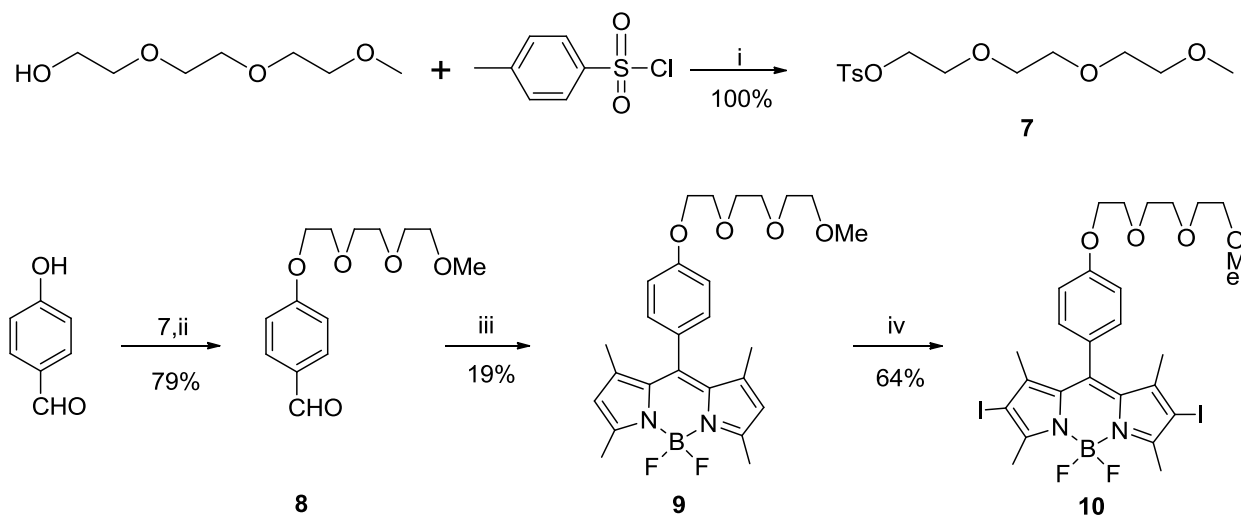


Figure 3-4. Synthesis of monomer **10**. (i) NaOH, THF, 0°C to r.t.; (ii) **7**, K_2CO_3 , DMF, 80°C, overnight; (iii-1) 2,4-Dimethylpyrrole, DCM, TFA (cat.) r.t., overnight; (iii-2) DDQ 3hr; (iii-3) TEA, BF_3OEt_2 , r.t., 30min; (iv) I_2 , HIO_3 , EtOH, r.t., overnight.

The monomers **6** and **10** were polymerized under Sonogashira cross-coupling conditions (Figure 3-5). The reaction was allowed to run for 36 hr under 60 °C, and the

mixture was passed through a short alumina oxide column to remove the catalysts before it was concentrated and then precipitated by addition of MeOH. The precipitate (polymer product) was redissolved in minimum amount of CHCl_3 and reprecipitated with MeOH. Such dissolving-precipitation process was repeated four times to yield the polymer protected by t-butyl esters (named as **PB-e**), which was analyzed by GPC and ^1H NMR.

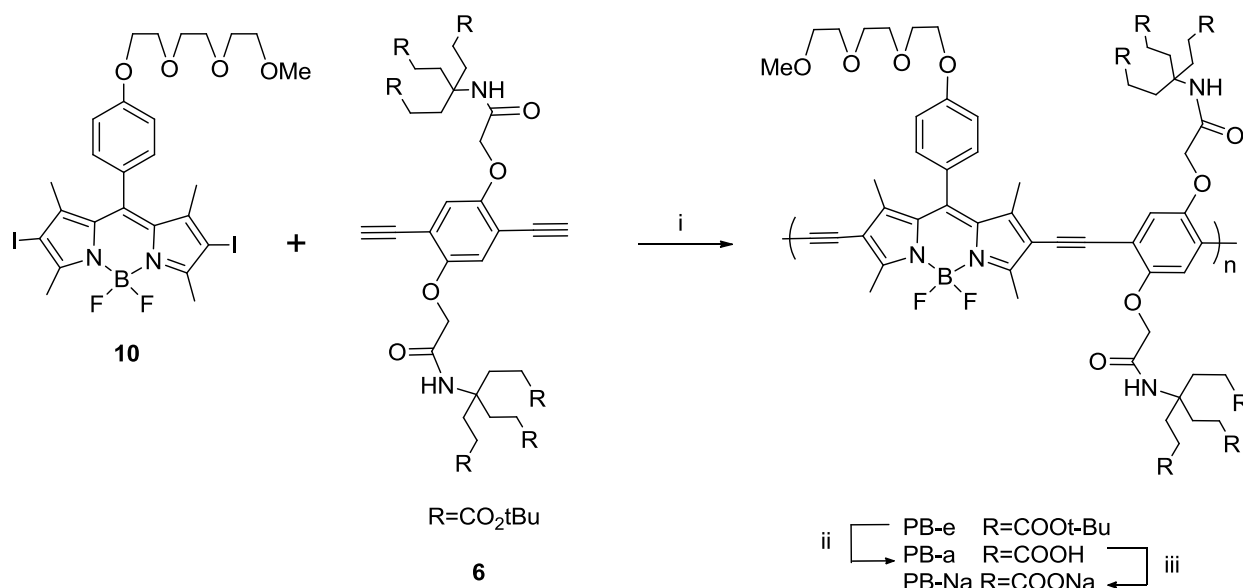


Figure 3-5. Polymerization and deprotection. (i) $\text{Pd}(0)$, CuI , THF, 60°C , 36hr; (ii) TFA, r.t. overnight; (iii) NaOH (10^{-4} M in MeOH).

GPC result suggested that the **PB-e** has a number averaged molecular weight of 28 kD (DP around 18) with PDI = 1.6. The t-butyl groups on **PB-e** were hydrolyzed by trifluoroacetic acid (TFA) using tetrahydrofuran (THF) as co-solvent (THF/TFA v/v=1:1). The deprotected polymer (where H replaced the t-butyl ester groups, named as **PB-a**) was precipitated and washed with acetone, and characterized by ^1H NMR in CDCl_3 . The ^1H NMRs of the monomer **6** and **10**, the **PB-e** and **PB-a** are compared in Figure 3-6. It is clearly shown that the chemical shifts of protons in **PB-e** appear in the same regions as those of the monomers, except that the peaks are broadened due to polymerization.

Protons on t-butyl groups appear as a strong singlet at $\delta = 1.43$ ppm. After hydrolysis, the **PB-a** shows almost no peak around 1.4-1.5 ppm, indicating that the t-butyl groups were completely removed from the polymer. Minimum amount of MeOH that contained 0.1 mM NaOH was used to dissolve **PB-a** and the resulting solution was slowly added to H₂O with pH=9. The water soluble polymer was dialyzed against a NaOH/water (Millipore Nanopure™) solution (pH = 8.5) in the dark for 3 days, resulting pure polyelectrolyte (named as **PB-Na**)-water solution. The concentration of the CPE was measured by gravimetric analysis, and the stock solution was degassed and stored away from light at 4°C.

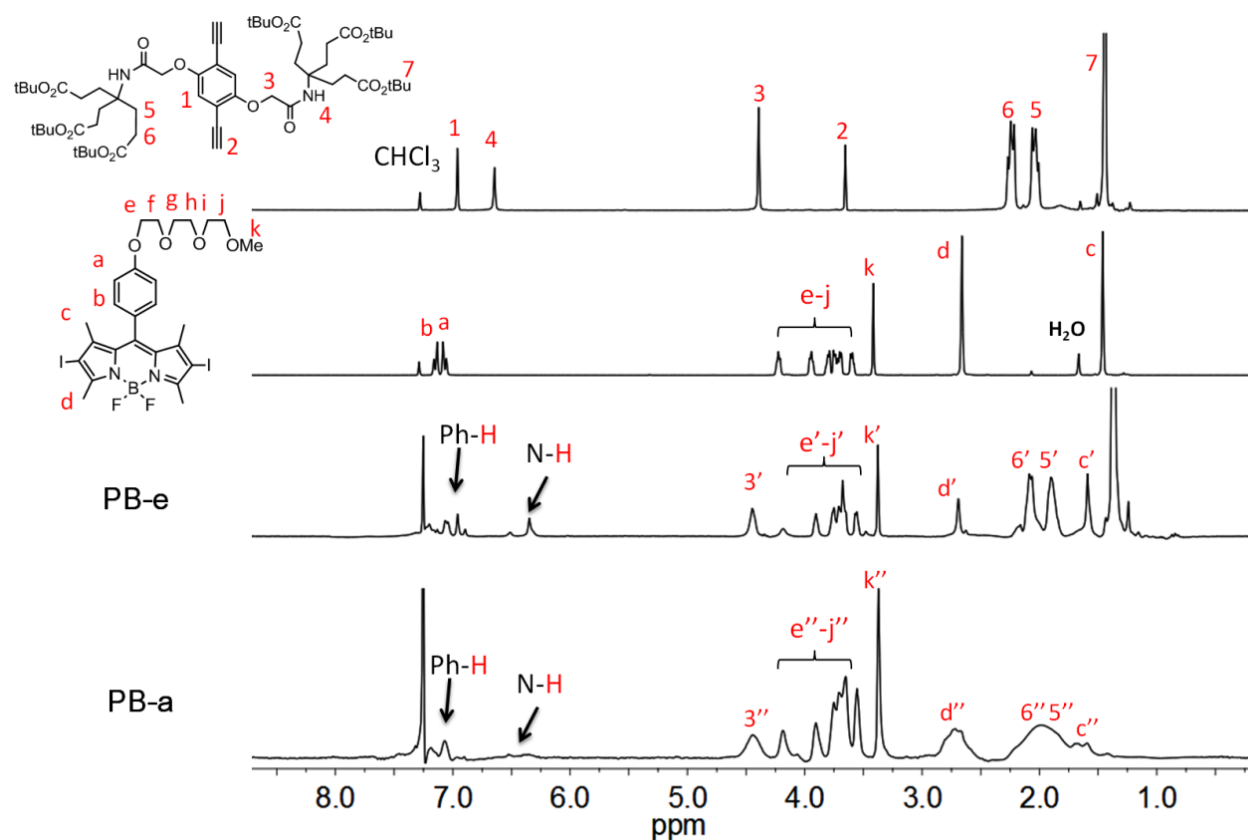


Figure 3-6. ¹H NMR spectra (in CDCl₃) and peak assignment for monomer **6**, monomer **10**, **PB-e** and **PB-a**

Photophysical Properties

The absorption and fluorescence spectra of **PB-e** and **PB-a** in THF and **PB-Na** in methanol are shown in Figure 3-7. Compared to BODIPY monomer **9**, both absorption and emission spectra of **PB-e** are red-shifted and broadened, which comes from the extension of conjugation on BODIPY units. The absorption of **PB-e** exhibits dual peaks at 400 nm and 591 nm respectively with high extinction coefficient, featuring a low band gap of 2.10 eV. The fluorescence spectrum of **PB-e** is a single emission at 631 nm. Compared to the literature reported BODIPY-phenylene ethynylene copolymers,¹²⁶ **PB-e** has a similar shaped spectrum. However, the wavelengths of absorption and fluorescence for **PB-e** are around 20 nm hypsochromically shifted than the reported polymer. A plausible rationalization of this observation is that the dendritic side groups that are applied to **PB-e** have given rise to much larger spatial hinderance than the reported polymer (which has linear side chains), so that the coplanarity of **PB-e** backbone decreases and thus the effective conjugation length is shorter.

As **PB-e** is hydrolyzed, the acid form of the polymer **PB-a** exhibits dramatic hypsochromic shift on absorption spectrum, increasing Stokes shift and lowered fluorescence quantum yield compared to **PB-e**. All the evidence is pointing to the formation of H aggregates of the polymer, and we believe that the aggregation is caused by intermolecular hydrogen bonding between the polymer chains. When **PB-a** was reacted with NaOH and transformed into the sodium salt counterpart **PB-Na**, which is dissolved in MeOH, it turns out that both absorption and emission wavelength shift bathochromically, with an increase in fluorescence quantum yield. While presumably the addition of NaOH could break up H bonding and thus diminish H aggregates, the absorption and emission wavelength of **PB-Na** remains hypsochromically shifted

compared to **PB-e**. One possible explanation is that with dendritic ionic side groups, the electrostatic repulsion induces even more torsional strain than that exists in the ester precursors, where steric repulsion has already impeded the polymer backbone from being coplanar. Similar observations have also been reported by other works.^{137,139}

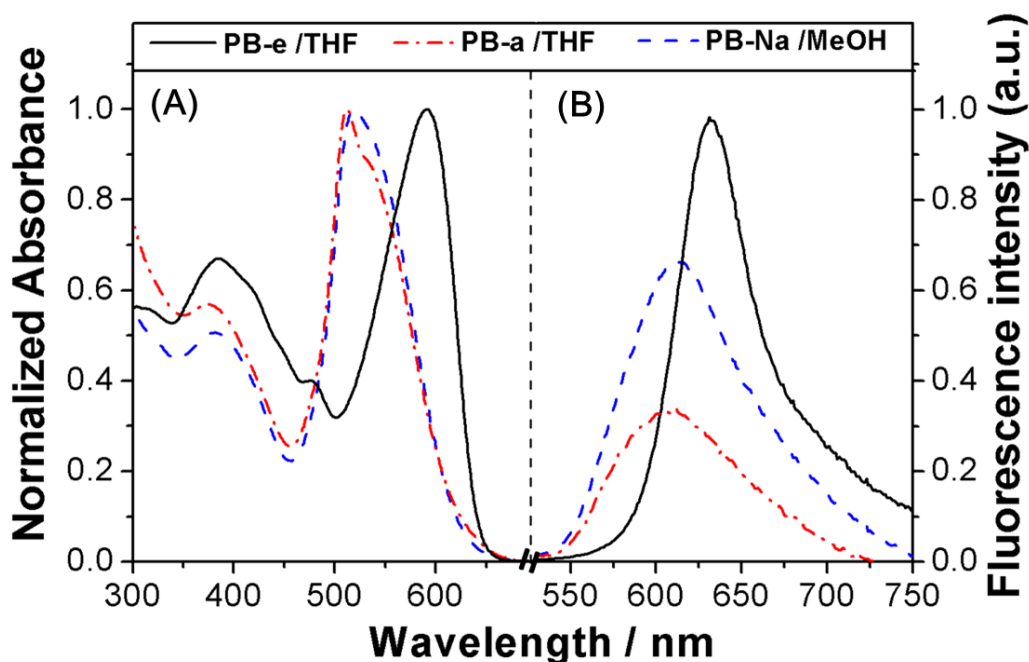


Figure 3-7. Normalized absorption (A) and fluorescence (B) spectra of **PB-e** (black solid lines) in THF, **PB-a** (red dash dot lines) in THF and **PB-Na** (blue dash lines) in MeOH (Fluorescence intensity reflects relative FI quantum yield).

To further characterize the aggregation-photophysical property relation of **PB-Na**, experiments with variable solvents were conducted. It has been discussed in the previous chapter that generally MeOH is considered as a “good” solvent for CPEs where the CPEs exhibit single-chain properties, while H₂O is a “poor” solvent where the CPEs form aggregates due to their amphiphilic nature. In this study, we examined the photophysical behavior of **PB-Na** in MeOH, H₂O, and two co-solvent systems where MeOH and H₂O are mixed (MeOH/H₂O v/v 1/1 and 1/2, respectively). The absorption and fluorescence spectra of the **PB-Na** in different solvents are recorded in Figure 3-8.

As the amount of H₂O increases, both absorption and fluorescence of **PB-Na** decreases. This indicates that the addition of H₂O induces some aggregation.

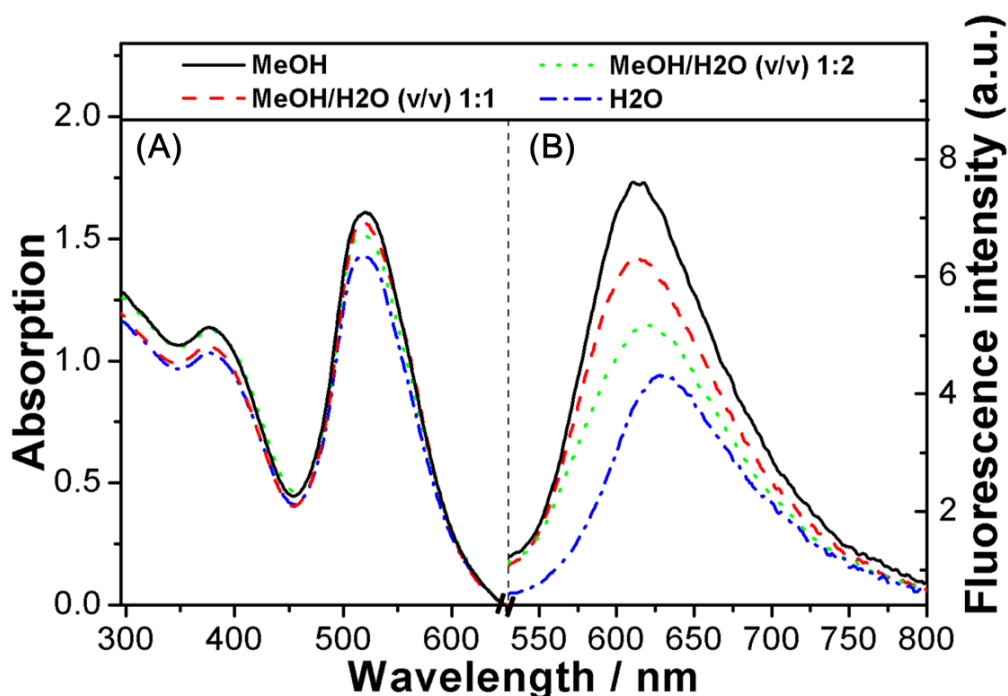


Figure 3-8. Absorption (A) and Fluorescence (B) spectra of **PB-Na** in a mixture of methanol and water (Fluorescence intensities reflects relative quantum yield).

More insights come from the comparison between **PB-Na** and CPEs with linear side ionic groups. Since reports of CPEs that contain BODIPYs with linear side-chain ionic groups are lacking in the literature (in fact, we have tried in vain to make such structures, but all attempts resulted in polymers that were not soluble in H₂O), we refer here to other CPEs that have linear side chains. In previous studies from Schanze and other groups^{22-24,30}, it was reported that CPEs with linear side chains tend to form aggregates upon addition of H₂O, resulting in the following characteristic features: 1) red shift of absorption spectra with appearance of a pronounced shoulder; 2) loss of well-structured emission with broadened, red-shifted structures; and 3) substantial decrease in fluorescence quantum yield coupled with an increase in the fluorescence lifetime. In this study, none of the above effects were observed for **PB-Na**. In particular,

as the solvent is changed from MeOH to H₂O, a limited change is seen in the absorption and emission spectrum. This observation suggests that **PB-Na** is less likely to form aggregates, even in H₂O.

It has been discussed previously that the coplanarity of the CPE backbone is impeded by the branched, dendritic ionic side groups by both steric and electrostatic repulsions,¹³⁷ thus it could be deduced that such CPE structures do not favor aggregation via a π - π stacking manner. Furthermore, the hydrophobic polymer backbones are well protected by high charge density of the dendritic ionic side groups, so that **PB-Na** is less likely to self-assemble as clusters in aqueous solution. Table 3-1 summarizes all the photophysical data for **PB-e**, **PB-a** and **PB-Na**, noting that the photophysical behavior for **PB-Na** in both MeOH and H₂O is similar.

Table 3-1. Photophysical data of **PB-e**, **PB-a** and **PB-Na**

Polymer /Solvent	$\lambda_{\max}^{\text{abs}}$	ϵ_{\max}	$\lambda_{\max}^{\text{Fl}}$	$\Phi_{\text{Fl}}^{\text{a}}$	τ_{Fl}		
	nm	10 ⁴ M ⁻¹ cm ⁻¹	nm		(ns)		
PB-e /THF	591	3.45	631	0.19	1.78(45.8%)	0.87(54.2%)	
PB-a /THF	512	2.57	609	0.07	2.40(11.3%)	0.93(45.2%)	0.32(43.5%)
PB-Na /MeOH	521	2.49	614	0.13	2.40(13.6%)	0.99(52.1%)	0.33(34.4%)
PB-Na /H ₂ O	522	2.13	630	0.05	2.70(20.0%)	1.09(47.2%)	0.38(32.8%)

^a Ru(bpy)₃Cl₂ in H₂O (Φ_{F} = 0.056, degassed) as standard

Above all, the first water-soluble BODIPY based CPE with modest fluorescence quantum yield has been introduced. The CPE is less likely to form aggregate in water and remains fluorescent, such property opens many opportunities for the CPE being applied to studies that are conducted in water or polar organic solvents. Some examples are (not limited to) amplified quenching, ion sensing, and layer-by-layer films.

Interaction with Quenchers- Amplified Quenching and Ion Sensing

With **PB-Na** in hand, we investigated the fluorescence quenching behavior of the CPE in the presence of several quenchers to determine whether the amplified quenching effect is observable.

First, N,N'-dimethyl-4,4'-bipyridinium (MV^{2+}) was applied to examine quenching by photo-induced electron transfer. MV^{2+} is used in a number of works as electron acceptor to quench the photoluminescence of other anionic CPEs with a $K_{SV} \sim 10^6 \text{ M}^{-1}$.^{1,21,23,25} Experimentally, a 5 μM **PB-Na** study solution was obtained by diluting the CPE stock solution. In parallel, MV^{2+} in MeOH solution was prepared with relatively higher concentration so that negligible volume of the solution could cause the designed concentration change of the quencher in the study solution. The evolution of absorption and fluorescence spectra of **PB-Na** in MeOH were recorded as varying amount of MV^{2+} was added, which is shown in Figure 3-9. Surprisingly, neither absorption nor emission of **PB-Na** was affected by addition of MV^{2+} . The absorption spectrum remains identical except that the absorption from MV^{2+} (less than 300 nm) gradually increases with added MV^{2+} , while the fluorescence intensity decreased less than 10% when up to 10 μM MV^{2+} is present in the solution. This result shows that the quenching of **PB-Na** at best occurs to only a limited extent. This relatively inefficient quenching ($K_{SV} \sim 1.5 \times 10^4 \text{ M}^{-1}$) is contrary to the common CPE systems with PPE type of backbones,^{12,21,24} where the fluorescence intensities are quenched at substantially high efficiency (K_{SV} usually at $\sim 10^6 \text{ M}^{-1}$).

Two possible explanations could be put forward to explain this phenomenon. The first possibility is that the singlet excitons are localized within each repeat unit so that the amplified quenching process is prohibited. However this is less likely to happen due

to the fact that the transition dipole of the BODIPY unit¹⁴⁰ is aligned with that of the phenylene ethynylene units (i.e. parallel to the backbone of the CPE). Thus theoretically the exciton migration is allowed through the backbone of **PB-Na**, which should give rise to amplified quenching effect as observed in other CPE systems.^{1,21,23,25} To clarify this point, more quenchers were applied to the **PB-Na** system as discussed later in this chapter.

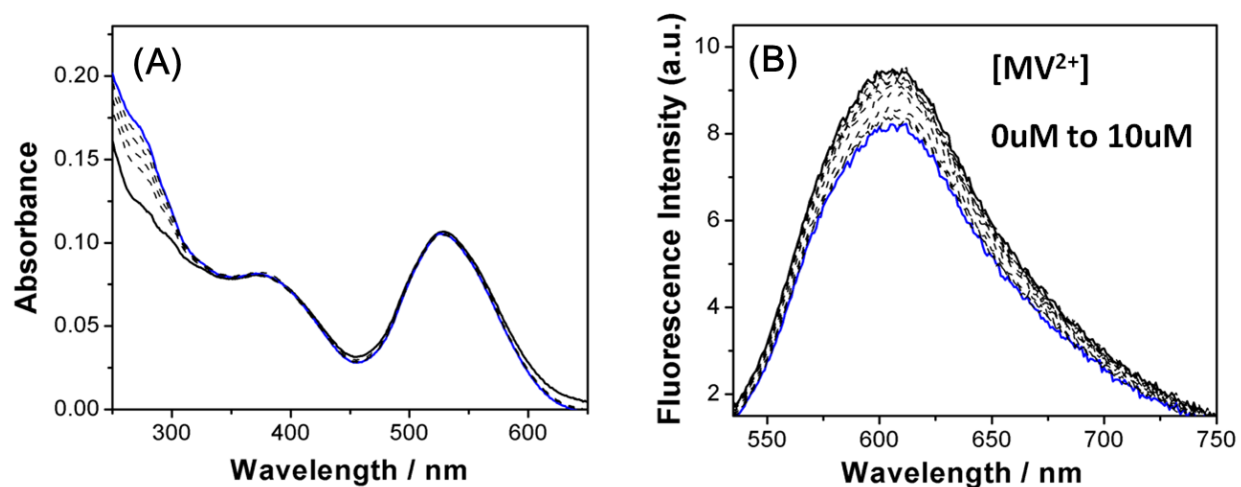


Figure 3-9. Absorption (A) and fluorescence (B) response of **PB-Na** in MeOH (5 μM) upon adding MV^{2+} (concentration range from 0 - 10 μM)

A second factor that may preclude the quenching of the **PB-Na** fluorescence by MV^{2+} is that the electron transfer reaction from the singlet excited state of **PB-Na** to MV^{2+} is thermodynamically unfavorable. To examine this possibility, electrochemical characteristics of the polymer were determined (this experiment was carried out by Romain Stalder from Dr. Reynolds' laboratory at University of Florida). **PB-a** was used in the experiment because of its good solubility in the electrochemical solvent (CH_2Cl_2). Here, we assume that the electrochemical properties of **PB-a** and **PB-Na** are similar. Figure 3-10 shows the cyclic voltammetry (CV) and differential pulse voltammetry (DPV) data of **PB-a** in DCM solution, from which an oxidation potential of ~ 1.0 V vs. Fc/Fc^+ is

observed. Given that Fc^+/Fc is 0.46 V vs. saturated calomel electrode (SCE),¹⁴¹ the oxidation potential of **PB-a** is 1.46 V vs. SCE. On the other hand, the reduction potential of $\text{MV}^{2+}/\text{MV}^+$ is -0.45 V vs. SCE,¹⁴² and the energy that is calculated from the fluorescence wavelength of **PB-a** (or **PB-Na**) is around 2.0 eV.



$$\Delta G_{\text{et}} = E_{\text{ox}} (\text{donor}) - E_{\text{red}} (\text{acceptor}) - E_{\text{fl}} \quad 2)$$

Considering a photo-induced electron transfer process that occurs between the singlet excited state of **PB-Na** and MV^{2+} , as illustrated in equation 1), the free energy change of the process can be estimated by equation 2), noting that with the polar solvent (MeOH) used in this case, the Coulombic term ($e^2/\epsilon r$) is considered negligible. Plugging in all the numbers discussed above, a free energy of ~ -0.10 eV was calculated for the process described in equation 1. This thermodynamic calculation shows that the electron transfer from the singlet excited state of **PB-Na** to MV^{2+} is at best only weakly exothermic. This result suggests that the weak quenching observed with MV^{2+} is due to the fact that the electron transfer reaction from **PB-Na** to MV^{2+} does not have sufficient driving force. For electron transfer from **PB-Na** to an electron acceptor to be efficient, the quencher must have a reduction potential less negative compared to MV^{2+} ($E_{\text{red}} > -0.4$ eV).

Further fluorescence quenching experiments that unveil the interactions between **PB-Na** and other quenchers via either charge transfer or energy transfer mechanisms were also conducted. Cupric ions (Cu^{2+}) has been found to be an efficient singlet exciton quencher in many anionic CPE systems,^{6,143,144} with quenching occur via charge

and/or energy transfer pathways. In this study, Cu^{2+} was chosen as a quencher ion due to its high affinity for CO_2^- groups. Figure 3-11 shows the fluorescence response of 5 μM **PB-Na** aqueous solution to incremental addition of Cu^{2+} . It is shown that the fluorescence of the CPE is quenched with a K_{SV} of $\sim 1.0 \times 10^6 \text{ M}^{-1}$ (For a curved Stern-Volmer plot, the first few points at low quencher concentration were used for K_{SV} calculation, Figure 3-11b), which is a typical value for Cu^{2+} quenching the CPEs that has been reported previously⁶. Without the appearance of any “aggregation band” on the emission spectra, we believe that the quenching involves energy and/or electron transfer from **PB-Na** to Cu^{2+} .

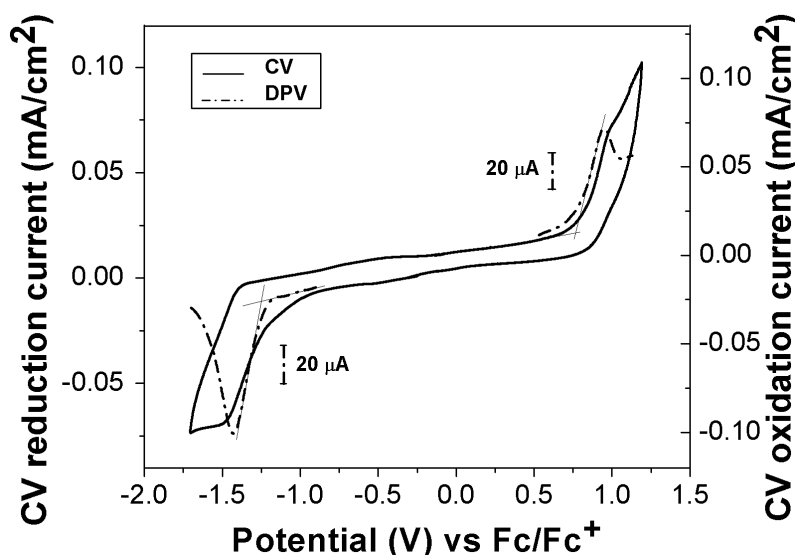


Figure 3-10. CV (solid line) and DPV (dash dot) of **PB-a**, recorded in a 0.1M TBAPF₆ in DCM solution calibrated against Fc/Fc^+

Interestingly, the fluorescence of **PB-Na** has very limited quenching (like the case of MV^{2+} , K_{SV} in the range of 10^3 M^{-1}) when other metal ions such as Ca^{2+} , Co^{2+} , Ni^{2+} , Zn^{2+} , Cd^{2+} and Pb^{2+} were titrated into the system with exactly the same condition of Cu^{2+} . These divalent ions were believed to induce aggregation of PPE based polyelectrolytes with linear side groups by bridging different polymer chains.²³ In

comparison, such “bridging effect” is much less pronounced in this study, presumably because the dendritic side groups that are modified on the polymer backbones offer a reasonable chelation to the metal ions within one unit and thus the interaction between the polymer chains is diminished.

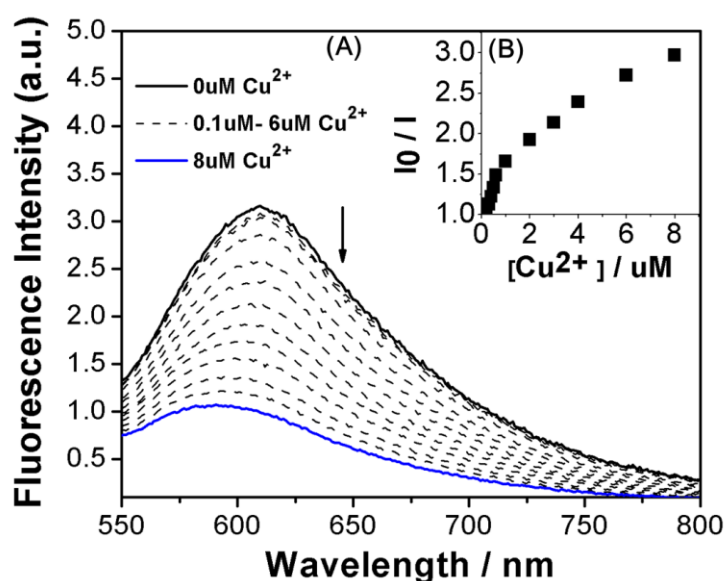


Figure 3-11. Fluorescence quenching of **PB-Na** by Cu^{2+} . A) fluorescence spectra of **PB-Na** (5 μM) with added Cu^{2+} (concentration range from 0-8.0 μM), and B) the S-V plot of the quenching process. ($K_{\text{sv}} \sim 1.0 \times 10^6 \text{ M}^{-1}$)

The amplified quenching effect was also investigated with the energy transfer quencher 3,3'-diethyloxatricarbocyanine iodide (DOTC). (The structure of DOTC is illustrated in Figure 3-12). The dye has been chosen for several reasons which include:

- 1) Good absorption spectral overlap with the fluorescence emission of **PB-Na** which gives rise to efficient Foster energy transfer.
- 2) High fluorescence quantum yield so that energy transfer can be monitored at relatively low quencher concentration.
- 3) Positively charged which facilitates the electrostatic binding between the polymer and the dye.

The fluorescence intensity of the **PB-Na** study solution (H_2O , 5 μM) was examined as a function of DOTC concentration with excitation at 450 nm, where no absorption from DOTC was observed.

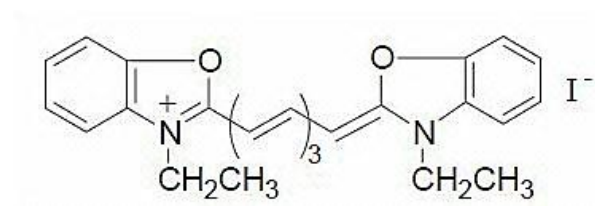


Figure 3-12. Chemical structure of DOTC

Figure 3-13 exhibits the evolution of the fluorescence of the study solution as DOTC was added. It is evident that the emission from **PB-Na** is quenched, while the emission from DOTC increases. For comparison, a control experiment was conducted where the same amount of DOTC was titrated into pure H₂O in the absence of **PB-Na**. When excited at 450 nm, there is almost no fluorescence detected from DOTC observed. This experiment clearly shows that energy transfer occurs from excited **PB-Na** to DOTC, i.e. the emission from DOTC is sensitized by the CPE. Based on the S-V plot of fluorescence quenching (Figure 3-13B), the quenching efficiency of **PB-Na** study solution is calculated to be $5.0 \times 10^5 \text{ M}^{-1}$, which is comparable to that of Cu²⁺ quenching ($1.0 \times 10^6 \text{ M}^{-1}$) discussed before.

In all the quenching experiments, the fluorescence lifetime of **PB-Na** study solution was monitored as quenchers were added. In all cases, no obvious evidence is found for lifetime-quenching, which indicates that the fluorescence quenching occurs by a static quenching process.

Above all, we have systematically investigated the fluorescence quenching behavior of this novel red-emitting CPE system featuring BODPIY-phenylene ethynylene copolymer backbone. Amplified quenching has been observed both with metal ion Cu²⁺ and cyanine dye DOTC. The quenching efficiency is comparable to typical PPE type of polyelectrolyte systems. Nonetheless, the interaction between the

PB-Na with commonly used electron acceptor MV^{2+} is not as pronounced as the literature reports, and this observation is attributed to the relatively high oxidation potential of the CPE.

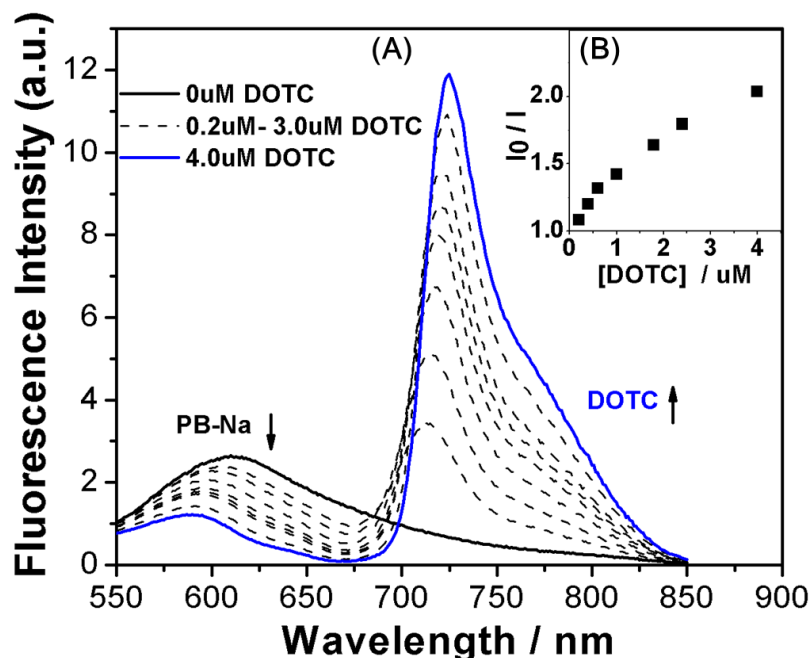


Figure 3-13. Fluorescence quenching of **PB-Na** by DOTC. A) fluorescence spectra of **PB-Na** (5 μM) with added DOTC (concentration range from 0-4.0 μM), and B) the S-V plot of the quenching process. ($K_{SV} \sim 5.9 \times 10^5 \text{ M}^{-1}$)

Application of PB-a in Dye-sensitized Solar Cells

As part of our efforts aimed at developing organic semi-conductive optoelectronic materials, we applied the **PB** system to the TiO_2 DSSCs, based on the following ideas:

1) The polymer has an extended absorption with onset at 600 nm with considerable molar absorptivity. 2) The electrochemical properties of the polymer suggest that there is a reasonable driving force for both electron injection and oxidized polymer regeneration in a TiO_2 based DSSC format. Specifically, the reductive potential E_{red} of **PB-a** (-1.4 V vs. Fc^+/Fc , Figure 3-10) is sufficiently more negative as compared to the TiO_2 conduction band (-0.9 V vs. Fc^+/Fc)¹⁴⁵, such that electron injection from **PB-a** into TiO_2 is expected. On the other hand, the oxidation potential E_{ox} of **PB-a** (1.0 V vs.

Fc^+/Fc , from Figure 3-10) is substantially more positive than the reduction potential of the iodine/iodide couple (0.24 V vs. Fc^+/Fc),¹⁴⁶ which allows the oxidized polymers to be reduced by iodide. 3) The **PB-a** is substituted with carboxylic acid groups which are widely applied as anchoring groups to bind organic dyes to the TiO_2 surfaces.^{147,148}

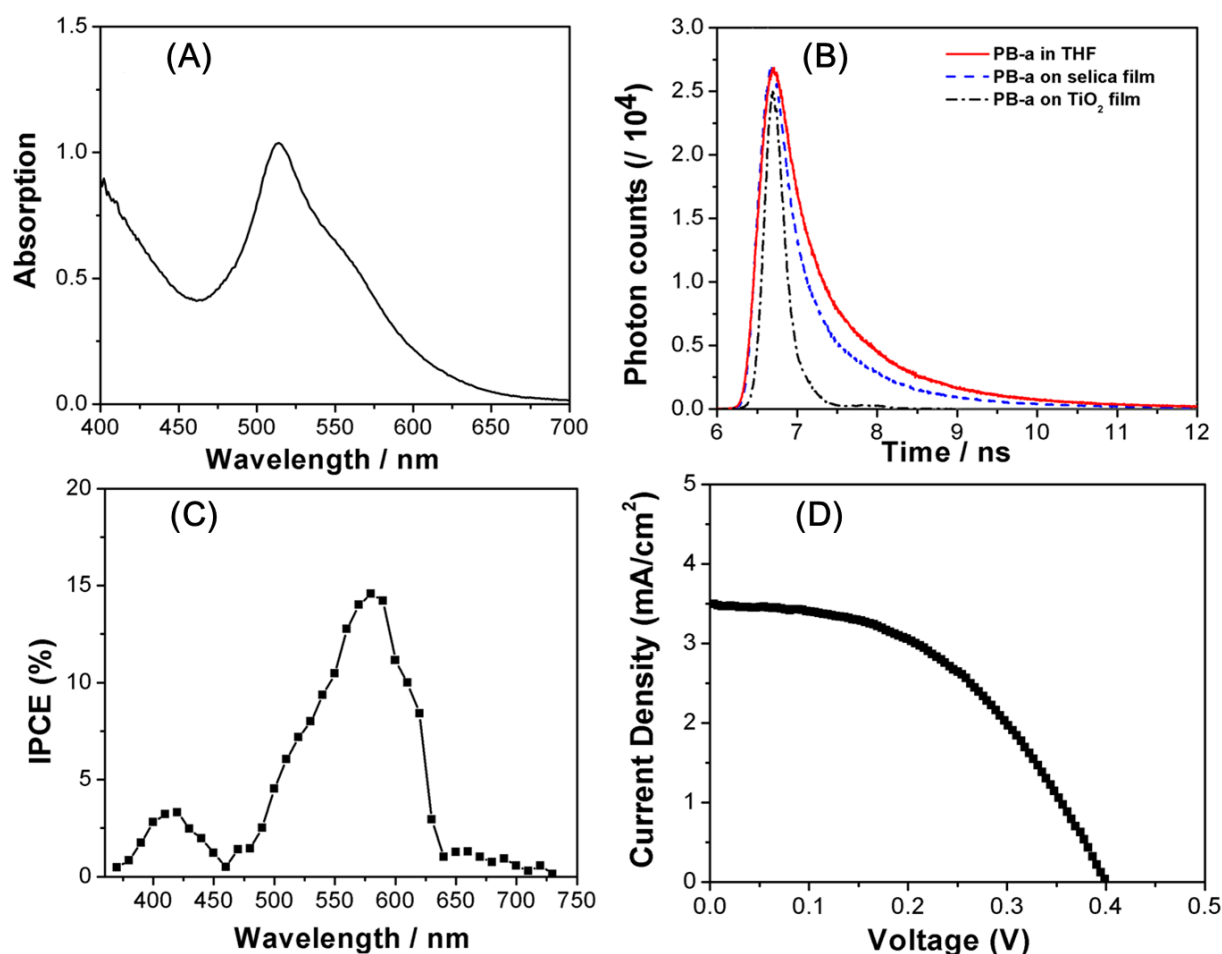


Figure 3-14. **PB-a** on TiO_2 films. A) film absorption; B) fluorescence lifetime comparison of **PB-a** in THF solution, on a silica film, and on a TiO_2 film; C) IPCE; D) J-V curve under solar AM 1.5 (PCE 0.7% FF 43%).

Experimentally, the **PB-a** coated TiO_2 films were tested in a modified reported DSSC format⁶¹ using a propylene carbonate solution of I_2/LiI as the electrolyte and a Pt/FTO counter electrode.

The IPCE and J-V curve of the as-prepared DSSC are exhibited in Figure 3-14 (Figure b and d, respectively). Comparing the IPCE curve with the film absorption profile

(Figure 3-14a), it is concluded that the main contribution to photocurrent comes from the BODIPY unit. Despite of that, the cell suffers from low photo current conversion efficiency, which leads to a rather poor cell performance (PCE~ 0.7%). To rationalize this observation and make suggestion for further improvement on the cell performances, several aspects are pointed out here. 1) It has been discussed in the photophysics of the polymer that the dendritic side group containing carboxylic acid is very likely to induce the dye aggregation. Although dye aggregation is preferable in terms of favoring light harvesting by broadening the absorption spectra, it is believed to hinder the electron injection efficiency,^{149,150} which would result in low power conversion efficiency. A general solution to this problem is either to co-adsorb the dye with additives that break the aggregation,¹⁵¹ or to structurally modify the dyes to prevent aggregation.¹⁵² 2) A recent study that was conducted in Schanze lab has revealed a correlation between polymer chain length and cell performance in DSSCs.⁶¹ It was demonstrated that unlike the conjugated polymer based bulk heterojunction solar cells, where the cell performance increases with polymer molecular weight,^{153,154} better performing cells were realized by low molecular weight polymers (PD ~ 5), which tend to achieve more surface coverage than the high molecular weight ones. By comparison, the **PB-a** used in this study has a relatively high molecular weight (DP ~18). Based on this argument, it might be worthwhile engineering the chain length of **PB-a** to optimize the dye coverage on the TiO₂ surface, and therefore increase the DSSC performance. 3) Another barrier for electron injection may come from the chemical structure of **PB-a** (Figure 3-5). It is obvious that instead of directly attached to the TiO₂, the backbone of **PB-a** is spaced

away from the “anchoring” carboxylic acid groups. Such insulation of the dye from TiO₂ surface could be a source preventing electron injection.¹⁵⁵

Finally, we looked into the photophysics of TiO₂ film adsorbed with **PB-a** for evidence of charge injection. Time resolved fluorescence spectroscopy was applied, and the fluorescence lifetime data of **PB-a** in THF solution, on a non-quenching silica gel, and on a TiO₂ film were obtained, as shown in Figure 3-14c. The fluorescence decay kinetics of **PB-a** in THF solution and adsorbed on silica are very similar, with median lifetimes of 1.51 and 1.39 ns, respectively. By contrast, when adsorbed on TiO₂ films, the **PB-a** fluorescence exhibits a 0.35 ns lifetime, indicating that the singlet excited state of **PB-a** is quenched by TiO₂. More insight is given by transient absorption (TA) measurement of **PB-a**/TiO₂ film. Figure 3-15 records the TA profile attributed to the radical cation of **PB-a** which is formed as a result of electron injection.^{61,156} The lifetime of the radical cation, which reflects the rate of charge recombination, is calculated to be 118 μ s. Compared to the literature values (200 – 300 μ s),^{61,156} the lifetime of the radical cation is relatively short, which provides another reason for low cell performance.

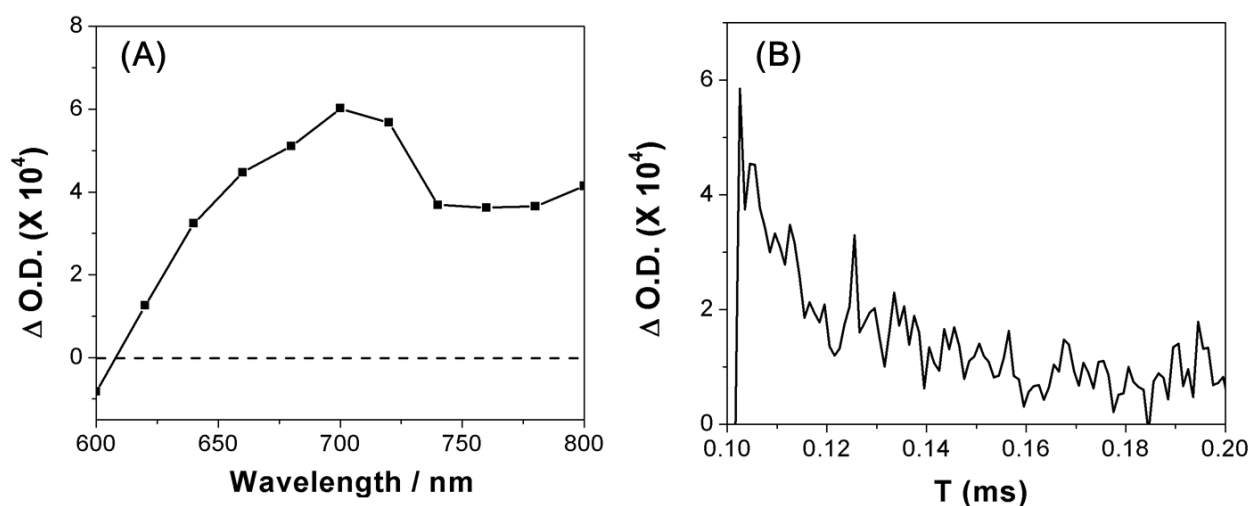


Figure 3-15. **PB-a**-TiO₂ film transient absorption. A) Transient absorption signal and B) decay profile at 700 nm. The lifetime of radical cation of **PB-a** (reflect the rate of charge recombination) was calculated to be 118 μ s.

The time-resolved fluorescence measurement and transient absorption of the **PB-a**/TiO₂ film have provided concrete evidence for electron injection, and depicted the dynamics of charge recombination. Nonetheless, the relatively low TA signal compared to the literature reports⁶¹ indicates that the charge injection yield is low, agreeing with the conclusion from IPCE results.

Summary and Conclusions

To conclude this chapter, we have synthesized a novel CPE featuring low band gap BODIPY-phenylene ethynylene copolymer backbone and branched anionic (CO₂⁻) side chains. The polymerization was effected via a precursor route utilizing a Sonogashira cross-coupling reaction that yielded the precursor polymer **PB-e**. Hydrolysis of **PB-e** was conducted under THF/TFA condition, which give rise to the carboxylic acid form of the polymer **PB-a**. The latter was treated with dilute NaOH solution and transformed to the salt form **PB-Na**. The photophysics of **PB-Na** in MeOH and H₂O is similar, indicating that the CPE is well dispersed, and thus applications of **PB-Na** in aqueous surroundings could be anticipated. The fluorescence quenching experiments show that **PB-Na** is quenched by Cu²⁺ selectively among a series of metal ions in an amplified quenching manner ($K_{sv} \sim 10^6 \text{ M}^{-1}$), and also, the energy transfer process was observed from **PB-Na** to cyanine dye DOTC. However, the electron acceptor MV²⁺ does not quench the CPE very efficiently. Electrochemical analysis shows that MV²⁺ is not a sufficiently strong oxidant to allow photo-induced electron transfer, underscoring the low HOMO energy level of the novel CPE **PB-Na**.

The carboxylic acid form **PB-a** was utilized as a sensitizer in DSSC cells with TiO₂. Electron injection from **PB-a** to TiO₂ is proved by fluorescence lifetime measurement and transient absorption experiment on **PB-a**-TiO₂ film. However, low transient

absorption signal together with relatively low IPCE suggest that insufficient electron injection yield is resulting from the cell. Structure-property discussions were initiated and future development on the **PB-a** based DSSCs are pointed out.

Experimental

Materials and Methods

All chemicals were purchased from either Fisher or Aldrich and used as received without further purification. NMR spectra were recorded either on a Varian Gemini-300 or a Mercury-300 spectrometer. Chemical shifts were referenced to residual signals from CHCl_3 (^1H 7.26 ppm and ^{13}C 77.23 ppm). UV-visible absorption spectra were obtained on a Varian Cary 100 absorption spectrometer using 1-cm quartz cells, and corrected for background due to solvent (HPLC grade). Fluorescence spectra were recorded on a Photon Technology International (PTI) fluorimeter. Fluorescence lifetime data was recorded on a PicoQuant Picoharp-300 TCSPC instrument.

E-chem measurement was conducted by Romain Stalder from Dr. Reynolds group. The electrochemistry was performed under inert atmosphere (Ar-filled glovebox) using a 3 electrode cell containing a solution of **PB-a** in 0.1 M tetrabutylammonium hexafluorophosphate (TBAPF_6) in DCM. The working electrode was a Pt-button, the counter-electrode was a Pt flag and we used a Ag/Ag^+ reference electrode calibrated against Fc/Fc^+ .

Film transient absorption experiment was conducted by Randi Price from Dr. Schanze group. The instrument setup is illustrated in Figure 3-16. A Surelite I-10 Nd:YAG laser with second and third harmonic generators delivered nanosecond pulses for excitation at 532 or 355 nm, respectively. A 250-watt quartz tungsten halogen lamp and power supply (Newport catalog #6334NS lamp and #69931 radiometric power supplies)

was used as the probe source. Light exposure of the sample is controlled by a series of shutters. Wavelengths of detection are isolated using a Cornerstone 130/m Motorized Monochromator. Transient absorption is collected using a Hamamatsu R928 PMT with an in-house custom wired base utilizing 5 of the 9 stages powered with 730 volts.

Dye-sensitized solar cells were fabricated as follows. First, a TiO_2 compact layer was spin-coated onto a clean FTO-glass slide.¹⁵⁷ The TiO_2 nanocrystalline paste (20 nm in diameter), which was received as a gift from Dr. Zhen Fang at Duke University, was doctor-bladed onto the slide with compact layer and sintered at 400°C for 30 min. The sintered electrode was immersed into the **PB-a** solution in DMF (~0.2 mM, based on repeat units) for 36 h to allow for polymer adsorption onto the TiO_2 film. The counter electrode was prepared by sputtering Pt on FTO glass with a thickness of 10 nm. Finally, an electrolyte solution containing 0.05 M I_2 and 0.1 M LiI in dry propylene carbonate was drawn into the sandwich between the TiO_2 working electrode and the Pt counter electrode by capillary action. The active area of the cell was 0.3 cm². The performance of the cells was measured immediately after they were assembled. The current-voltage characteristics of the cells were measured with a Keithley 2400 source meter under AM1.5 (100 mW/cm²) solar simulator. As for the IPCE measurements, the cells were illuminated by monochromatic light from an Oriel Cornerstone spectrometer, and the current response under short circuit conditions was recorded at 10 nm intervals using a Keithley 2400 source meter. The light intensity at each wavelength was calibrated with an energy meter (S350, UDT Instruments).

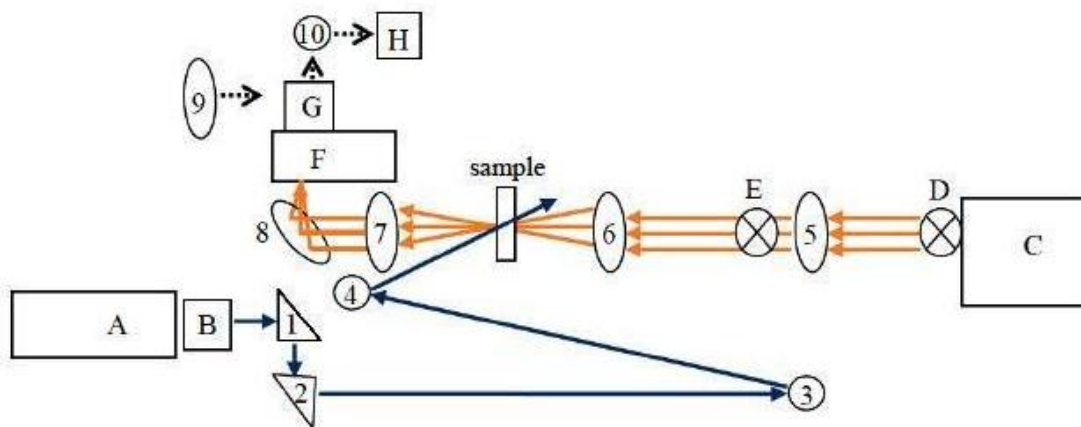


Figure 3-16. Transient absorption setup for films. *Components:* **A.** Surelite I-10 Nd: YAG laser; **B.** Second and Third Harmonic Generator; **C.** 250W QTH Lamp; **D.** Slow Shutter; **E.** Fast Shutter; **F.** Cornerstone 130/m Monochromator; **G.** PMT; **H.** APD. *Optics:* **1,2.** 1"prisms; **3,4,10.** 1"mirrors; **5,6,7.** 10cm fl. Plano convex 2" lens; **8.** 10 cm fl. Concave mirror; **9.** 5 cm Fl. Plano convex 2" lens; **10.** 5 cm fl. concave mirror.

Synthetic Procedures

Compound **1-4** were synthesized by following the literature procedures.¹⁵⁸

Compound **5**. This compound was synthesized by a modified literature procedure.¹⁵⁹ To a 250-mL round-bottom flask were charged compound **2** (5 g, 12.1 mmol), 5 mL of Et₃N and 50 mL distilled DCM. The mixture was cooled with an ice/water bath before 45 mg **4** (5.5 mmol) in 30 mL dry DCM was added via a syringe. After 2 hr, the reaction mixture was allowed to warm to room temperature and further stirred for 10 hr. The solvent was removed by vacuo, and the crude product was purified by flash chromatography (silica gel, EtOAc/hexane (1/3 v/v)) to give **5** as white powder (yield 85%). ¹H NMR (300 MHz CDCl₃, ppm): 7.13 (s, 2H), 6.60 (s, 2H), 4.35 (s, 4H), 2.25 (m, 12H), 2.03 (m, 12H), 1.42 (s, 27H). ¹³C NMR (75 MHz, CDCl₃, ppm): 172.18, 165.72, 151.57, 122.63, 86.29, 80.63, 68.83, 57.80, 30.17, 29.74, 28.09.

Compound **6**. This compound was synthesized in two steps. Step 1 is the Sonogashira cross coupling reaction between compound **5** and TMS acetylene. To a

100-mL round-bottom flask was charged compound **5** (2.55 g 2 mmol), 20 mL THF and 10 mL di-isopropyl amine (DIPA). With stirring, the solution was degassed by an argon flow for 30 min before Pd(PPh₃)₄ (10 mg) and CuI (8 mg) were charged into the reaction mixture. After the system was degassed for another 5 min, 0.84 mL (8 mmol) of trimethylsilyl acetylene was added to the reaction mixture by syringe. The reaction was allowed to run for 5 hr at room temperature before the precipitates were filtered. The filtrate was evaporated by vacuo and the solid was redissolved in DCM. The solution was washed by saturated NH₄Cl solution (30 mL × 2), brine (30 mL × 2) and water (30 mL). The organic layers were combined and dried over anhydrous Na₂SO₄ before they are passed through a short column (silica gel) to remove residue catalyst. Then DCM was evaporated, the crude product was dried under vacuum and directly used in the next step, without further purification. Step 2 is the deprotection of TMS group to yield compound **6**. The crude product of step 1 was dissolved in 30 mL DCM, the solution was degassed for 20 min before excess amount of tetra-n-butylammonium fluoride (TBAF) (2 mL) was charged into the round bottom flask. The solution turned brown immediately. After 10 min, 5 mL MeOH was added by syringe and the reaction was allowed to run for another 20 min before all solvent was removed in vacuo. The crude product was applied to flash chromatography (silica gel) using DCM/hexane (2:1 v/v) as eluent. Compound **6** was obtained as white powder after dried under vacuum. Yield 1.54 g (72% for two steps). ¹H NMR (300 MHz, CDCl₃, ppm) δ 6.94 (s, 2H), 6.63 (s, 2H), 4.37 (s, 4H), 3.63 (s, 2H), 2.23 (t, 12H), 2.01 (t, 12H), 1.42 (s, 54H). ¹³C NMR (75 MHz, CDCl₃, ppm) δ 172.46, 166.47, 153.12, 117.87, 114.07, 85.05, 80.87, 79.00, 68.44,

57.78, 30.39, 29.85, 28.30. ESI-TOF-MS calcd for $C_{58}H_{88}N_2O_{16}Na$ 1091.6026, found $[M+Na]^+$ at 1091.6070.

2-(2-(2-Methoxyethoxy)ethoxy)ethyl p-tosylate (7). This compound was prepared by a modified reported procedure.¹⁶⁰ To a 500-mL round-bottom flask was added sodium hydroxide (8 g, 0.2 mol) in water (30 mL) with vigorous stirring. When NaOH was fully dissolved, triethylene glycol monomethyl ether (16 g, 0.1 mol) in THF (50 mL) was charged. The reaction mixture was cooled to 0°C by ice bath before a solution of p-tosyl chloride (19 g, 0.1 mol) in THF (50 mL) was added dropwise over 30 min. The reaction mixture was then warmed to room temperature and stirred for overnight. Water (100 mL) was then added to the resulting solution which was acidified by sulfuric acid (3 M). The solution was extracted with DCM (3 × 50 mL), the combined organic layers were washed with brine (3 × 100 mL), dried with sodium sulfate anhydrous, and concentrated in vacuo to give 27.67 g (0.087 mol, 87%) of pure **7** as a colorless oil. ¹H NMR (300 MHz, CDCl₃, ppm) δ 7.79 (d, J = 8.2 Hz, 2H), 7.33 (d, J = 8.7 Hz, 2H), 4.16-4.14 (m, 2H), 3.69-3.67 (m, 2H), 3.59-3.56 (m, 6H), 3.51-3.49 (m, 2H), 3.35 (s, 3H), 2.43 (s, 3H). ¹³C NMR (75 MHz, CDCl₃, ppm) δ 144.62, 132.66, 129.54, 127.82, 71.60, 70.42, 69.02, 68.26, 58.59, 21.30.

4-(2-(2-(2-Methoxyethoxy)ethoxy)ethoxy)benzaldehyde (8). This compound was synthesized by a modified literature procedure.¹⁶¹ To a 500-mL round-bottom flask was added 2.05 g (20.5 mmol) 4-hydroxybenzaldehyde, 8.4 g (60 mmol) anhydrous K₂CO₃ powder and 150 mL DMF. The reaction mixture was heated to 85°C before 6.85 g (21 mmol) compound **7** was charged to the reaction mixture. The reaction was allowed to run for overnight before 200 mL H₂O was added. The mixture was extracted

with DCM (3 × 80 mL), the organic layers were combined and washed by 0.1 M HCl solution (2 × 30 mL) and brine (2 × 30 mL) before drying with anhydrous Na₂SO₄. The crude product was purified by flash chromatography (silica gel) using DCM as eluent. Yield 4.23g (79%). ¹H NMR (300 MHz, CDCl₃, ppm) δ 9.81 (s, 1H), 7.77 (d, 2H), 6.96 (d, 2H), 4.16 (t, 2H), 3.83 (t, 2H), 3.70-3.67 (m, 2H), 3.64-3.58 (m, 4H), 3.50-3.47 (m, 2H), 3.31 (t, 3H). ¹³C NMR (75 MHz, CDCl₃, ppm) δ 190.88, 163.97, 132.05, 130.14, 115.02, 72.06, 71.04, 70.80, 70.72, 69.62, 67.93, 59.18.

BODIPY compound (9). This compound was prepared by a modified literature procedure.¹²⁶ To a 500-mL round-bottom flask was charged 2.30 g (8.57 mmol) of compound **8** and 200 mL of freshly distilled DCM. The reaction mixture was degassed for 30 min before 2,4-dimethylpyrrole (1.64 g, 17.2 mmol) was added quickly to the solution along with a few drops of trifluoroacetic acid (TFA). The reaction was covered by aluminum foil and allowed to run for 12 hr. Then 1.8 g of 2,3-dichloro-5,6-dicyano-1,4-benzoquinone (DDQ) was quickly added to the reaction mixture with vigorous stirring. The reaction was continued for 1 hr before 18 mL of triethylamine (TEA) and 18 mL of BF₃•OEt₂ was charged into the solution. The reaction was quenched by adding 200 mL H₂O after another hour stirring. The organic layer was washed by saturated NH₄Cl solution (3 × 80 mL) and H₂O (2 × 50 mL) and dried with anhydrous Na₂SO₄. After filtration, DCM was evaporated under reduced pressure. The dark crude product was allowed to pass through a 3-inch column (silica gel) quickly under pressure. The eluent was a mixture of DCM and hexane (1:8 v/v). The resulting brown oil (0.7 g, ~ 1.4 mmol) was directly used without further purification in the preparation of compound **10**.

BODIPY monomer (10). This compound was prepared using a modified literature procedure.¹²⁶ All compound **9** (0.7 g, 1.4 mmol) from the last step (could contain some impurity) was charged into a 100-mL round-bottom flask with 45 mL of absolute EtOH. With stirring, 0.5 g of I₂ (4 mmol I atom) and 0.5 g of (2.8 mmol) HIO₃ were charged into the flask. 30 min later the color of the reaction mixture turned from green to red-orange. The reaction was allowed to run under room temperature for 5 hr before 50 mL of DCM was added to the solution. With stirring, saturated Na₂S₂O₃ aqueous solution was added to quench the excess I₂, the aqueous layer was extracted with DCM, which is later combined with the organic layer. The organic layer was washed with saturated Na₂SO₃ solution (2 × 50 mL), saturated Na₂CO₃ solution (2 × 50 mL), and H₂O (2 × 50 mL) before drying with anhydrous Na₂SO₄. The organic solvent was evaporated and the crude product was purified by flash chromatography (silica gel) using ethyl acetate/hexane (1:4 v/v) as eluent. Yield 0.66 g (64%). ¹H NMR (300 MHz, CDCl₃, ppm) δ 7.12 (d, 2H), 7.05 (d, 2H), 4.20 (t, 2H), 3.92 (t, 2H), 3.78-3.66 (m, 6H), 3.57 (t, 2H), 3.39 (s, 3H), 2.63 (s, 6H), 1.43 (s, 6H). ¹³C NMR (75 MHz, CDCl₃, ppm) δ 160.01, 156.78, 145.60, 141.77, 131.92, 129.26, 127.07, 115.73, 85.73, 72.17, 71.13, 70.90, 70.82, 69.92, 67.81, 59.29, 17.41, 16.23. ESI-TOF-MS calcd for C₂₆H₃₁BF₂I₂N₂O₄Na 761.0332, found [M+Na]⁺ at 761.0434.

PB-e was synthesized by a modified literature procedure.¹²⁶ To a 25-mL Schlenk flask, 150 mg (0.14 mmol) of dendritic monomer **6** and 103 mg (0.14mmol) of BODIPY monomer **10** were dissolved in a mixed solvent of 5 mL of THF and 5 mL of DIPA. The system was degassed by bubbling argon flow for 30 min. The system was subsequently frozen by liquid N₂ before 10 mg of Pd(PPh₃)₄ and 8 mg of CuI were charged to the flask.

The reaction mixture was allowed to go another two freezing- argon cycle before they were heated to 60°C. The reaction was vigorously stirred avoiding light under the protection of argon for 36 hr. A dark red fluorescent solution resulted. The reaction mixture was passed through a 4-inch aluminum oxide column (with argon pressure and flushed by THF) to remove the catalysts and ionic side products (ammonium iodide salts) before it was concentrated under vacuum to around 3 mL. The concentrated solution was added to 30 mL of MeOH whereupon a dark purple precipitate formed. The precipitate was washed by MeOH and redissolved in 3-5 mL of CHCl₃. The CHCl₃ solution was precipitated by MeOH again. Such precipitation- redissolving process was repeated for 3 times before GPC and NMR characterization suggested achieving of pure polymer. Yield 118 mg. GPC: Mn = 28,150, PDI = 1.6. ¹H NMR (300 MHz, CDCl₃, ppm) δ 7.23- 6.96 (broad, Ph-H, 6-7 H) 6.35 (broad, NH-H, 2H), 4.45 (broad, 4-5 H), 4.18 (broad, 2H) 3.90 (broad, 2-3 H), 3.75-3.65 (broad, 12H), 3.59-3.55 (broad, 3-4H), 3.38 (s, 3H), 2.70-2.63 (broad, 6H), 2.14-2.05 (broad, 14-15H), 2.00-1.88 (broad, 14H), 1.59 (broad, 6H), 1.37 (broad, 72H).

PB-a In a 50-mL round-bottom flask, 80 mg of **PB-e** was dissolved in a mixed solvent of 10 mL of THF and 10 mL of TFA. With vigorous stirring, the reaction was allowed to run for overnight. The dark red fluorescence was almost quenched. The reaction mixture was concentrated and **PB-a** was precipitated and washed with acetone. The product was dried under vacuum before it was characterized by NMR. ¹H NMR (300 MHz, CDCl₃, ppm) δ 7.23-7.00 (broad Ph-H 6H) 6.56-6.26 (broad, N-H 2H), 4.52-4.30 (broad, 12H), 4.23-4.11 (broad, 8H), 3.95-3.48 (broad, 36H), 3.38-3.33 (broad 18H), 2.86-2.57 (broad, 24H), 2.20-1.76 (broad, 50H).

PB-Na MeOH (2 mL) that contained 0.1 mM NaOH was used to dissolve **PB-a** and the resulting solution was slowly added to 50 mL H₂O with pH 9. The water soluble polymer was dialyzed against a NaOH/water (Millipore NanopureTM) solution (pH 8.5) under dark for 3 days. The resulting polyelectrolyte (**PB-Na**) aqueous solution was concentrated by means of freeze drying to ~10 mL. The concentration of the CPE was measured by gravimetric analysis, which was calculated as 0.8 mg/ mL, or 0.6 mM (repeat unit). The stock solution was degassed and stored from light under 4°C.

CHAPTER 4
PHOSPHONIC ACID FUNCTIONALIZED π -CONJUGATED PHOTOACTIVE
OLIGOMERS: PHOTOPHYSICAL PROPERTIES, INTERACTIONS WITH CDSE
NANOCRYSTALS, AND APPLICATION IN DYE-SENSITIZED SOLAR CELLS

Hybrid Materials Based on Conjugated Oligomers

Organic/inorganic hybrid materials are broadly defined as mixtures of organic molecules and inorganic materials at molecular level.¹⁶² First introduced in the late 1980s, these materials have shown promising functionalities and applications in photocatalysis,¹⁶³ solar fuels,¹⁶⁴ and photovoltaics.^{165,166} Specifically, organic semiconductor/inorganic nanocrystal (NC) hybrids are materials that not only inherit characteristics from both the organic and inorganic components, but also exhibit new features due to the interactions (such as energy transfer/charge transfer) between different phases.⁶² Inspired by Alivisatos and co-workers' early work on optoelectronic devices based on conjugated polymer/CdSe NCs hybrid films,^{63,64} a great deal of research interest has focused on developing organic semiconductor/inorganic NC hybrids and exploring their applications in photovoltaic energy harvesting and optoelectronic devices.⁶⁵⁻⁷⁶

The major challenge that these devices faced was that device performance was the dramatic effect of morphology of the mixtures on device performance.⁶⁸ It was demonstrated that inorganic NCs tend to aggregate to form NC cluster islands in the organic polymer matrix.¹⁶⁷ Such "phase segregation" effect, unfortunately, diminished the interaction between components, thus largely limiting device performance. Coating surfactants on the surface of inorganic NCs facilitated their dispersion in organic phases, but the insulating nature of the surfactants largely reduced the efficiency of charge transfer between the organic SC and inorganic NCs.⁹⁹ Another strategy to improve

communication between the NCs and organic SCs was to engineer the shapes of the inorganic NCs on a three-dimensional scale, so that the interpenetration of the organic and inorganic phases was optimized.^{79,168,169} Unfortunately, state-of-art intimate nanocomposites of organic semiconductor and inorganic NC hybrids were hardly achieved.⁶⁸

A third approach has proven to provide better control of both the morphology of the hybrid films and the surfactant composition on the NC surfaces. Instead of physically blending the components, the organic molecules were functionalized with “anchoring groups” that attach to the surface of the NCs through covalent bonds. For instance, in an early work that studied the morphology of regioregular poly(3-hexylthiophene) (P3HT)/CdSe NC films, Frechet and co-workers discovered that end-functionalized P3HT enhanced the performance of P3HT/CdSe solar cells by increasing the dispersion of CdSe nanocrystals without introducing insulating surfactants.⁶⁸ To date, a number of “anchoring groups” have been employed to facilitate the communication between organic SCs and inorganic NCs. Among them, phosphine oxide,^{75,76} thiol groups,^{83,84} carbodithioic acids,^{73,85,86} carboxylic acids,⁸⁷⁻⁸⁹ phosphonic acids,^{67,90} amines,⁶⁸ and anilines⁷³ are commonly described in the literatures. Regarding the synthetic methodology of these hybrid materials, both “graft to”^{67,68,71,73,75,76} (by synthesis of organic oligomer/polymers prior to linking to NCs) and “graft from”⁶⁹ (precursors modification on NCs prior to formation of oligomer/polymer phases) methods have been developed. As introduced in Chapter1, the “graft to” method, although relatively more tedious in terms of synthesis, has the advantage of providing

mono-dispersed hybrid materials, resulting in better processability,⁶⁷ energy^{70,75}/ charge transfer⁶⁷ at the molecular level, and increased device performance.⁶⁸

In this chapter, we will discuss a series of π -conjugated oligomers with different bandgaps. These oligomers are all functionalized with a phosphonic acid group on terminal for attachment to the surfaces of CdSe NCs. The interactions between the oligomers and CdSe NCs are studied both in solution and in the form of solid hybrid films. As part of our efforts to develop high efficiency photovoltaics, the functionalized oligomers are also utilized in dye-sensitized solar cells (DSSCs) with TiO₂ NC films. Preliminary results show that these conjugated oligomers have promising applications in DSSCs.

The project being described in this chapter involves a combination of efforts from several research groups at the University of Florida, as listed in Table 4-1. The focus of this chapter will be on the work conducted in the Schanze group, yet to maintain the integrity of the entire “story” and the flow of the paper, data and figures from the other two groups will also be briefly covered (with consent of the collaborators).

Table 4-1. Contributions made by several groups to the project

Research group (PI / Researcher)	Kirk Schanze / Dongping Xie	John Reynolds / Romain Stalder	Jiangeng Xue / Renjia Zhou
Contributions	Synthesis of OPE		
	Photophysical and PL quenching measurements	Syntheses of T6 and T4BTD	Syntheses of CdSe NCs
	Syntheses of oligomer-CdSe hybrids	Electro-chemical measurements	Hybrid device fabrications and IPCE measurements
	DSSC devices	TGA	TEM imaging

Results and Discussions

Synthesis and Structural Characterizations

The oligomers were designed as electroactive rods bearing a phosphonic acid functional group at one end (Figure 4-1). Achieving such asymmetric structures normally requires stepwise synthesis, in which the aromatic units are installed one after another onto the conjugated backbones, a process known as “combinatorial chemistry”.¹⁷⁰ In this work, we employed an alternative method in which a series of subunits was synthesized before assembled with a “central” unit in a one-pot reaction to provide the final product. This method is much less tedious without compromising product yield, thanks to the large difference in polarity between the products and side products. In Figure 4-2, we use the synthesis of **OPE** oligomer as an example to discuss the methodology.

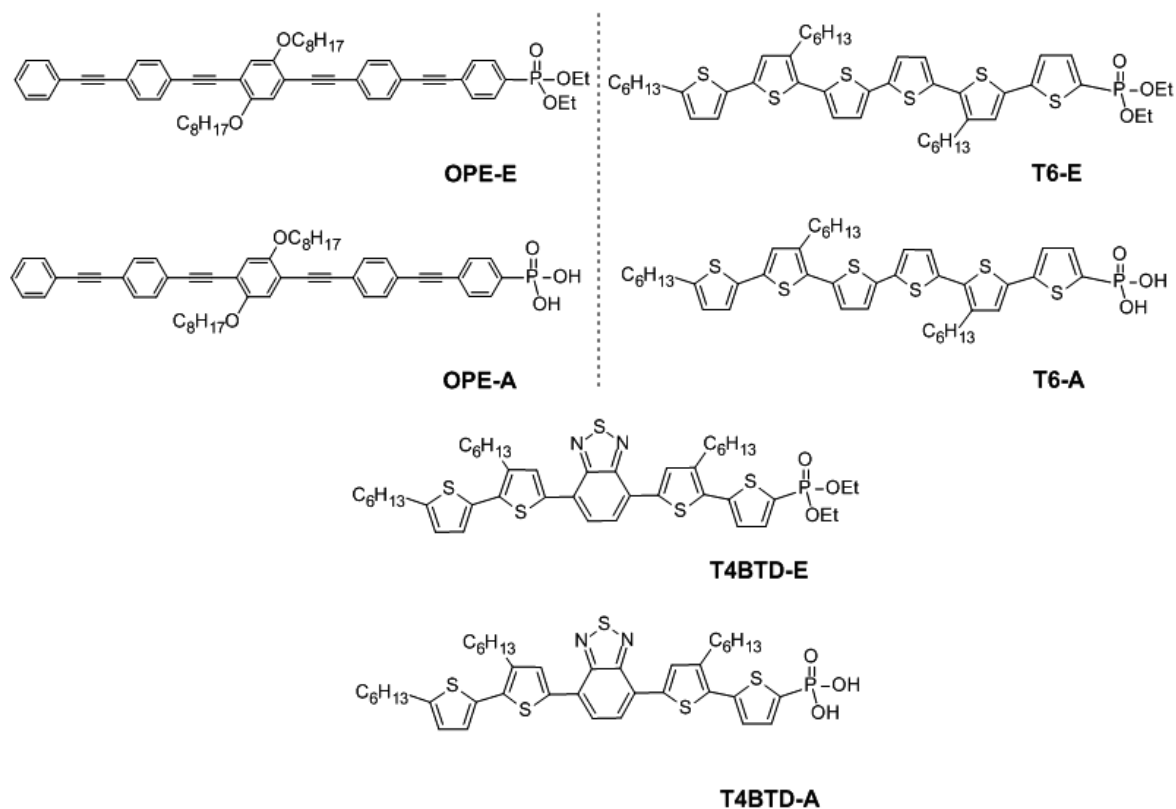


Figure 4-1. Chemical structures of conjugated oligomers studied in this work.

Synthesis of the **OPE** oligomer bearing one phosphonic acid group (**OPE-A**) begins with the alkylation of hydroquinone into **1** followed by iodination of the benzene ring to afford **2**, which is the precursor to the central benzene ring in **OPE-A**. The two other precursors to **OPE-A**, the extended phenylene ethynylene moieties **4** and **7**, were both synthesized from 1,4-diiodobenzene. Under Sonogashira cross-coupling conditions, phenylene acetylene and propargyl alcohol were added to yield **3**, which was subsequently deprotected under basic conditions to afford the di(phenylene ethynylene) **4**. In a nickel-mediated Arbuzov type reaction with one equivalent of triethylphosphite, 1,4-diiodobenzene was converted to diethyl (4-iodophenyl)phosphonate **5**. Similar conditions as described for **3** were applied to transform 1,4-diiodobenzene into intermediate **6**, which was then coupled with **5** to generate the di(phenylene ethynylene) **7**, bearing a phosphonate group on one end and a terminal alkyne on the other. Precursors **2**, **4** and **7** were then reacted in a one-pot reaction to yield the phosphonate-mono-functionalized oligo(phenylene ethynylene) **OPE-E**. The symmetrical side products (the non-functionalized and the di-functionalized OPEs) were readily removed by column chromatography, based on the substantial difference in polarities of the compounds. The last steps towards the phosphonic acid **OPE-A** involved treatment of the phosphonate **OPE-E** with trimethylsilyl bromide in DCM, followed by hydrolysis with methanol.

The detailed synthetic procedures for the **T6** and **T4BTD** oligomers are not discussed in this work (Table 4-1). In brief, the oligomer backbones were built under Pd-catalyzed Suzuki or Stille coupling conditions. The same methodology used in **OPE** synthesis was applied to prepare the **T6** and **T4BTD** oligomers. In each case, the

phosphonic acid group was first introduced as ethyl ester **T6-E** or **T4BTD-E**, which was subsequently hydrolyzed to yield the acid products **T6-A** or **T4BTD-A**. In all, we collected six conjugated oligomers end-capped with either phosphonate or phosphonic acid groups (Figure 4-1). The purity of the oligomers was demonstrated by NMR and MS spectroscopy.

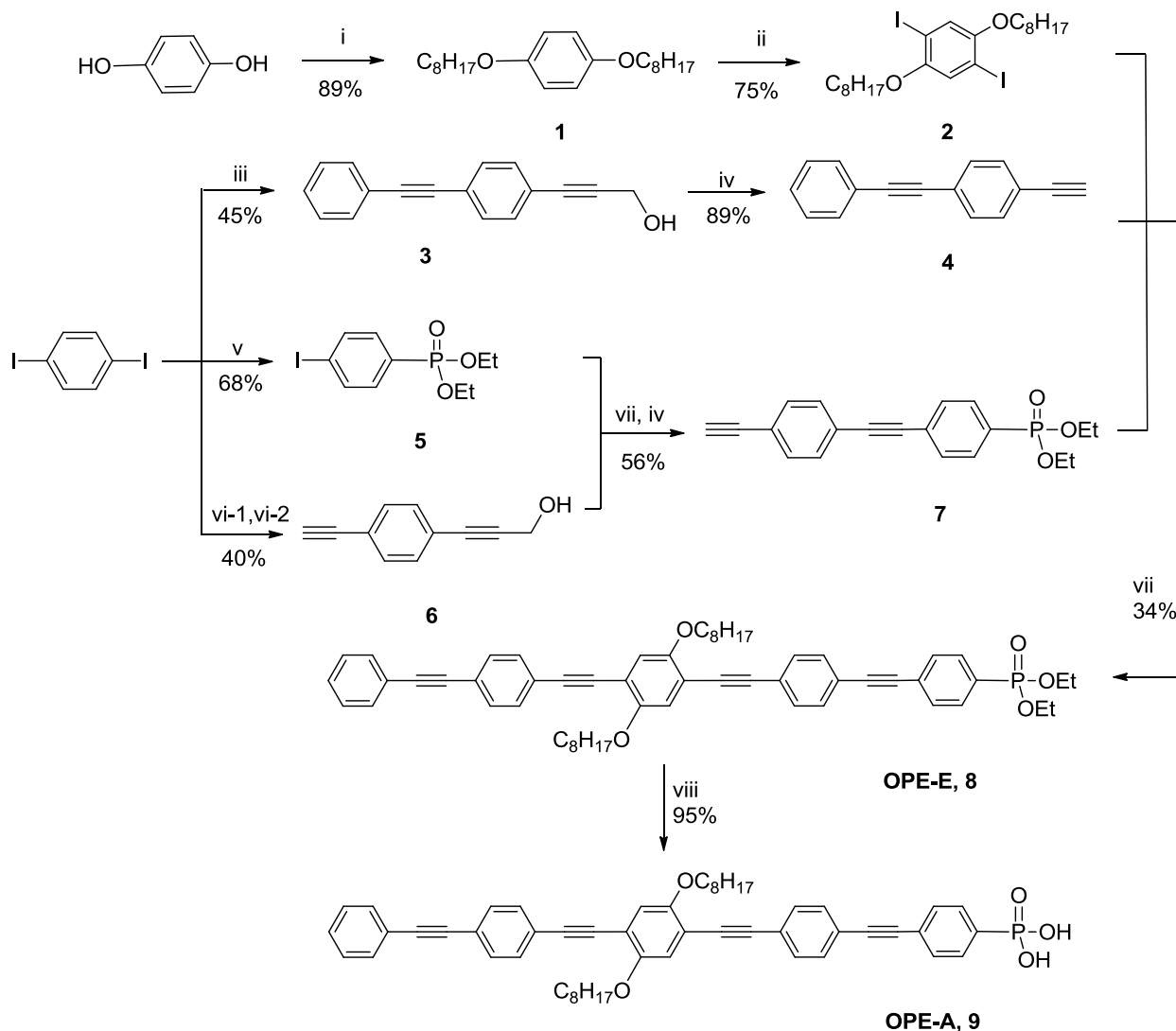


Figure 4-2. Synthesis of **OPE-E** and **OPE-A**. (i) KOH, C₈H₁₇Br, DMF; 80°C, overnight; (ii) I₂, KIO₃, AcOH, H₂SO₄, H₂O; reflux, 24hr; (iii) propargyl alcohol, phenylene acetylene, Pd(PPh₃)₄, CuI, THF, r.t; overnight; (iv) MnO₂, KOH, Et₂O r.t; 5h; (v) P(OEt)₃, NiCl₂, neat; 145°C, 30min; (vi-1) trimethylsilyl acetylene, propargyl alcohol, Pd(PPh₃)₄, CuI, THF, r.t; overnight; (vi-2) K₂CO₃, DCM, MeOH, r.t. 4h; (vii) Pd(PPh₃)₄, CuI, THF, r.t; overnight; (viii) trimethylsilyl bromide, MeOH

The CdSe NCs used in this study were synthesized by Dr. Xue's group at the University of Florida (Table 4-1), following a previously reported procedure with modifications.^{171,172} The NCs were nano-spherically shaped with 6.5 nm diameter (by TEM), carrying trioctylphosphine oxide (TOPO) as the surfactant.

Photophysics of the Oligomers and CdSe NCs

The UV-vis absorption and fluorescence spectra of **OPE-A**, **T6-A**, **T4BTD-A** and CdSe NCs were obtained as shown in Figure 4-3. All the absorption spectra feature a strongly allowed long wavelength absorption band, which shifts systematically from 393 nm for **OPE** to 425 nm for **T6** to 505 nm for **T4BTD**. High molar absorptivities of 30,000 – 50,000 M⁻¹cm⁻¹ were calculated, as summarized in Table 4-2. From the absorption onset of **OPE-A** and **T6-A** in solution, relatively high energy gaps of 2.8 eV and 2.4 eV respectively, were calculated, as expected of oligomers with homogeneous π -electron systems. The **T4BTD** oligomer, on the other hand, features a longer wavelength absorption onset corresponding to a lower HOMO-LUMO gap of 2.0 eV. This is due to the donor-acceptor (DA) interaction attributed to the mixing of the BTD acceptor unit with the flanking bithiophene donors.¹⁷³ The extinction coefficient of **T4BTD** is lower compared to that for **OPE** or **T6**, which is consistent with the DA transition.

The photoluminescence of each oligomer, in both the ester and acid forms were recorded in dilute chloroform solution. All oligomers exhibit intense fluorescence with quantum yield near or above 50%. The peak emission wavelengths red-shifted proceeding from **OPE** to **BTD**, 434 nm for **OPE-A**, 565 nm for **T6-A** and 676 nm for **T4BTD-A**. This trend agrees with the phenomena observed in UV-vis spectra. Additionally, the emission band width and the Stokes shift are greater for BTD, reflecting the charge transfer nature of the excited states. Fluorescence lifetimes were determined

for the oligomers. In each case, the fluorescence decay exhibits single exponential kinetics. Little difference between the acid and ester forms for each oligomer was observed, indicating that the acid forms of the oligomers are well dispersed in dilute solutions. While the **OPE** and **T6** oligomers show short fluorescence lifetime of 0.9 – 1.0 ns, the **T4BTD** oligomers exhibit significantly longer lifetimes of 5 ns. The longer lifetime for **T4BTD** results from a much lower radiative rate (ca. 0.16 ns^{-1}), and this is again consistent with the DA nature of the fluorescent excited state.

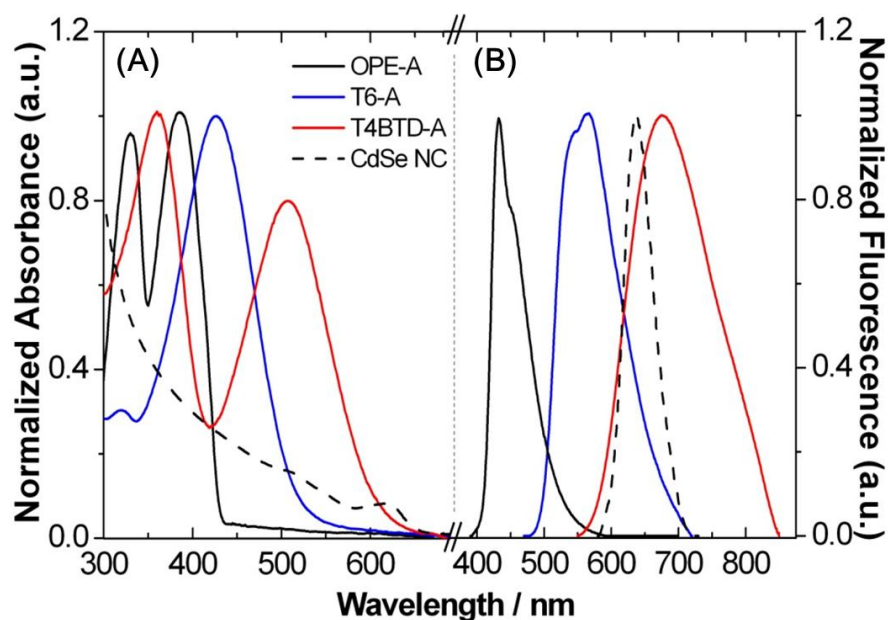


Figure 4-3. Photophysical characterization of the oligomers. A) Normalized UV-vis absorption and B) photoluminescence spectra of **OPE-A** (black), **T6-A** (blue), **T4BTD-A** (red) and the CdSe NCs (dashed) in chloroform.

The CdSe NCs have a long wavelength absorption peak at 624 nm, characteristic of the quantum confinement effect, and the absorption rises steadily towards the UV region of the spectrum. An optical energy gap of 1.9 eV is calculated from the onset of absorption, which is in accordance with the size of the NCs.¹⁷⁴ The low PL quantum yield of CdSe NPs is presumably due to formation of defect states at the CdSe NC surfaces during the removal of excess TOPO and oleic acids (reagents that are used

during the syntheses of the NCs).¹⁷¹ Compared to passivated CdSe NCs that are surrounded by TOPO groups, the CdSe NCs used in this study have relatively both shorter PL lifetime and lower PL quantum yield.¹⁷⁵ Table 4-2 summarizes all the photophysical characterizations of the oligomers and the CdSe NCs in chloroform solution.

Table 4-2. Photophysical data for the oligomers and CdSe NCs in CHCl₃ solution.

	$\lambda_{\text{max}}^{\text{abs}}$ (nm)	Optical ΔE^a (eV)	$\epsilon_{\text{abs}}^{\text{abs}}$ (M ⁻¹ cm ⁻¹)	$\lambda_{\text{max}}^{\text{Fl}}$ (nm)	Stokes Shift (cm ⁻¹)	Φ_F	τ_{Fl} (ns)
OPE-E	381	2.8	42700	436	3100	0.79 ^c	0.91
OPE-A	383	2.8	33800	434	3068	0.53 ^c	0.89
T6-E	424	2.4	55600	537/564	5854	0.54 ^c	0.86
T6-A	426	2.4	48700	539/565	5775	0.49 ^c	0.85
T4BTD-E	504	2.1	30000	675	5026	0.71 ^d	5.60
T4BTD-A	508	2.0	21000	676	4892	0.71 ^d	5.55
CdSe NC	624	1.9	632000 ^b	650	641	0.001 ^d	1.26 ^e

^a from low-energy onset of absorption in the solution UV-vis spectra. ^b calculated by the method described in ref¹⁷⁴. ^c quinine sulfate in 0.1 M sulfuric acid ($\Phi_F = 0.54$) as standard. ^d Ru(bpy)₃Cl₂ in H₂O ($\Phi_F = 0.056$, degassed) as standard ^e average lifetime from a multi-exponential decay

E-chem Characterizations

The measurement of redox properties of the oligomers was conducted in Dr. Reynolds group, and detailed experimental procedures can be found in Romain Stalder's dissertation (2012 University of Florida). Briefly, the HOMO and LUMO levels of the oligomers in solution were investigated by means of both cyclic voltammetry (CV) and differential pulse voltammetry (DPV). **OPE-A** has a HOMO energy level at −5.84 eV, **T6-A** at −5.32 eV and **T4BTD-A** at −5.50 eV vs vacuum. In the case of **T4BTD-A**, the LUMO energy is measured from the reductive DPV onset to be at −3.55 eV, giving an

electrochemical energy gap of 1.95 eV, which is quite close to the optical energy gap value of 2.0 eV calculated from its UV-vis spectrum. Unfortunately, the reductive DPV for **OPE-A** or **T6-A** were difficult to measure due to the electron-rich nature of the two oligomers. Thus the electrochemical estimation of LUMO energies for the latter two oligomers is not available. Given the fact that for **T4BTD** the energy gap measured electronically is reasonably close to that calculated from the optical spectra, we make the assumption that the spectral values are valid in the cases **OPE** and **T6** oligomers. Therefore, the corresponding optical energy gaps listed in Table 4-2 were employed to deduce the energies of the LUMOs for **OPE-A** and **T6-A**, which were calculated at – 3.04 eV and –2.92 eV vs vacuum, respectively. Figure 4-4 depicts the position of the HOMO and LUMO energy levels for the three oligomers.

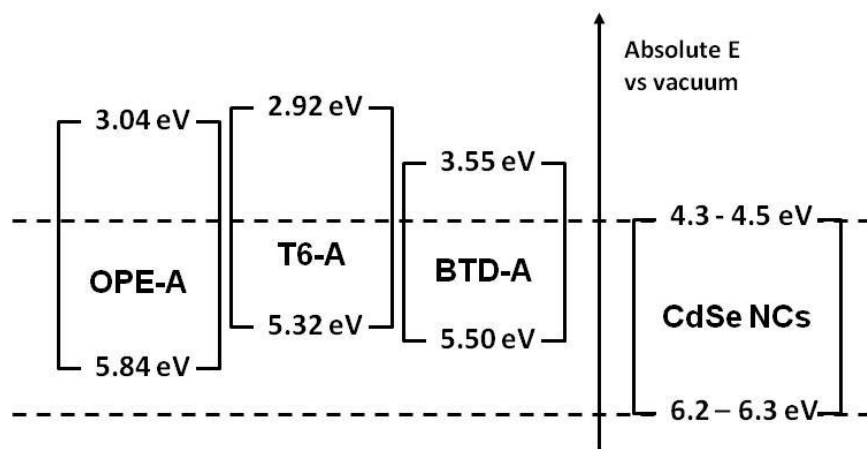


Figure 4-4. Energy level alignment of the oligomers and CdSe. Band structure diagram comparing the HOMO and LUMO levels of **OPE-A**, **T6-A** and **T4BTD-A** and their offsets relative to the CdSe NCs.

According to the literature, the positions of the conduction band (CB) and valence band (VB) of the CdSe NCs used in this study are set between –4.3 and –4.5 eV, and between –6.22 and –6.3 eV respectively.¹⁷¹ The energy diagram of CdSe NCs is drawn parallel with those of the oligomers in Figure 4-4. In each case, the LUMO level of the

oligomer is more than 1 eV higher than the CB of the NCs and the HOMO level of the oligomer is more than 0.5 eV higher than the VB of the NCs. Based on such energy configuration, it is expected that upon formation of hybrids between the oligomers and the CdSe NCs, photoexcitation of either the oligomer or the NC will give rise to electron transfer from the oligomer to the NC.

Photoluminescence Quenching of the Oligomers and NCs

As described in Chapter 1, photoluminescence quenching has been used as a “indicator” for energy/charge transfer between chromophores. Applying the same method, we sought evidence of energy/charge transfer at the oligomer/CdSe NCs interfaces by examining the evolution of the fluorescence spectra of the oligomers upon incremental addition of CdSe NCs in CHCl_3 solution. Furthermore the difference between evolutions for the phosphonate ester protected oligomers was compared with the oligomers modified by phosphonic acid groups. Figure 4-5a shows the PL evolution for **OPE-E** and **OPE-A** in dilute chloroform (5 μM) as CdSe NCs (chloroform solution) was titrated into the study solution. The increments were chosen so that each addition doubled the concentration of CdSe NCs in the oligomer solution, until an oligomer: CdSe molar ratio of 50:1 was reached. The relative concentrations of the starting solutions (oligomer and CdSe NCs) were such that only microliters of CdSe solution were needed for a fixed volume of 2 mL of oligomer solution to achieve the designed ratio. Therefore the effect of dilution on the PL intensity could be neglected.

For **OPE-E**, the addition of the CdSe reduced the oligomer fluorescence by 25% at the 50:1 ratio. Since the fluorescence lifetime of the result solution remained the same with that of the pure **OPE-E**, diffusional quenching could be ruled out. We believe that the reduction of **OPE-E** fluorescence is due to the absorption of CdSe NCs at 436 nm

(acting as a neutral density filter). By comparison, when the acid form **OPE-A** was subjected to the same procedure, significant luminescence quenching was observed. Over 90% of fluorescence was quenched when the molar ratio of **OPE-A**: CdSe NCs equaled 50:1.

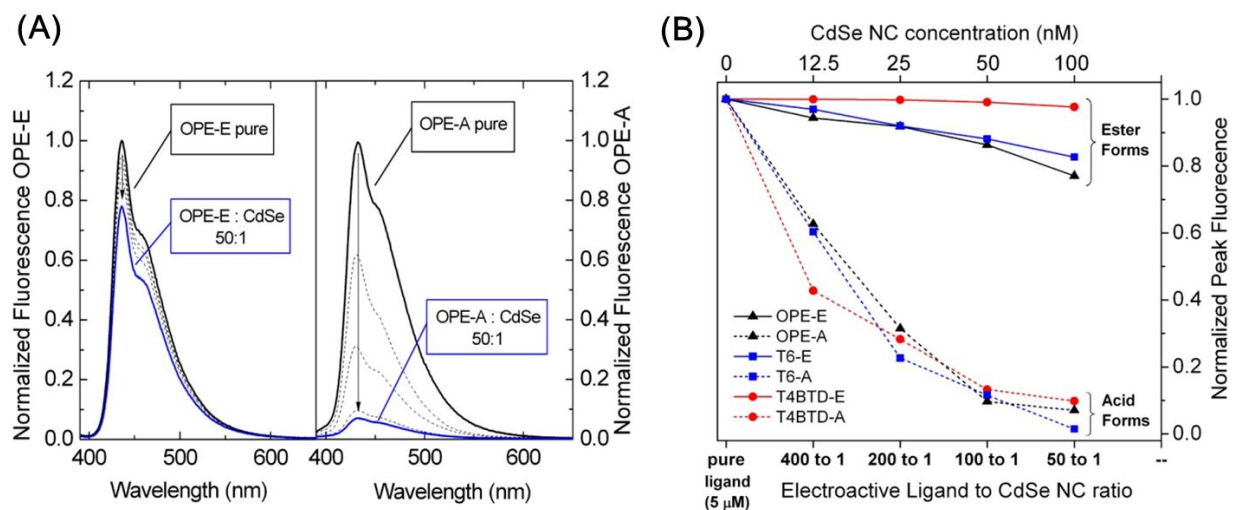


Figure 4-5. Fluorescence quenching of the oligomers by CdSe. A) Evolution of the fluorescence of **OPE-E** and **OPE-A** upon addition of CdSe NCs, and B) evolution of the peak fluorescence intensities for the ester (squares) and acid (circles) forms of **OPE** (black), **T6** (blue) and **T4BTD** (red) upon addition of CdSe NCs. The concentration for each oligomer solution was 5 μ M

The same set of experiments was carried out for **T6** and **T4BTD** oligomers as well. Figure 4-5b summarizes the evolution of the peak fluorescence intensities for all six oligomers. The fluorescence intensity of **T4BTD-E** does not decrease as much as those of **T6-E** and **OPE-E**. This observation can be explained by referring to Figure 4-3a. There is almost no absorption for CdSe NCs at the emission wavelength of **T4BTD-E**, while the absorption is much stronger at wavelengths where **T6-E** and **OPE-E** emit. Furthermore, it is commonly true that the fluorescence of the ester forms decreases by a limited amount upon addition of the CdSe NCs, while the fluorescence of the acid form is quenched by more than 90% under the same conditions. Noting that the

substantial fluorescence quenching of the acid form of the oligomers occurs at very low quencher concentration (in the range of nanomolar), and diffusional quenching could be ruled out, it can thus be deduced that any evolution in the PL intensity would be due to oligomer/NC complex formation, i.e. direct interaction between the two. The PL quenching results suggest that the phosphonate ester forms have, at best, a weak interaction and thus there is little binding of the oligomers to the NCs, while the phosphonic acid forms bind strongly to the NC surface.

In the experiments described above, no luminescence increase was observed while carefully monitoring the 640 to 660 nm region for any enhancement of the emission from the CdSe in the oligomer/CdSe mixture. Considering both the low fluorescence quantum yield and the negligible concentration of CdSe NCs used in the study, this observation alone was not sufficient to rule out the possibility of energy transfer from oligomers to the CdSe NCs. To further decipher the mechanism of interactions between the oligomers and CdSe NCs, the reverse experiment was conducted, which involved investigation of the change of photoluminescence intensity of CdSe NCs emission upon addition the oligomers. For **OPE**, the procedure began with mixing 0.5 mL of a 1 μ M CdSe solution with 1.5 mL of oligomer solution of the following concentrations: 16.7 μ M (for 50:1 oligomer:CdSe); 33.4 μ M (for 100:1 oligomer:CdSe) and 66.8 μ M (for 200:1 oligomer:CdSe). The solutions were stirred and irradiated with light at the CdSe peak absorption wavelength (where no absorption for **OPE** was observed). Figure 4-6 records the change of CdSe NCs emission upon titration with **OPE-A** as described above. As a control experiment, the same process was applied to **OPE-E**. The photoluminescence of CdSe decreased upon addition of **OPE-A**, while the

same amount of **OPE-E** had almost no influence on the CdSe emission. This result again supports the proposal that **OPE-A** binds strongly to the surface of the CdSe NCs, so that the interaction between the two species is possible. Furthermore, the mutual quenching behavior of CdSe NCs and **OPE-A** indicates that when either component in the complex is photoexcited, a charge transfer process results. Either electrons are injected from **OPE-A** to CdSe NC, or holes migrate in the other direction. Similar results were observed for the **T6** derivatives.

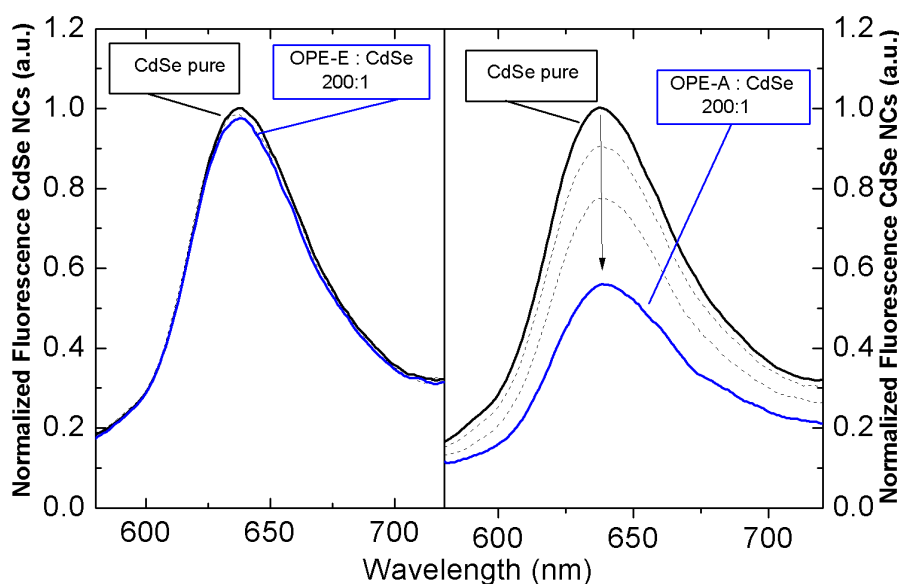


Figure 4-6. Evolution of the fluorescence of CdSe NCs upon addition of **OPE-E** and **OPE-A**. Excitation at 630 nm

Unfortunately, the same experiment was difficult to perform on **T4BTD**, since the absorption and emission of both organic and inorganic species overlapped significantly, making it impossible to look into the emission of CdSe without interference from the emission of **T4BTD** (The charge transfer between **T4BTD** and CdSe NCs will be demonstrated later in the incident photon-to-electron conversion efficiency (IPCE) results).

Referring back to the energy diagram of the oligomers and CdSe, it is true that the interaction between the oligomers and CdSe NCs occurs via electron transfer, and this interaction is strongly facilitated by attaching the oligomers onto CdSe NCs with binding groups (in this case the phosphonic acid).

Oligomer-CdSe Hybrids and IPCE Results

Now that it has been demonstrated that the acid forms of oligomers tend to bind with CdSe NCs to form complex in solution, we further explored the possibility of synthesizing hybrid materials based on the oligomer/CdSe complex. From the PL quenching experiments, a 200:1 molar ratio of oligomer:NC was sufficient to quench more than half of the luminescence of the NCs. We thus stipulated that such a ratio or higher would be reasonable for the synthesis of hybrids consisting of CdSe NC cores saturated by the oligomers at the surfaces. Since phosphonic acid groups have higher affinity to the CdSe NCs than TOPO groups (the initial ligands on the CdSe NCs), the hybrid preparation utilizes the exchange of the superficial TOPO groups of the NCs with **OPE-A**, **T6-A** or **T4BTD-A** oligomers.

As a general procedure, oligomers and CdSe NCs were mixed in chloroform solutions, followed by precipitation of the NC/oligomer hybrid in an appropriate solvent and centrifugation to remove the supernatant containing any unbound organic ligands (TOPO and excess oligomers). Experimentally, 10 mg of the oligomer was dissolved in 5 mL of degassed chloroform, to which was added a solution of the CdSe NCs in chloroform at the appropriate concentration for an excess of 200:1 ratio (oligomer:NCs, M:M). The mixture was stirred vigorously in the absence of light at room temperature for 30 minutes. The mixture was then precipitated in a poor solvent for the NCs/oligomer hybrids which still dissolves the unbound surfactants and excess oligomers. For the

T6/CdSe hybrid, ethyl acetate was used to precipitate the hybrids, while methanol was employed to precipitate the **OPE**/CdSe and **T4BTD**/CdSe hybrids. After centrifugation of the suspension and removal of the supernatant, the precipitates were redissolved in chloroform and precipitated once again in the proper solvent. This was repeated several times, and meanwhile the UV-vis absorption spectrum of the chloroform solutions was recorded in each step. As unbound oligomers were removed after each precipitation, the overall absorption profile of the redissolved precipitates featured less absorption contribution from the oligomers. Once the relative absorption intensities of the NCs versus that of the oligomer stabilized, the chloroform solution containing the redissolved oligomer/NC hybrid was considered free of unbound oligomers (This usually required 3-4 precipitation-redissolve cycles). The UV-vis absorption spectra of as-prepared hybrids solutions are shown in Figure 4-7.

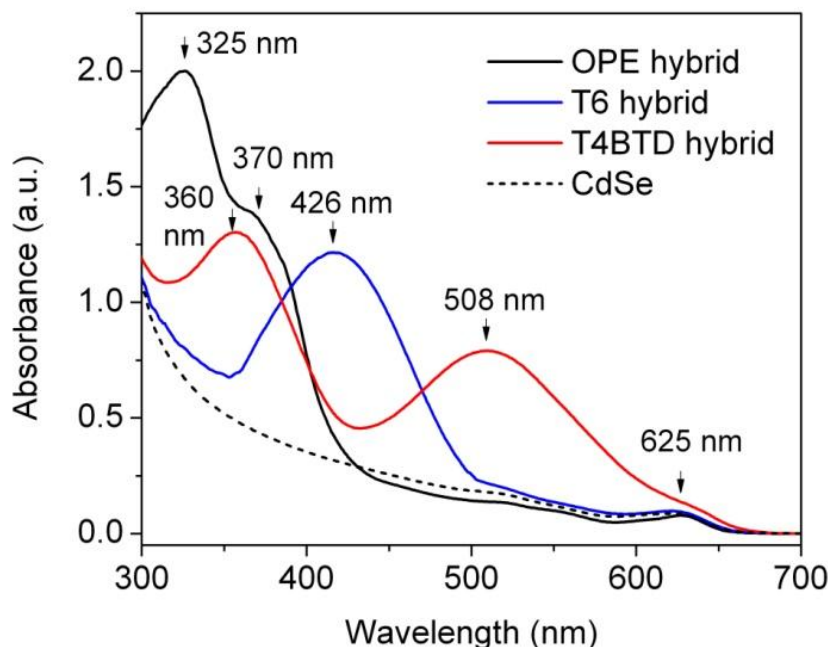


Figure 4-7. Absorbance comparison of the hybrids with parental CdSe NCs. Absorption spectra of the **OPE**-CdSe (black), the **T6**- CdSe (blue) and the **T4BTD-A**-CdSe (red) along with the spectrum of free CdSe NCs (dashed) in solution.

Compared to the absorption of pure NC solution (dashed line), the profile of the **OPE**/CdSe hybrid (black line) shows an absorption band emerging at 410 nm towards shorter wavelengths, and peaking at 325 nm with a shoulder at 370 nm, indicating the contribution of the bound **OPE-A**. The **T6**/CdSe hybrid (blue line) has a broad absorption band centered at 426 nm from the contribution of the bound T6-PA oligomers. Likewise the absorption profile for the **T4BTD**/CdSe hybrid shows the contribution of the NC-bound **T4BTD-A** peaking at 360 nm and 508 nm. In all three spectra, the contribution of the NCs to the overall absorption is observed as a peak or shoulder around 625 nm.

With the hybrids in hand, a quantitative estimation of the average number of oligomers at the NCs surface was attempted. Thermogravimetric analysis is carried out to determine the total weight loss difference between the pristine CdSe NCs and the ones functionalized with the electroactive oligomers. In principle, during the ligand exchange process, if a native surfactant such as TOPO (MW = 415 g/mol) is replaced by **OPE-A** (MW = 815 g/mol), **T6-A** (MW = 827 g/mol) or **T4BTD-A** (MW = 797 g/mol), then an oligomer/NC hybrid should have a higher organic content by weight than the original NCs. Displayed in Figure 4-8, the TGA thermograms for a CdSe sample before ligand exchange (dashed line) and after ligand exchange with **OPE-A** (black line), **T6-A** (blue line) or **T4BTD-A** (red line) were plotted. Weight loss differences in the 4% to 8% range at 500°C were observed for the hybrids compared to the pristine CdSe sample. This implies that the ligand exchange process did increase the organic content in the hybrid, supporting the presence of higher molecular weight species bound to the surface of the NCs. One obvious limitation to this method is that it is in fact very difficult

to determine the exact number of native surfactants before ligand exchange. The results from a TGA experiment on hybrids are thus, at best, qualitative.

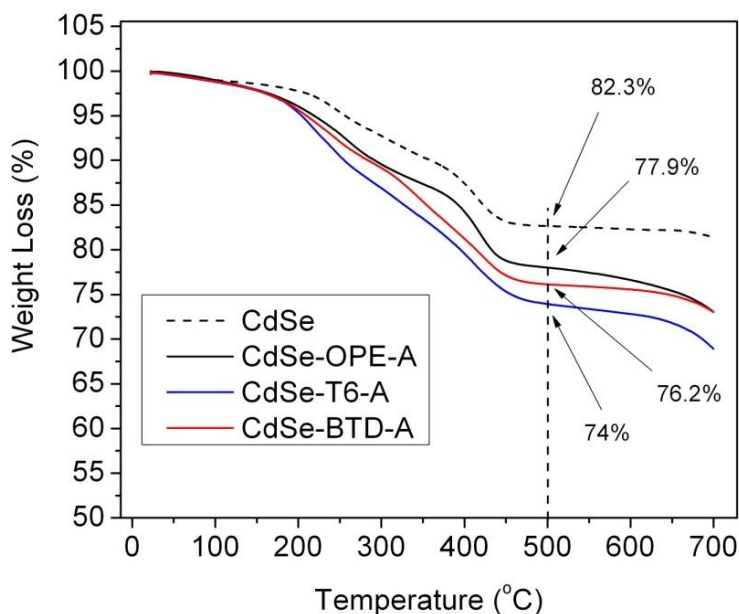


Figure 4-8. TGA thermograms of the pristine CdSe NCs (dashed line) and the hybrids with **OPE-A** (black line), **T6-A** (blue line) and **T4BTD-A** (red line) under nitrogen flow, 10°C/min heating rate.

A more quantitative way to estimate the number of surface-bound oligomers involves a careful comparison of the hybrid's absorption with that of the pristine NCs and the free oligomers. Figure 4-9 illustrates the method of such estimation using the **T6**/CdSe hybrid system as an example. The relative absorbance of the free oligomer **T6-A** (dash-dot line) and the free CdSe NCs (dashed line) was adjusted so that: 1) the absorbance from the free CdSe NCs is identical to that of **T6**/CdSe hybrid at 634nm (no absorption contribution from the **T6-A**); 2) the sum of their absorption spectra (black solid line) resulted in a profile for which the intensities at the respective absorption maxima (at 426 nm and 624 nm) matched that of the hybrid's (solid blue line). This was achieved for an absorbance of 0.912 at 426 nm for **T6-A** and 0.087 at 624 nm for the CdSe NCs. From Beer's law and referring to the extinction coefficients listed in Table 4-

2, concentrations of 18.7 μM for **T6-A** and 136 nM for CdSe NCs were calculated, respectively, resulting in an oligomer to CdSe NC ratio of 137:1. The same spectral analysis and calculations were applied to the **OPE** and **T4BTD** hybrids, suggesting ratios of 200:1 for **OPE**/CdSe hybrid and 140:1 for **T4BTD**/CdSe hybrid, respectively. While we succeeded in estimating the ratio between organic ligands and CdSe NCs, it is necessary to point out that the major limitation of this estimation is application of Beer's Law in a non-linear region of the absorption-concentration function. Based on the down-curvature of the function, the actual oligomer ratio should be higher than the estimated values. Overall, however, the estimation offers direct evidence that a significant coverage of the CdSe NCs was achieved using phosphonic acid-functionalized oligomers.

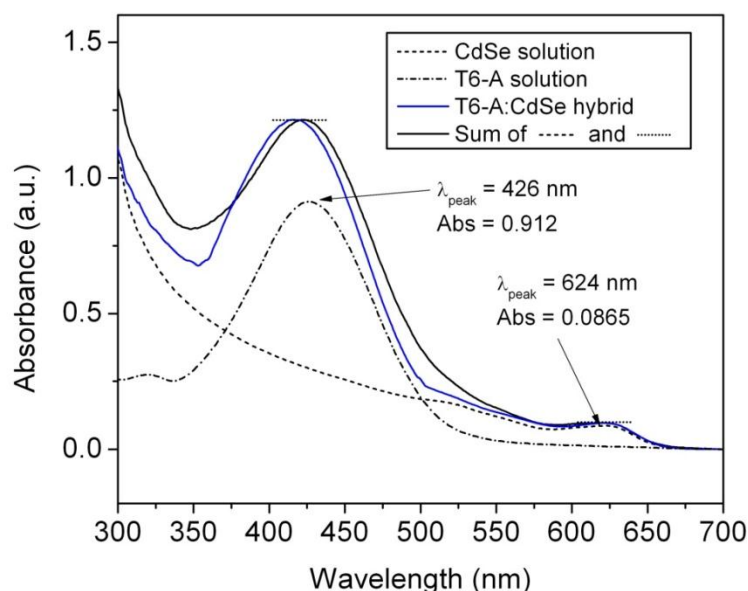


Figure 4-9. Comparison of absorption of **T6-A**/CdSe hybrid and the free components. Absorption profiles of the **T6-A**/CdSe hybrid (blue line), the free **T6-A** (dash-dot line), the free CdSe NCs (dashed line) and the sum of the latter two (black solid line).

The optical properties of the hybrids are summarized in Table 4-3. Extremely weak fluorescence was detected for chloroform solutions of the hybrids, with quantum yields

below 0.1% at 433 nm for the **OPE** hybrid solution, 564 nm for the **T6** hybrid solution and at 676 nm for the **T4BTD** hybrid solution. Seeking evidence for the dynamics of the hybrids' fluorescence, we measured the fluorescence lifetimes of the hybrids solutions as recorded in Table 4-3. Two components are contributing to the average lifetime of the hybrids fluorescence. One from the ligand emission and the other from the CdSe emission. Compared with the fluorescence lifetime of the free ligands or CdSe NCs (Table 4-2), it is clear that the components of hybrids fluorescence have almost identical lifetime with their corresponding parental oligomer or CdSe NCs. This observation suggests that the fluorescence of the hybrids comes from the residual unbound free ligands and CdSe NCs, while the hybrids themselves are non-emissive, presumably due to rapid charge transfer between the components. Transient absorption was measured for the hybrid materials to investigate the rate of the charge transfer. Unfortunately, we were not able to capture any information on the nano-second scale instrumental setup, suggesting that a rapid photophysical process occurred.

Table 4-3. Optical data of the oligomer/CdSe hybrids in CHCl₃ solution.

	λ_{\max} abs (nm)	λ_{\max} FI (nm)	Φ_{FI}	T_{FI} (ns)
OPE hybrid	325/370/625	433	<0.1%	0.88(450nm)/1.24(650nm)
T6 hybrid	426/625	564	<0.1%	0.83(560nm)/1.23(650nm)
T4BTD hybrid	360/508/625	676	<0.1%	5.2(680nm) / 1.68(650nm)

As the mechanism of photo-induced charge transfer process is concerned, either (or both) of the following scenario are to be considered. 1) Direct excitation of the organic ligands (CdSe NCs) followed by the electron injection (hole migration) from the ligands (CdSe NCs) to the CdSe NCs (the ligands), or 2) Energy transfer happens from the singlet excited state of the ligands to the CdSe NCs generating excitons in the NCs

before the hole migration from NCs back to the ligands. In all events, charge separation between the components of the hybrid materials is involved, which is demonstrated by the IPCE of the hybrids (described later in this chapter). Further study (eg. ultrafast transient absorption) is needed to discover the dynamics of the photophysical process at the interface of the hybrids.

To further demonstrate photo-induced electron transfer between the oligomers and CdSe NCs, and to study the potential application of these hybrid materials for photovoltaics (PV), we fabricated hybrid PV devices with a structure of ITO/PEDOT: PSS/Oligomer: CdSe/ZnO/Al, in which the oligomer:CdSe is the active layer, and ZnO NCs serve as optical spacer and hole-blocking layer.¹⁷⁶ The IPCE was recorded for each hybrid as displayed in Figure 4-10. The IPCE for the **OPE**/CdSe hybrid peaks at 350 nm to 10%, with little response below 3% at wavelengths higher than 500 nm except for a small shoulder at 640 nm that is likely due to the contribution of CdSe NCs. For the **T6**-based hybrid, a broader band reaching 12% appears in the IPCE from 400 nm to 550 nm corresponding to photons absorbed by the **T6** ligands bound on the CdSe NC surface. A shoulder at 640 nm was observed, implying the contribution from the CdSe NC absorption to the overall photocurrent. The IPCE for the **T4BTD** hybrid is broadened further to 650 nm, with two bands centered at 371 nm and 505 nm, and a value of 13%. The IPCE parallels the absorption of the **T4BTD**/CdSe hybrid, and a slight shoulder around 650 nm can be distinguished for CdSe contribution. Overall, the IPCE spectra for the three hybrids indeed indicate that the photocurrent contributions are from both oligomers and CdSe NCs, providing additional evidence of charge separation happening at the interface of the hybrid material.

Unfortunately, the device performances of the hybrids discussed above are disappointing (less than 0.3%). Many possible factors both from molecular design and engineering aspects are to be optimized for better devices. For example, the oligomer based hybrid active layers do not have sufficient viscosity for the devices to be successfully processed. This problem could be potentially solved by blending the hybrids with a high molecular weight conjugated polymer (eg. P3HT). Otherwise, the functionalized oligomers applied in DSSC format achieved reasonable power conversion efficiencies (This topic will be covered later in this chapter). In all, the oligomers developed in this project are promising candidates for high efficiency photovoltaics.

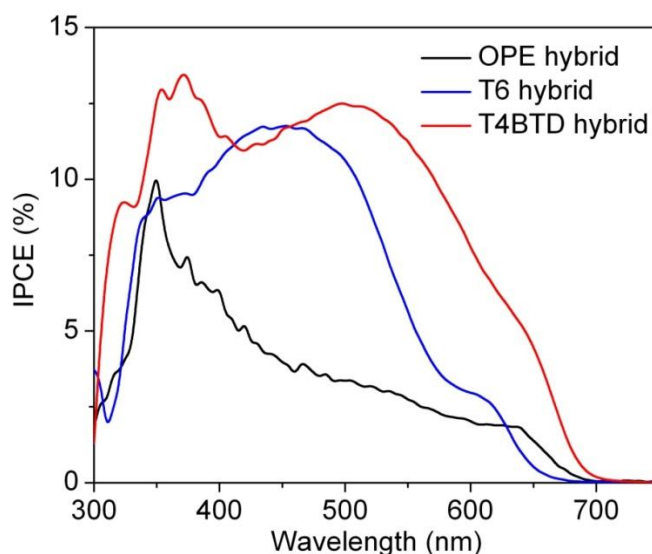


Figure 4-10. IPCE of **OPE**/CdSe (black line), **T6**/CdSe (blue line) and **T4BTD**/CdSe (red line) hybrids films in a simple device architecture under AM1.5 illumination.

Application of the Oligomers in Dye-sensitized Solar Cells

It has been reviewed in Chapter 1 that dye-sensitized solar cells (DSSCs) have gained striking progress with transition-metal based complexes as sensitizers. Recently, metal-free organic molecules are receiving increasing research attention due to the

concern that the long-term availability of the transition metals is limited.⁵⁵ To date, various organic dyes for DSSCs have been developed, such as coumarin dyes,¹⁵¹ merocyanine derivatives,¹⁷⁷ and polyene dyes.¹⁷⁸ Power conversion efficiency (PCE) that is comparable with transition-metal dyes has been achieved so far (over 10%).⁵⁵

Previously we applied the BODIPY based conjugated polyelectrolyte as sensitizers in TiO₂ DSSC devices. As our continuing investigation, we constructed DSSCs using the phosphonic acid oligomers. **T6** and **T4BTD** oligomers were chosen to build the devices for their capability of utilizing the majority of visible lights. Additionally, the phosphonic acid functional groups provide connection of the oligomers to the TiO₂ NCs. Experimentally, the oligomer coated TiO₂ films were tested in a modified reported DSSC format⁶¹ using a propylene carbonate solution of I₂/LiI as the electrolyte and a Pt/FTO counter electrode.

Figure 4-11 shows the J-V curve and IPCE plot of **T6** and **T4BTD** dyes. It is clear that the IPCE for both oligomers mimics their absorption spectra, indicating sufficient utilization of photons absorbed. Noting that without any device optimization involved, the oligomers already offer moderate PCE (1.4% and 2.2% for **T6** and **T4BTD**, respectively). It is expected that the oligomers developed in this project are promising candidates for photovoltaic applications, which is endorsed by their capability of interacting with semiconductor NCs via electron transfer.

Finally, the performance of the oligomers in the CdSe-based hybrid solar cells and those in the TiO₂-based DSSCs are surprisingly different. We propose that this different is caused by the nature of the devices. It was proven that in heterojunction cells, the device performance increase with polymer molecular weight,^{153,154} due to increased

structural order in the films. Such structural order facilitates the charge mobility in the hybrid cells. On the contrary, in DSSCs, inverse correlation between polymer chain length and cell performance was observed,⁶¹ presumably due to the fact that small molecules have better coverage on the TiO₂ surfaces. Indeed, the up-to-date efficient sensitizers used in DSSCs are all small molecules/oligomers. Based on the above arguments, it is reasonable that the oligomers developed in this project fit better for DSSC cells. More studies on morphologies need to be done to support the conclusion.

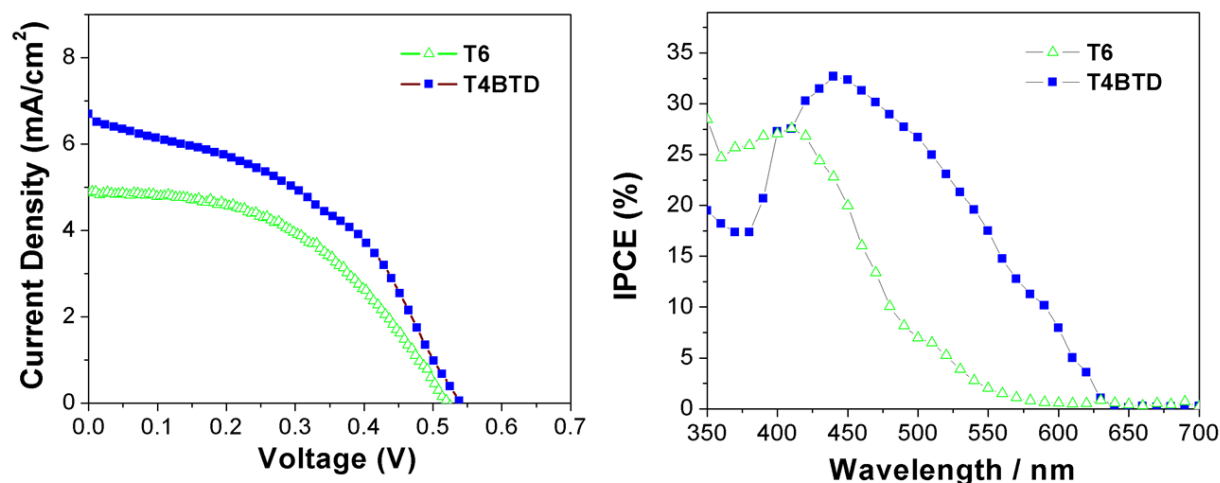


Figure 4-11. J-V curve (A) and IPCE (B) of **T6** (blue squares) and **T4BTD** (green triangles) in TiO₂ based DSSCs.

Summary and Conclusions

This chapter described three mono-functionalized conjugated oligomers with variable band gaps and their interactions with CdSe nanocrystals.

First, the syntheses of phosphonic acid functionalized oligo phenylene ethynylene **OPE-A** was introduced. Instead of applying the conventional synthetic procedure for the OPE backbones, we developed a subunit-core one-pot assembling methodology where the desired product and side product were easily separated by the polarity differences.

The novel methodology was less tedious in terms of synthesis, without compromising the overall yield of the oligomers.

Second, the photophysics and electrochemical properties of the **OPE**, **T6** and **T4BTD** were carefully characterized. By means of donor-acceptor-donor designing, the HOMO-LUMO gaps of the oligomer were varied, from 2.8 eV for **OPE** to 2.0 eV for **T4BTD**.

Third, it has been demonstrated in the study from several aspects that electron transfer occurs from the oligomers to the CdSe NCs. The process is assisted by the phosphonic acid group modified on the oligomers as evidenced by two observations. 1) The fluorescence of the acid form of the oligomers are effectively quenched at low CdSe concentration (nanomolar range), while the ester forms remain unquenched. Likewise addition of oligomers with acid groups to CdSe NCs quenches the CdSe fluorescence. The mutual quenching of the oligomers and CdSe NCs is not surprising, since electrochemical studies have indicated that the charge transfer process between the species is favored. 2) IPCE measurements on the oligomer/CdSe hybrid materials offer solid evidence for photon-induced current to occur, which is a direct result of charge separation at the oligomer/CdSe interface.

Finally, the application of the oligomers in DSSC devices was investigated in parallel. Preliminary results show that the oligomers are promising candidates for high efficiency DSSCs.

Experimental

Materials and Methods

All chemicals were purchased from either Fisher or Aldrich and used as received without further purification. NMR spectra were recorded on either a Varian Gemini-300

or a Mercury-300 spectrometer. Chemical shifts were referenced to residual signals from CHCl_3 (^1H 7.26 ppm and ^{13}C 77.23 ppm). UV-visible absorption spectra were obtained on a Varian Cary 100 absorption spectrometer using 1-cm quartz cells, and corrected for background due to solvent (HPLC grade). Fluorescence spectra were recorded on a Photon Technology International (PTI) fluorimeter. Fluorescence lifetime data was recorded on a PicoQuant PicoHarp-300 TCSPC instrument.

Dye-sensitized solar cells were fabricated as follows. First, a TiO_2 compact layer was spin-coated onto a clean FTO-glass slide.¹⁵⁷ The TiO_2 nanocrystalline paste (20 nm in diameter), which was received as a gift from Dr. Felix N. Castellano at Bowling Green State University, was doctor-bladed onto the slide with compact layer and sintered at 400°C for 30 min. The sintered electrode was immersed into the oligomer solution in DMF (~ 0.5 mM) for 36 h to allow for oligomer adsorption onto the TiO_2 film. The counter electrode was prepared by sputtering Pt on FTO glass with a thickness of 10 nm. Finally, an electrolyte solution containing 0.05 M I_2 and 0.1 M LiI in dry propylene carbonate was drawn into the sandwich between the TiO_2 working electrode and the Pt counter electrode by capillary action. The active area of the cell was 0.3 cm². The performance of the cells was measured immediately after they were assembled. The current-voltage characteristics of the cells were measured with a Keithley 2400 source meter under AM1.5 (100 mW/cm²) solar simulator. As for the IPCE measurements, the cells were illuminated by monochromatic light from an Oriel Cornerstone spectrometer, and the current response under short circuit conditions was recorded at 10 nm intervals using a Keithley 2400 source meter. The light intensity at each wavelength was calibrated with an energy meter (S350, UDT Instruments).

Synthetic Procedures

1,4-Bis(octyloxy)benzene (1). This compound was prepared by a modified literature procedure.¹⁷⁹ 8.6 g KOH powder and 50 mL DMSO were added to a 200-mL round bottom flask. The mixture was degassed for 15 min before 5.5 g (0.05 mol) hydroquinone was added. The system was heated to 80°C. After the hydroquinone dissolved, 19.3 g (0.1 mol) 1-bromooctane was added via syringe. The reaction was then allowed to run for 12 hours. After the cooled down, the mixture was poured into 600 mL ice-cold water and the crude product was precipitated as tan solid. The crude product was recrystallized by ethanol and then dried as colorless crystals. Yield 89%. ¹H NMR (300 MHz, CDCl₃, ppm) δ 6.82 (s, 4H), 3.90 (t, 4H), 1.75 (pentet, 4H), 1.45-1.30 (m, 20H), 0.88(t, 6H). ¹³C NMR (75 MHz, CDCl₃, ppm) δ 153.15, 115.34, 68.61, 31.80, 31.49, 29.37, 29.24, 26.03, 22.64, 14.09.

1,4-Diiodo-2,5-bis(octyloxy)benzene (2).¹⁸⁰ 14.5 g (0.043 mol) of **1** and a mixture of 200 mL of acetic acid and 40 mL of DI water was heated to 80°C in a 500-mL 3-necked round-bottom flask with a condenser installed. After 30 min, compound **1** was well mixed with acetic/H₂O (Since the melting point of **1** was around 60°C, it actually melted while heating). Then 13 g (0.05 mol) I₂ and 6.9 g KIO₃ was added while the system was kept stirring. After attaining reflux, a solution of sulfuric acid (4 mL in 10 mL water) was added slowly to the reaction. The reaction was then allowed to run 24 hr while the color of the iodine (purple) faded. After cooling, a saturated aqueous solution of Na₂S₂O₄ was added until the color of the reaction mixture turned pale yellow. The mixture was poured into ice-cold water, and the crude product precipitated as a light yellow solid. The crude product was dissolved in DCM and washed with DI water twice. DCM was then evaporated and the crude product was recrystallized in ethanol as a

white solid, yield 18.8g (75%). ^1H NMR (300 MHz, CDCl_3 , ppm) δ 7.17 (s, 2H), 3.93 (t, 4H), 1.80 (pentet, 4H), 1.45-1.30 (m, 20H), 0.89 (t, 6H). ^{13}C NMR (75 MHz, CDCl_3 , ppm) δ 152.79, 122.68, 86.29, 70.29, 31.77, 29.21, 29.10, 25.98, 22.63, 14.10.

3-(4-(Phenylethynyl)phenyl)prop-2-yn-1-ol (3).¹⁸¹ 1,4-diiodobenzene (5 g, 15.2 mmol) was dissolved in a mixture of 50 mL of THF and 15 mL of diisopropylamine (DIPA) in a 250-mL round-bottom flask. The solution was degassed under argon flow for 40 min before 20 mg $\text{Pd}(\text{PPh}_3)_4$ and 15 mg CuI were charged. Under the protection of argon, propargyl alcohol (15 mmol) was injected slowly via syringe. The reaction mixture turned cloudy after 30 min, and then phenylene acetylene (15.2 mmol) was added to the mixture under argon. The reaction was allowed to run overnight before the mixture was filtered. The filtrate was concentrated to remove free amines. The crude product was dissolved in DCM and washed with saturated ammonium chloride (20 mL \times 2) and brine (20 mL \times 3). The organic layers were combined and dried, and the crude product was purified by flash chromatography (DCM: hexane 2:1 v/v). Yield 2.2g (45%). ^1H NMR (300 MHz, CDCl_3 , ppm) δ 7.52 (m, 5H), 7.42 (m, 4H), 4.52 (d, 2H), 1.63 (t, 1H). ^{13}C NMR (75 MHz, CDCl_3 , ppm) δ 131.62, 131.48, 128.44, 128.37, 123.43, 122.93, 122.28, 91.24, 88.87, 85.37, 51.64.

1-Ethynyl-4-(phenylethynyl)benzene (4).¹⁸² 500 mg (2.2 mmol) of compound 3 was dissolved by 50 mL of diethyl ether in a 200-mL round-bottom flask. The system was degassed for 30 min. Then, 10 equivalents of MnO_2 (22 mmol) and KOH (22 mmol) powder were well mixed and divided into three portions. One portion was added every one hour with vigorous stirring. The reaction was allowed to run for another 2 hr after the addition of the last portion of MnO_2/KOH . The reaction mixture was filtered and

passed through a short silica-gel column by DCM and dried under vacuo. Compound **4** was obtained as a pale white solid. Yield 89%. ^1H NMR (300 MHz, CDCl_3 , ppm) δ 7.55 (m, 2H), 7.49 (s, 4H), 7.37 (m, 3H), 3.19 (s, 1H). ^{13}C NMR (75 MHz, CDCl_3 , ppm) δ 132.15, 131.72, 131.56, 128.62, 128.46, 123.85, 122.99, 91.46, 88.91, 83.35, 78.96.

Diethyl-(4-iodophenyl)phosphonate (5).¹⁸³ 16.5 g (50 mmol) of 1,4-diiodobenzene and 0.33 g (2.5 mmol) of anhydrous NiCl_2 were charged into a 100-mL 3-necked round-bottom flask with an argon inlet and outlet. The mixture was degassed for 20 min and then melted. (the temperature should not exceed 145°C). While stirring, 10.4 mL (60 mmol) of $\text{P}(\text{OEt})_3$ was slowly added to the flask via syringe with argon flow. 30 min later, the reaction mixture turned brown. The product was purified by flash chromatography. Hexane was employed first to remove free $\text{P}(\text{OEt})_3$ and 1,4-diiodobenzene, and then the product was eluted with DCM. Evaporation of solvents provided pure product as light yellow oil. Yield 70%. ^1H NMR (300 MHz, CDCl_3 , ppm) δ 7.83 (m, 2H), 7.52 (m, 2H), 4.10 (m, 4H), 1.30 (m, 6H). ^{13}C NMR (75 MHz, CDCl_3 , ppm) δ 138.02, 133.30, 128.35, 100.21, 62.40, 16.34. ^{31}P NMR (CDCl_3 , against H_3PO_4 , ppm): 19.1.

3-(4-Ethynylphenyl)prop-2-yn-1-ol (6).¹⁸⁴ This compound was synthesized in a two-step reaction. Step 1 was a Sonogashira cross-coupling reaction that was carried out under similar conditions as compound **3**, except that trimethylsilyl acetylene (instead of phenylene acetylene) was added. The intermediate was subsequently deprotected in step 2, where mild basic conditions were employed. 500 mg of intermediate (3-(4-((trimethylsilyl)ethynyl)phenyl)prop-2-yn-1-ol) was dissolved in DCM (20 mL) and MeOH (20 mL) mixed solvent and the system was degassed for 30 min. Excess amount of

K₂CO₃ (3.5 g) solid was added and the reaction was vigorously stirred for 4 hr. The reaction mixture was filtered and the filtrate was concentrated under vacuo to yield the title compound as a white solid. Yield for 2 steps is 40%. ¹H NMR (300 MHz, CDCl₃, ppm) δ 7.47-7.35 (m, 4H), 4.51 (d, 2H), 3.18 (s, 1H), 1.69 (t, 1H). ¹³C NMR (75 MHz, CDCl₃, ppm) δ 132.23, 131.68, 123.15, 122.32, 89.25, 85.30, 83.34, 79.13, 51.65.

Diethyl-(4-((4-ethynylphenyl)ethynyl)phenyl)phosphonate (7). This compound was synthesized in a two-step reaction. Step 1: compound **5** (150 mg, 0.44 mmol) and **6** (68.8 mg 0.44 mmol) were dissolved in a mixed solvent of 15 mL of THF and 5 mL of DIPA in a 50-mL round-bottom flask. The system was degassed with argon for 25 min before 8 mg Pd(PPh₃)₄ and 5 mg CuI were added. The reaction was gently heated to 50°C and allowed to run for 12 hr. The reaction mixture was filtered and the filtrate was concentrated and redissolved in DCM. After washing with saturated ammonium chloride (20 mL × 2) and brine (20 mL × 3), the crude product was dried under vacuo and purified by flash chromatography (DCM: MeOH v/v 20:1). Step 2: the intermediate was deprotected at the propargyl alcohol site using the same conditions described for compound **4**. The deprotected product was obtained as pale yellow powder. Yield for 2 steps 68%. ¹H NMR (300 MHz, CDCl₃, ppm) δ 7.80 (m, 2H), 7.60 (m, 2H), 7.49 (s, 4H), 4.16 (m, 4H), 3.19 (s, 1H), 1.35 (t, 3H). ¹³C NMR (75 MHz, CDCl₃, ppm) δ 132.00, 131.89, 131.78, 131.58, 129.65, 127.40, 122.89, 91.73, 82.42, 62.57, 51.77, 16.60. ³¹P NMR (CDCl₃, against H₃PO₄, ppm) 19.0. ESI-TOF-MS calcd for C₂₀H₁₉O₃PNa (M+Na) 361.0970, found 361.0958. Anal. calcd for C₂₀H₁₉O₃P: C, 71.00; H, 5.66, found: C, 69.85; H, 5.70.

OPE-E (8). In a 100-mL round-bottom flask, compounds **2** (176 mg 0.3 mmol) and **7** (100 mg, 0.296 mmol) were dissolved by a mixed solvent of 20 mL THF and 10 mL DIPA. The system was degassed with argon for 40 min before 10 mg Pd(PPh₃)₄ and 8 mg CuI were added. The mixture was stirred at room temperature for 1 hr and then **4** (60.7 mg 0.3 mmol) was quickly added to the system under argon. The reaction was then gently heated to 50°C and allowed to run overnight. The reaction mixture was filtered and the filtrate was concentrated and redissolved in DCM. After washing with saturated ammonium chloride (20 mL × 2) and brine (20 mL × 3), the crude product was dried under vacuo and purified by flash chromatography using DCM as eluent. Yield 80 mg (31%). ¹H NMR (300 MHz, CDCl₃, ppm) δ 7.80 (m, 2H), 7.62 (m, 2H), 7.54 (m, 9H), 7.35 (m, 4H), 7.03 (s, 2H), 4.15 (m, 4H), 4.05 (t, 4H), 1.86 (pentet, 4H), 1.50-1.30 (m, broad, 20H), 1.31 (t, 6H), 0.88 (t, 6H). ¹³C NMR (75 MHz, CDCl₃, ppm) δ 14.1, 16.4, 23.1, 26.0, 29.3, 29.6, 33.2, 61.8, 67.9, 96.0, 120.0, 128.4, 124.0, 133.1, 134.4. ³¹P NMR (300MHz CDCl₃, ppm) δ 19.5 ppm. HRMS (APCI) *m/z* calcd for C₅₈H₆₃O₅PH (MH⁺) 871.4491, found 871.4482. Anal. calcd for C₅₈H₆₃O₅P: C, 79.97; H, 7.29, found C, 79.80; H, 7.36.

OPE-A (9). To a round bottom flask equipped with stirring bar, **OPE-E** was dissolved in DCM. Upon stirring, excess amount (10 mL) of trimethylsilyl bromide (TMSBr) was added via syringe. The reaction was allowed to run for 30 min before nitrogen inlet and outlet were set up. After all the DCM and free TMSBr were evaporated under nitrogen flow, MeOH was added and the mixture was kept stirring for another 30 min. The crude product was dried under vacuo and dissolved in a few drops of CHCl₃. 10 mL MeOH was added to obtain the title compound as yellow precipitate,

which was collected by centrifuge. Yield (95%). ^1H NMR (300 MHz, CDCl_3 , ppm) δ 10.25 (broad, 2H) 7-8 (broad, 16H), 4.20 (broad, 4H), 1.0-1.8 (broad, 22H). ^{31}P NMR (300 MHz CDCl_3 , ppm) δ 22ppm. Anal. calcd. for $\text{C}_{54}\text{H}_{55}\text{O}_5\text{P}$: C, 79.58; H, 6.80, found C, 79.57; H, 6.95.

CHAPTER 5

CONCLUSIONS AND FUTURE WORK

The studies described in this dissertation involve conjugated polyelectrolytes and conjugated oligomers based on phenylene/arylene- ethynylene backbones. In detail, we have discussed the synthesis, characterization, and photophysical properties of several CPEs and oligomers with newly designed chemical structures. Meanwhile, their applications on solar cells were explored. In Chapter 2, two CPEs with interrupted conjugation were synthesized and their structure-property relations were investigated. In Chapter 3, the first CPE with BODIPY unit in the backbone was prepared by applying dendritic ionic side groups. Fundamentally, the interaction of the CPE and a series of quenchers were systematically studied. As the aspect of application, the CPE was used as sensitizer in DSSC cells. In Chapter 4, the interfaces of conjugated oligomers with variable band gaps and inorganic nano-sized materials were explored. In the first part, hybrid materials with oligomer/CdSe NCs were studied. The charge transfer between the species was demonstrated from several aspects, which nominates them potential candidates in organic-inorganic photovoltaic materials. In addition, the oligomers were applied to DSSC devices with considerable power conversion efficiencies. Finally, possible reasons for the oligomers' different behaviors in two solar cell formats were discussed.

Aggregation Induced Amplified Quenching

Two anionic conjugated polyelectrolytes that contain three-ring (phenylene ethynylene) units linked by a single $-\text{CH}_2-$ or $-\text{O}-$ tether (**C-PPE** and **O-PPE**, respectively) were characterized. Polymer **C-PPE** did not exhibit emission from an aggregate state in either MeOH or H_2O , and while the quenching of this polymer was

enhanced slightly compared to that of a monomeric chromophore, the polymer exhibited only a modest amplified quenching effect. By contrast, polymer **O-PPE** exhibited both monomer and aggregate emission, and the aggregate state was quenched 200-fold more efficiently compared to the monomer state with a K_{SV} value rivaling the maximum efficiency seen for fully conjugated polyelectrolytes. This study provides insight concerning the effect of “interrupted conjugation” on the photophysical properties and amplified quenching of conjugated polyelectrolytes. Evidence has shown that **O-PPE** forms “loose aggregates” that exhibit excimer-like emission, while **C-PPE** forms non-emissive aggregates with much larger sizes. These results underscore the important role played by chromophore aggregation in promoting efficient exciton transport, which is key to the amplified quenching effect.

More work is needed to discover how the subtle structural difference between the two CPEs has induced the major differences in terms of photophysical properties. Molecular modeling and computation can be conducted to assist understanding the two CPEs. Meanwhile, it can be helpful to synthesize the “polymer” forms (which are dissolved in organic solvents like CHCl_3) of the CPEs, so that the aggregation effect can be minimized. Photophysical study of the polymer forms will reveal the role of chemical structure difference of the two polymers in their photophysical natures.

BODIPY in the Backbone

The BODIPY-phenylene-ethynylene copolymer was converted to CPE by installing branched anionic side groups (**PB-Na**). The similar photophysics of **PB-Na** in both MeOH and H_2O indicates that the CPE is less likely to aggregate, which result in moderate fluorescence quantum yields in water. The fluorescence quenching experiment showed that **PB-Na** could be quenched by Cu^{2+} selectively among a series

of metal ions in an amplified quenching manner ($K_{sv} \sim 10^6 \text{ M}^{-1}$). Also, the energy transfer process was observed from **PB-Na** to cyanine dye DOTC ($K_{sv} \sim 10^6 \text{ M}^{-1}$). However, treatment with commonly used electron acceptor MV^{2+} caused little change in the photophysical properties of the CPE. Electrochemical analysis showed that MV^{2+} is not a sufficiently strong oxidant to allow the electron transfer process to occur, underlying low LUMO energy level of the novel CPE **PB-Na**. The development of this novel CPE has opened many opportunities for applications in studies conducted in aqueous environments.

The carboxylic acid form **PB-a** was utilized as sensitizer in DSSC cells with TiO_2 . Evidence for electron injection between **PB-a** and TiO_2 was provided by fluorescence lifetime measurements and TA experiments on **PB-a**- TiO_2 films. The low transient absorption signal together with relatively inadequate IPCE suggest that insufficient electron injection yield is resulting from the cell. Structure-property discussions were initiated and future development on the **PB-a** based DSSCs were pointed out.

Further work can be designed from two aspects. First, for DSSC applications, the side groups and polymer chain length can be engineered to optimize the device performance. Second, for CPE application in aqueous media, ionic side groups can be introduced into the BODIPY unit. For example, the phenyl group at the *meso* position of the BODIPY unit can be replaced by hydrophilic groups. Although the proposed structure will be harder to achieve synthetically, it really can help to yield BODIPY based CPEs with high fluorescence quantum yields.

Conjugated Oligomers with Mono Phosphonic Acid Functionality

Through synthetic tailoring of the conjugated chromophore, the absorption of the conjugated oligomers was varied from 380 to 600 nm in solution. The asymmetrically

modified phosphonic acid group on the oligomers offered strong anchoring of the electroactive ligands at the CdSe NCs surface. Effective photoluminescence quenching was observed for both the oligomer and CdSe while the other species was titrated. Hybrid materials based on the oligomers and CdSe NCs were prepared and purified, leading to composites with significant coverage of the NCs by more than a hundred electroactive ligands. This effectively increased the absorption of the hybrids in the visible region of the spectrum, especially as the donor-acceptor-donor molecule was used, and the photocurrent response of hybrid thin films reflected the increased absorption at wavelengths longer than 400 nm. We anticipate that the phosphonic acid-functionalized conjugated molecules described here are good candidates as active layer components for efficient hybrid organic-inorganic solar cells, especially as the absorption is further increased by taking advantage of the donor-acceptor approach. The oligomers were also used as sensitizers in DSSC format. The cell performance was encouraging, especially for the low band gap **T4BTD** oligomer. We believe that the difference on the architecture of oligomer/CdSe hybrid solar cells and TiO₂ based DSSC devices is responsible for explaining the disparity of the cell performance using the same oligomers.

LIST OF REFERENCES

- (1) Jiang, H.; Taranekar, P.; Reynolds, J. R.; Schanze, K. S. *Angew. Chem., Int. Ed.* **2009**, *48*, 4300.
- (2) Patil, A. O.; Ikenoue, Y.; Wudl, F.; Heeger, A. J. *J. Am. Chem. Soc.* **1987**, *109*, 1858.
- (3) Shi, S.; Wudl, F. *Macromolecules.* **1990**, *23*, 2119.
- (4) Feng, F.; He, F.; An, L.; Wang, S.; Li, Y.; Zhu, D. *Adv. Mater.* **2008**, *20*, 2959.
- (5) Hoven, C. V.; Garcia, A.; Bazan, G. C.; Nguyen, T.-Q. *Adv. Mater.* **2008**, *20*, 3793.
- (6) Zhao, X.; Liu, Y.; Schanze, K. S. *Chem. Commun.* **2007**, 2914.
- (7) Thomas, S. W.; Joly, G. D.; Swager, T. M. *Chem. Rev* **2007**, *107*, 1339.
- (8) Duarte, A.; Pu, K.-Y.; Liu, B.; Bazan, G. C. *Chem. Mater.* **2011**, *23*, 501.
- (9) Liu, Y.; Ogawa, K.; Schanze, K. S. *J. Photochem. Photobiol., C* **2009**, *10*, 173.
- (10) Chen, L.; McBranch, D. W.; Wang, H.-L.; Helgeson, R.; Wudl, F.; Whitten, D. G. *Proc. Natl. Acad. Sci. U.S.A.* **1999**, *96*, 12287.
- (11) Hoven, C. V.; Yang, R.; Garcia, A.; Crockett, V.; Heeger, A. J.; Bazan, G. C.; Nguyen, T.-Q. *Proc. Natl. Acad. Sci. U.S.A.* **2008**, *105*, 12730.
- (12) Pinto, M. R.; Schanze, K. S. *Proc. Natl. Acad. Sci. U.S.A.* **2004**, *101*, 7505.
- (13) Pu, K.-Y.; Liu, B. *Adv. Funct. Mater.* **2009**, *19*, 277.
- (14) Mwaura, J. K.; Zhao, X.; Jiang, H.; Schanze, K. S.; Reynolds, J. R. *Chem. Mater.* **2006**, *18*, 6109.
- (15) McRae, R. L.; Phillips, R. L.; Kim, I.-B.; Bunz, U. H. F.; Fahrni, C. J. *J. Am. Chem. Soc.* **2008**, *130*, 7851.
- (16) Björk, P.; Peter R. Nilsson, K.; Lenner, L.; Kågedal, B.; Persson, B.; Inganäs, O.; Jonasson, J. *Mol. Cell Probe.*, *21*, 329.

- (17) Miyaura, N.; Suzuki, A. *Chem. Rev.* **1995**, *95*, 2457.
- (18) Wallow, T. I.; Novak, B. M. *J. Am. Chem. Soc.* **1991**, *113*, 7411.
- (19) Brookins, R. N.; Schanze, K. S.; Reynolds, J. R. *Macromolecules*. **2007**, *40*, 3524.
- (20) Peng, Z.; Xu, B.; Zhang, J.; Pan, Y. *Chem. Commun.* **1999**, 1855.
- (21) Tan, C.; Pinto, M. R.; Schanze, K. S. *Chem. Commun.* **2002**, 446.
- (22) Zhao, X.; Pinto, M. R.; Hardison, L. M.; Mwaura, J.; Müller, J.; Jiang, H.; Witker, D.; Kleiman, V. D.; Reynolds, J. R.; Schanze, K. S. *Macromolecules*. **2006**, *39*, 6355.
- (23) Jiang, H.; Zhao, X.; Schanze, K. S. *Langmuir*. **2006**, *22*, 5541.
- (24) Tan, C.; Atas, E.; Muller, J. G.; Pinto, M. R.; Kleiman, V. D.; Schanze, K. S. *J. Am. Chem. Soc.* **2004**, *126*, 13685.
- (25) Pinto, M. R.; Kristal, B. M.; Schanze, K. S. *Langmuir*. **2003**, *19*, 6523.
- (26) Nelson, T. L.; O'Sullivan, C.; Greene, N. T.; Maynor, M. S.; Lavigne, J. J. *J. Am. Chem. Soc.* **2006**, *128*, 5640.
- (27) Sun, H.; Feng, F.; Yu, M.; Wang, S. *Macromol. Rapid. Comm.* **2007**, *28*, 1905.
- (28) Kaur, P.; Yue, H.; Wu, M.; Liu, M.; Treece, J.; Waldeck, D. H.; Xue, C.; Liu, H. *J. Phys. Chem. B* **2007**, *111*, 8589.
- (29) Prince, R. B.; Saven, J. G.; Wolynes, P. G.; Moore, J. S. *J. Am. Chem. Soc.* **1999**, *121*, 3114.
- (30) Tan, C.; Pinto, M.; Kose, M.; Ghiviriga, I.; Schanze, K. *Adv. Mater.* **2004**, *16*, 1208.
- (31) Zhao, X.; Schanze, K. S. *Langmuir*. **2006**, *22*, 4856.
- (32) Arnt, L.; Tew, G. N. *Macromolecules*. **2004**, *37*, 1283.
- (33) Xie, D.; Parthasarathy, A.; Schanze, K. S. *Langmuir*. **2011**, *27*, 11732.

- (34) Lakowicz, J. R. *Principles of Fluorescence Spectroscopy*, 2nd ed.; Kluwer Academic/Plenum Publishers: New York, 1999.
- (35) Zhou, Q.; Swager, T. M. *J. Am. Chem. Soc.* **1995**, *117*, 12593.
- (36) Thomas, S. W.; Joly, G. D.; Swager, T. M. *Chem. Rev.* **2007**, *107*, 1339.
- (37) Achyuthan, K. E.; Bergstedt, T. S.; Chen, L.; Jones, R. M.; Kumaraswamy, S.; Kushon, S. A.; Ley, K. D.; Lu, L.; McBranch, D.; Mukundan, H.; Rininsland, F.; Shi, X.; Xia, W.; Whitten, D. G. *J. Mater. Chem.* **2005**, *15*, 2648.
- (38) Onitsuka, O.; Fou, A. C.; Ferreira, M.; Hsieh, B. R.; Rubner, M. F. *J. Appl. Phys.* **1996**, *80*, 4067.
- (39) Baur, J. W.; Kim, S.; Balanda, P. B.; Reynolds, J. R.; Rubner, M. F. *Adv. Mater.* **1998**, *10*, 1452.
- (40) Ma, W.; Iyer, P. K.; Gong, X.; Liu, B.; Moses, D.; Bazan, G. C.; Heeger, A. J. *Adv. Mater.* **2005**, *17*, 274.
- (41) Hoven, C.; Yang, R.; Garcia, A.; Heeger, A. J.; Nguyen, T.-Q.; Bazan, G. C. *J. Am. Chem. Soc.* **2007**, *129*, 10976.
- (42) Garcia, A.; Yang, R.; Jin, Y.; Walker, B.; Nguyen, T.-Q. *Appl. Phys. Lett.* **2007**, *91*, 153502.
- (43) Baur, J. W.; Durstock, M. F.; Taylor, B. E.; Spry, R. J.; Reulbach, S.; Chiang, L. Y. *Synthetic. Met.* **2001**, *121*, 1547.
- (44) Pu, K.-Y.; Li, K.; Shi, J.; Liu, B. *Chem. Mater.* **2009**, *21*, 3816.
- (45) Parthasarathy, A.; Ahn, H.-Y.; Belfield, K. D.; Schanze, K. S. *ACS Appl. Mater. Interfaces* **2010**, *2*, 2744.
- (46) Corbitt, T. S.; Ding, L.; Ji, E.; Ista, L. K.; Ogawa, K.; Lopez, G. P.; Schanze, K. S.; Whitten, D. G. *Photochem. Photobiol. Sci.* **2009**, *8*, 998.
- (47) Ding, L.; Chi, E. Y.; Chemburu, S.; Ji, E.; Schanze, K. S.; Lopez, G. P.; Whitten, D. G. *Langmuir.* **2009**, *25*, 13742.
- (48) Kim, J.; McQuade, D. T.; McHugh, S. K.; Swager, T. M. *Angew. Chem., Int. Ed.* **2000**, *39*, 3868.

- (49) Fan, C.; Wang, S.; Hong, J. W.; Bazan, G. C.; Plaxco, K. W.; Heeger, A. J. *Proc. Natl. Acad. Sci. U.S.A.* **2003**, *100*, 6297.
- (50) O'Regan, B.; Gratzel, M. *Nature* **1991**, *353*, 737.
- (51) Hagfeldt, A.; Boschloo, G.; Sun, L.; Kloo, L.; Pettersson, H. *Chem. Rev.* **2010**, *110*, 6595.
- (52) Grätzel, M. *Inorg. Chem.* **2005**, *44*, 6841.
- (53) Chiba, Y.; Islam, A.; Watanabe, Y.; Komiya, R.; Koide, N.; Han, L. *Jpn. J. Appl. Phys.* **2006**, *45*, L638.
- (54) Yella, A.; Lee, H.-W.; Tsao, H. N.; Yi, C.; Chandiran, A. K.; Nazeeruddin, M. K.; Diao, E. W.-G.; Yeh, C.-Y.; Zakeeruddin, S. M.; Grätzel, M. *Science* **2011**, *334*, 629.
- (55) Zeng, W.; Cao, Y.; Bai, Y.; Wang, Y.; Shi, Y.; Zhang, M.; Wang, F.; Pan, C.; Wang, P. *Chem. Mater.* **2010**, *22*, 1915.
- (56) Koumura, N.; Wang, Z.-S.; Mori, S.; Miyashita, M.; Suzuki, E.; Hara, K. *J. Am. Chem. Soc.* **2006**, *128*, 14256.
- (57) Kim, Y.-G.; Walker, J.; Samuelson, L. A.; Kumar, J. *Nano Lett.* **2003**, *3*, 523.
- (58) Jiang, H.; Zhao, X.; Shelton, A. H.; Lee, S. H.; Reynolds, J. R.; Schanze, K. S. *ACS Appl. Mater. Interfaces* **2009**, *1*, 381.
- (59) Senadeera, G. K. R.; Nakamura, K.; Kitamura, T.; Wada, Y.; Yanagida, S. *Appl. Phys. Lett.* **2003**, *83*, 5470.
- (60) Kanimozhi, C.; Balraju, P.; Sharma, G. D.; Patil, S. *J. Phys. Chem. C* **2010**, *114*, 3287.
- (61) Fang, Z.; Eshbaugh, A. A.; Schanze, K. S. *J. Am. Chem. Soc.* **2011**, *133*, 3063.
- (62) Reiss, P.; Couderc, E.; De Girolamo, J.; Pron, A. *Nanoscale* **2011**, *3*, 446.
- (63) Colvin, V. L.; Schlamp, M. C.; Alivisatos, A. P. *Nature* **1994**, *370*, 354.
- (64) Huynh, W. U.; Dittmer, J. J.; Alivisatos, A. P. *Science* **2002**, *295*, 2425.

- (65) Lee, J.; Sundar, V. C.; Heine, J. R.; Bawendi, M. G.; Jensen, K. F. *Adv. Mater.* **2000**, *12*, 1102.
- (66) Coe, S.; Woo, W.-K.; Bawendi, M.; Bulovic, V. *Nature* **2002**, *420*, 800.
- (67) Milliron, D. J.; Alivisatos, A. P.; Pitois, C.; Edder, C.; Fréchet, J. M. J. *Adv. Mater.* **2003**, *15*, 58.
- (68) Liu, J.; Tanaka, T.; Sivula, K.; Alivisatos, A. P.; Fréchet, J. M. J. *J. Am. Chem. Soc.* **2004**, *126*, 6550.
- (69) Skaff, H.; Sill, K.; Emrick, T. *J. Am. Chem. Soc.* **2004**, *126*, 11322.
- (70) Chen, C.-H.; Liu, K.-Y.; Sudhakar, S.; Lim, T.-S.; Fann, W.; Hsu, C.-P.; Luh, T.-Y. *J. Phys. Chem. B* **2005**, *109*, 17887.
- (71) Chen, C.-T.; Pawar, V. D.; Munot, Y. S.; Chen, C.-C.; Hsu, C.-J. *Chem. Commun.* **2005**, 2483.
- (72) Gur, I.; Fromer, N. A.; Geier, M. L.; Alivisatos, A. P. *Science* **2005**, *310*, 462.
- (73) Querner, C.; Reiss, P.; Zagorska, M.; Renault, O.; Payerne, R.; Genoud, F.; Rannou, P.; Pron, A. *J. Mater. Chem.* **2005**, *15*, 554.
- (74) Solomeshch, O.; Kigel, A.; Saschiuk, A.; Medvedev, V.; Aharoni, A.; Razin, A.; Eichen, Y.; Banin, U.; Lifshitz, E.; Tessler, N. *J. Appl. Phys.* **2005**, *98*, 074310.
- (75) Odoi, M. Y.; Hammer, N. I.; Sill, K.; Emrick, T.; Barnes, M. D. *J. Am. Chem. Soc.* **2006**, *128*, 3506.
- (76) Sudeep, P. K.; Early, K. T.; McCarthy, K. D.; Odoi, M. Y.; Barnes, M. D.; Emrick, T. *J. Am. Chem. Soc.* **2008**, *130*, 2384.
- (77) Rogach, A. L.; Eychmüller, A.; Hickey, S. G.; Kershaw, S. V. *Small* **2007**, *3*, 536.
- (78) Park, J.; Joo, J.; Kwon, S. G.; Jang, Y.; Hyeon, T. *Angew. Chem., Int. Ed.* **2007**, *46*, 4630.
- (79) Yin, Y.; Alivisatos, A. P. *Nature* **2005**, *437*, 664.
- (80) Holder, E.; Tessler, N.; Rogach, A. L. *J. Mater. Chem.* **2008**, *18*, 1064.

- (81) Rogach, A. L.; Talapin, D. V.; Shevchenko, E. V.; Kornowski, A.; Haase, M.; Weller, H. *Adv. Funct. Mater.* **2002**, *12*, 653.
- (82) Murray, C. B.; Kagan, C. R.; Bawendi, M. G. *Annu. Rev. Mater. Sci.* **2000**, *30*, 545.
- (83) Javier, A.; Yun, C. S.; Sorena, J.; Strouse, G. F. *J. Phys. Chem. B* **2002**, *107*, 435.
- (84) Sih, B. C.; Wolf, M. O. *J. Phys. Chem. C* **2007**, *111*, 17184.
- (85) Querner, C.; Reiss, P.; Bleuse, J.; Pron, A. *J. Am. Chem. Soc.* **2004**, *126*, 11574.
- (86) Querner, C.; Benedetto, A.; Demadrille, R.; Rannou, P.; Reiss, P. *Chem. Mater.* **2006**, *18*, 4817.
- (87) Shallcross, R. C.; D'Ambruso, G. D.; Korth, B. D.; Hall, H. K.; Zheng, Z.; Pyun, J.; Armstrong, N. R. *J. Am. Chem. Soc.* **2007**, *129*, 11310.
- (88) Pokrop, R.; Pamuła, K.; Deja-Drogomirecka, S.; Zagorska, M.; Borysiuk, J.; Reiss, P.; Pron, A. *J. Phys. Chem. C* **2009**, *113*, 3487.
- (89) Zotti, G.; Vercelli, B.; Berlin, A.; Pasini, M.; Nelson, T. L.; McCullough, R. D.; Virgili, T. *Chem. Mater.* **2010**, *22*, 1521.
- (90) Locklin, J.; Patton, D.; Deng, S.; Baba, A.; Millan, M.; Advincula, R. C. *Chem. Mater.* **2004**, *16*, 5187.
- (91) De Girolamo, J.; Reiss, P.; Pron, A. *J. Phys. Chem. C* **2007**, *111*, 14681.
- (92) Liao, H.-C.; Chen, S.-Y.; Liu, D.-M. *Macromolecules.* **2009**, *42*, 6558.
- (93) Peng, X.; Zhang, L.; Chen, Y.; Li, F.; Zhou, W. *Appl. Surf. Sci.* **2010**, *256*, 2948.
- (94) Majetich, S. A.; Carter, A. C.; Belot, J.; McCullough, R. D. *J. Phys. Chem.* **1994**, *98*, 13705.
- (95) Fritzinger, B.; Moreels, I.; Lommens, P.; Koole, R.; Hens, Z.; Martins, J. C. *J. Am. Chem. Soc.* **2009**, *131*, 3024.
- (96) Stalder, R.; Mei, J.; Subbiah, J.; Grand, C.; Estrada, L. A.; So, F.; Reynolds, J. R. *Macromolecules.* **2011**, *44*, 6303.

- (97) Hu, D.; Shen, F.; Liu, H.; Lu, P.; Lv, Y.; Liu, D.; Ma, Y. *Chem. Commun.* **2012**, 48, 3015.
- (98) Xu, J.; Wang, J.; Mitchell, M.; Mukherjee, P.; Jeffries-El, M.; Petrich, J. W.; Lin, Z. *J. Am. Chem. Soc.* **2007**, 129, 12828.
- (99) Greenham, N. C.; Peng, X.; Alivisatos, A. P. *Phys. Rev. B* **1996**, 54, 17628.
- (100) Dayal, S.; Kopidakis, N.; Olson, D. C.; Ginley, D. S.; Rumbles, G. *Nano Lett.* **2010**, 10, 239.
- (101) Bozano, L.; Carter, S. A.; Scott, J. C.; Malliaras, G. G.; Brock, P. J. *Appl. Phys. Lett.* **1999**, 74, 1132.
- (102) Sun, B.; Snaith, H. J.; Dhoot, A. S.; Westenhoff, S.; Greenham, N. C. *J. Appl. Phys.* **2005**, 97, 014914.
- (103) Peng, X. G.; Manna, L.; Yang, W. D.; Wickham, J.; Scher, E.; Kadavanich, A.; Alivisatos, A. P. *Nature* **2000**, 404, 59.
- (104) Wang, D.; Gong, X.; Heeger, P. S.; Rininsland, F.; Bazan, G. C.; Heeger, A. J. *Proc. Natl. Acad. Sci. U.S.A.* **2002**, 99, 49.
- (105) Jin, Y.; Bazan, G. C.; Heeger, A. J.; Kim, J. Y.; Lee, K. *Appl. Phys. Lett.* **2008**, 93, 123304/1.
- (106) Swager, T. M. *Acc. Chem. Res* **1998**, 31, 201.
- (107) He, C.; Zhong, C.; Wu, H.; Yang, R.; Yang, W.; Huang, F.; Bazan, G. C.; Cao, Y. *J. Mater. Chem.* **2010**, 20, 2617.
- (108) Burrows, H. D.; Tapia, M. J.; Fonseca, S. M.; Valente, A. J. M.; Lobo, V. M. M.; Justino, L. n. L. G.; Qiu, S.; Pradhan, S.; Scherf, U.; Chattopadhyay, N.; Knaapila, M.; Garamus, V. M. *ACS Appl. Mater. Interfaces* **2009**, 1, 864.
- (109) Yue, H.; Wu, M.; Xue, C.; Velayudham, S.; Liu, H.; Waldeck, D. H. *J. Phys. Chem. B* **2008**, 112, 8218.
- (110) Wang, F.; Bazan, G. C. *J. Am. Chem. Soc.* **2006**, 128, 15786.
- (111) McQuade, D. T.; Pullen, A. E.; Swager, T. M. *Chem. Rev.* **2000**, 100, 2537.

- (112) Lu, L.; Helgeson, R.; Jones, R. M.; McBranch, D.; Whitten, D. *J. Am. Chem. Soc.* **2002**, *124*, 483.
- (113) Gaylord, B. S.; Wang, S.; Heeger, A. J.; Bazan, G. C. *J. Am. Chem. Soc.* **2001**, *123*, 6417.
- (114) Tang, Y.; Zhou, Z.; Ogawa, K.; Lopez, G. P.; Schanze, K. S.; Whitten, D. G. *Langmuir*. **2008**, *25*, 21.
- (115) Friedman, A. E.; Chambron, J. C.; Sauvage, J. P.; Turro, N. J.; Barton, J. K. *J. Am. Chem. Soc.* **1990**, *112*, 4960.
- (116) Kumar, C. V.; Barton, J. K.; Turro, N. J. *J. Am. Chem. Soc.* **1985**, *107*, 5518.
- (117) Loudet, A.; Burgess, K. *Chem. Rev.* **2007**, *107*, 4891.
- (118) Erten-Ela, S.; Yilmaz, M. D.; Icli, B.; Dede, Y.; Icli, S.; Akkaya, E. U. *Org. Lett.* **2008**, *10*, 3299.
- (119) Ulrich, G.; Ziesel, R.; Harriman, A. *Angew. Chem., Int. Ed.* **2008**, *47*, 1184.
- (120) Nagai, A.; Miyake, J.; Kokado, K.; Nagata, Y.; Chujo, Y. *J. Am. Chem. Soc.* **2008**, *130*, 15276.
- (121) Li, J.; Kim, I. H.; Roche, E. D.; Beeman, D.; Lynch, A. S.; Ding, C. Z.; Ma, Z. *Bioorg. Med. Chem. Lett* **2006**, *16*, 794.
- (122) Ekmekci, Z.; Yilmaz, M. D.; Akkaya, E. U. *Org. Lett.* **2008**, *10*, 461.
- (123) Wan, C.-W.; Burghart, A.; Chen, J.; Bergström, F.; Johansson, L. B. Å.; Wolford, M. F.; Kim, T. G.; Topp, M. R.; Hochstrasser, R. M.; Burgess, K. *Chem-eur. J.* **2003**, *9*, 4430.
- (124) Kim, B.; Ma, B.; Donuru, V. R.; Liu, H.; Frechet, J. M. J. *Chem. Commun.* **2010**, *46*, 4148.
- (125) Ziesel, R.; Ulrich, G.; Harriman, A. *New J. Chem.* **2007**, *31*, 496.
- (126) Donuru, V. R.; Vegesna, G. K.; Velayudham, S.; Green, S.; Liu, H. *Chem. Mater.* **2009**, *21*, 2130.

- (127) Goze, C.; Ulrich, G.; Mallon, L. J.; Allen, B. D.; Harriman, A.; Ziesse, R. *J. Am. Chem. Soc.* **2006**, *128*, 10231.
- (128) Goze, C.; Ulrich, G.; Ziesse, R. *J. Org. Chem.* **2006**, *72*, 313.
- (129) Goze, C.; Ulrich, G.; Ziesse, R. *Org. Lett.* **2006**, *8*, 4445.
- (130) Popere, B. C.; Della Pelle, A. M.; Thayumanavan, S. *Macromolecules*. **2011**, *44*, 4767.
- (131) Dodani, S. C.; He, Q.; Chang, C. J. *J. Am. Chem. Soc.* **2009**, *131*, 18020.
- (132) Zhu, S.; Zhang, J.; Vegesna, G.; Luo, F.-T.; Green, S. A.; Liu, H. *Org. Lett.* **2010**, *13*, 438.
- (133) Li, L.; Han, J.; Nguyen, B.; Burgess, K. *J. Org. Chem.* **2008**, *73*, 1963.
- (134) Niu, S. L.; Ulrich, G.; Ziesse, R.; Kiss, A.; Renard, P.-Y.; Romieu, A. *Org. Lett.* **2009**, *11*, 2049.
- (135) Gießler, K.; Griesser, H.; Göhringer, D.; Sabirov, T.; Richert, C. *Eur. J. Org. Chem.* **2010**, *2010*, 3611.
- (136) Jiao, L.; Li, J.; Zhang, S.; Wei, C.; Hao, E.; Vicente, M. G. H. *New J. Chem.* **2009**, *33*, 1888.
- (137) Lee, S. H.; Kömürlü, S.; Zhao, X.; Jiang, H.; Moriena, G.; Kleiman, V. D.; Schanze, K. S. *Macromolecules*. **2011**, *44*, 4742.
- (138) Zhao, X. *PhD. Dissertation, University of Florida* **2007**, p144.
- (139) Huang, Y.-Q.; Fan, Q.-L.; Lu, X.-M.; Fang, C.; Liu, S.-J.; Yu-Wen, L.-H.; Wang, L.-H.; Huang, W. *J. Polym. Sci., Part A: Polym. Chem.* **2006**, *44*, 5778.
- (140) Bergström, F.; Mikhalyov, I.; Hägglöf, P.; Wortmann, R.; Ny, T.; Johansson, L. B. Å. *J. Am. Chem. Soc.* **2001**, *124*, 196.
- (141) Connelly, N. G.; Geiger, W. E. *Chem. Rev.* **1996**, *96*, 877.
- (142) Liao, Y.-T.; Zang, L.; Akins, D. L. *Catal. Commun.* **2005**, *6*, 141.
- (143) Fan, L.-J.; Jones, W. E. *J. Am. Chem. Soc.* **2006**, *128*, 6784.

- (144) Fabbrizzi, L.; Licchelli, M.; Pallavicini, P. *Acc. Chem. Res.* **1999**, 32, 846.
- (145) Hagfeldt, A.; Graetzel, M. *Chem. Rev.* **1995**, 95, 49.
- (146) Lenzmann, F.; Krueger, J.; Burnside, S.; Brooks, K.; Grätzel, M.; Gal, D.; Rühle, S.; Cahen, D. *J. Phys. Chem. B* **2001**, 105, 6347.
- (147) Argazzi, R.; Bignozzi, C. A.; Heimer, T. A.; Castellano, F. N.; Meyer, G. J. *Inorg. Chem.* **1994**, 33, 5741.
- (148) Hagfeldt, A.; Grätzel, M. *Acc. Chem. Res.* **2000**, 33, 269.
- (149) Kay, A.; Graetzel, M. *J. Phys. Chem.* **1993**, 97, 6272.
- (150) Hara, K.; Dan-oh, Y.; Kasada, C.; Ohga, Y.; Shinpo, A.; Suga, S.; Sayama, K.; Arakawa, H. *Langmuir*. **2004**, 20, 4205.
- (151) Wang, Z.-S.; Hara, K.; Dan-oh, Y.; Kasada, C.; Shinpo, A.; Suga, S.; Arakawa, H.; Sugihara, H. *J. Phys. Chem. B* **2005**, 109, 3907.
- (152) Hara, K.; Kurashige, M.; Dan-oh, Y.; Kasada, C.; Shinpo, A.; Suga, S.; Sayama, K.; Arakawa, H. *New J. Chem.* **2003**, 27, 783.
- (153) Coffin, R. C.; Peet, J.; Rogers, J.; Bazan, G. C. *Nature Chem.* **2009**, 1, 657.
- (154) Bijleveld, J. C.; Zoombelt, A. P.; Mathijssen, S. G. J.; Wienk, M. M.; Turbiez, M.; de Leeuw, D. M.; Janssen, R. A. J. *J. Am. Chem. Soc.* **2009**, 131, 16616.
- (155) Hardin, B. E.; Sellinger, A.; Moehl, T.; Humphry-Baker, R.; Moser, J.-E.; Wang, P.; Zakeeruddin, S. M.; Grätzel, M.; McGehee, M. D. *J. Am. Chem. Soc.* **2011**, 133, 10662.
- (156) Wang, P.; Zakeeruddin, S. M.; Moser, J.-E.; Humphry-Baker, R.; Grätzel, M. *J. Am. Chem. Soc.* **2004**, 126, 7164.
- (157) Burke, A.; Ito, S.; Snaith, H.; Bach, U.; Kwiatkowski, J.; Grätzel, M. *Nano Lett.* **2008**, 8, 977.
- (158) Zhao, X. *PhD. Dissertation, Univeristy of Florida* **2007**, p169.
- (159) Lee, S. H. *PhD. Dissertation, Univeristy of Florida* **2010**, p78.

- (160) Stone, M. T.; Moore, J. S. *Org. Lett.* **2004**, 6, 469.
- (161) Xiao, Z.-Y.; Hou, J.-L.; Jiang, X.-K.; Li, Z.-T.; Ma, Z. *Tetrahedron* **2009**, 65, 10182.
- (162) Yoshiki, C. *Curr. Opin. Solid State Mater. Sci.* **1996**, 1, 806.
- (163) Hoffmann, M. R.; Martin, S. T.; Choi, W.; Bahnemann, D. W. *Chem. Rev.* **1995**, 95, 69.
- (164) Walter, M. G.; Warren, E. L.; McKone, J. R.; Boettcher, S. W.; Mi, Q.; Santori, E. A.; Lewis, N. S. *Chem. Rev.* **2010**, 110, 6446.
- (165) Kamat, P. V.; Tvrđy, K.; Baker, D. R.; Radich, J. G. *Chem. Rev.* **2010**, 110, 6664.
- (166) Grätzel, M. *Acc. Chem. Res.* **2009**, 42, 1788.
- (167) Huynh, W. U.; Dittmer, J. J.; Libby, W. C.; Whiting, G. L.; Alivisatos, A. P. *Adv. Funct. Mater.* **2003**, 13, 73.
- (168) Jun, Y.-w.; Choi, J.-s.; Cheon, J. *Angew. Chem., Int. Ed.* **2006**, 45, 3414.
- (169) Zhang, F.; Svensson, M.; Andersson, M. R.; Maggini, M.; Bucella, S.; Menna, E.; Inganäs, O. *Adv. Mater.* **2001**, 13, 1871.
- (170) Hwang, J.-J.; Tour, J. M. *Tetrahedron* **2002**, 58, 10387.
- (171) Yang, J.; Tang, A.; Zhou, R.; Xue, J. *Sol. Energ. Mat. Sol. C.* **2011**, 95, 476.
- (172) Peng, Z. A.; Peng, X. *J. Am. Chem. Soc.* **2000**, 123, 183.
- (173) Beaujuge, P. M.; Amb, C. M.; Reynolds, J. R. *Acc. Chem. Res.* **2010**, 43, 1396.
- (174) Yu, W. W.; Qu, L.; Guo, W.; Peng, X. *Chem. Mater.* **2003**, 15, 2854.
- (175) Jones, M.; Nedeljkovic, J.; Ellingson, R. J.; Nozik, A. J.; Rumbles, G. *J. Phys. Chem. B* **2003**, 107, 11346.
- (176) Qian, L.; Yang, J.; Zhou, R.; Tang, A.; Zheng, Y.; Tseng, T.-K.; Bera, D.; Xue, J.; Holloway, P. H. *J. Mater. Chem.* **2011**, 21, 3814.

- (177) Horiuchi, T.; Miura, H.; Sumioka, K.; Uchida, S. *J. Am. Chem. Soc.* **2004**, *126*, 12218.
- (178) Kitamura, T.; Ikeda, M.; Shigaki, K.; Inoue, T.; Anderson, N. A.; Ai, X.; Lian, T.; Yanagida, S. *Chem. Mater.* **2004**, *16*, 1806.
- (179) Lynch, P. J.; O'Neill, L.; Bradley, D.; Byrne, H. J.; McNamara, M. *Macromolecules.* **2007**, *40*, 7895.
- (180) Lee, J.; Cho, H.-J.; Cho, N. S.; Hwang, D.-H.; Kang, J.-M.; Lim, E.; Lee, J.-I.; Shim, H.-K. *J. Polym. Sci., Part A: Polym. Chem.* **2006**, *44*, 2943.
- (181) Fang, J.-K.; An, D.-L.; Wakamatsu, K.; Ishikawa, T.; Iwanaga, T.; Toyota, S.; Matsuo, D.; Orita, A.; Otera, J. *Tetrahedron Lett.* **2010**, *51*, 917.
- (182) Li, K.; Wang, Q. *Chem. Commun.* **2005**, 4786.
- (183) Brunet, E.; Alhendawi, H. M. H.; Cerro, C.; de la Mata, M. J.; Juanes, O.; Rodríguez-Ubis, J. C. *Micropor. Mesopor. Mat.* **2011**, *138*, 75.
- (184) Ko, E.; Liu, J.; Perez, L. M.; Lu, G.; Schaefer, A.; Burgess, K. *J. Am. Chem. Soc.* **2010**, *133*, 462.

BIOGRAPHICAL SKETCH

Dongping Xie was born in 1985 in Sichuan, China, where he grew up and finished high school. At the age of 18 he attended Fudan University in Shanghai majored in applied chemistry. In 2007, he graduated with honor and continued immediately on to graduate work at the University of Florida, pursuing a doctorate in chemistry. Under the supervision of Dr. Kirk Schanze, he conducted a series of researches on conjugated polyelectrolytes and conjugated oligomers. After graduation in May, 2012, Dongping will be starting his professional career as an investment analyst for the industry of chemistry and chemical engineering in Beijing, China.